

Abstract

In high-pH (pH > 10) fluids that have participated in low-temperature (< 150 °C) serpentinization, the dominant form of C is often methane (CH₄), but the origin of this CH₄ is uncertain. To assess CH₄ origin during low-temperature serpentinization, we pumped fluids from aquifers within the Samail Ophiolite, Oman. We determined fluid chemical compositions, analyzed taxonomic profiles of fluid-hosted microbial communities, and measured isotopic compositions of hydrocarbon gases. We found that 16S rRNA gene sequences affiliated with methanogens were widespread in the aquifer. We measured clumped isotopologue (¹³CH₃D and ¹²CH₂D₂) relative abundances less than equilibrium, consistent with substantial microbial CH₄ production. Further, we observed an inverse relationship between dissolved inorganic C concentrations and δ¹³C_{CH₄} across fluids bearing microbiological evidence of methanogenic activity, suggesting that the apparent C isotope effect of microbial methanogenesis is modulated by C availability. A second source of CH₄ is evidenced by the presence of CH₄-bearing fluid inclusions in the Samail Ophiolite and our measurement of high δ¹³C values of ethane and propane, which are similar to those reported in studies of CH₄-rich inclusions in rocks from the oceanic lithosphere. In addition, we observed 16S rRNA gene sequences affiliated with aerobic methanotrophs and, in lower abundance, anaerobic methanotrophs, indicating that microbial consumption of CH₄ in the ophiolite may further enrich CH₄ in ¹³C. We conclude that substantial microbial CH₄ is produced under varying degrees of C limitation and mixes with abiotic CH₄ released from fluid inclusions. This study lends insight into the functioning of microbial ecosystems supported by water/rock reactions.

Plain Language Summary

Rocks from beneath Earth’s crust can be thrust to the surface, where they are exposed to rain and air containing carbon dioxide (CO₂). The groundwaters that become stored in these rocks often contain methane (CH₄, a major component of “natural gas”), which can be formed from carbon dioxide in the subsurface. To investigate these methane-forming processes, we sampled water, gas, and suspended particles from groundwaters using wells previously drilled into the rocks. The particles contained microbes with the genetic ability to produce methane. We also precisely measured the masses of C and H atoms (isotopes) and their arrangements (isotopologues) in the natural gas to determine how it was formed. The results of these measurements suggest that microbes could actively produce a considerable amount of the methane, which mixes with methane from another source that was formed by non-biological processes, possibly long ago under different conditions than today’s. Rocks like those studied here are widespread in the Solar System, so our finding that microbes live and produce methane in these rocks could help guide the search for life beyond Earth.

1 Introduction

At temperatures and pressures near the Earth’s surface (< 400 °C, < 100 MPa), ultramafic rocks such as peridotite in contact with water are thermodynamically driven to hydrate and oxidize, forming variable amounts of serpentine, magnetite, brucite, hydrogen (H₂), and other phases (Evans, 1977; Frost, 1985; McCollom & Bach, 2009; Klein & Bach, 2009; Klein et al., 2009, 2019). This process, often called “serpentinization”, can produce H₂ at temperatures at least as low as 55 °C (Miller, Mayhew, et al., 2017). The resultant H₂ can be thermodynamically favored to reduce carbon dioxide (CO₂) to methane (CH₄) (Shock, 1992). The reduction of CO₂ by H₂ to form CH₄ can be catalyzed on mineral surfaces as in the Sabatier reaction (Etiopie & Ionescu, 2015; Klein et al., 2019), or enzymatically through microbial methanogenesis (Whiticar, 1999).

In continental settings undergoing serpentinization, where fluid-rock reactions typically occur at low temperatures (< 150 °C), there is disagreement regarding the ori-

gin of CH₄. Three key potential CH₄ sources have been identified in these environments. One potential source is the abiotic reduction of CO₂ to CH₄ at warmer-than-present temperatures in fluid inclusions within crystals that can store CH₄ and subsequently release it. Another potential source is the abiotic, mineral-catalyzed reduction of CO₂ to CH₄ at the low temperatures that prevail in the present-day weathering environment. A third potential source is microbial methanogenesis.

Storage of CH₄ produced at temperatures of 270 °C to 800 °C in fluid inclusions in minerals such as olivine and the release of this CH₄ through subsequent chemical/physical alteration are the dominant processes contributing to CH₄ fluxes from sediment-poor seafloor hydrothermal vents (Kelley, 1996; Kelley & Früh-Green, 1999; McDermott et al., 2015; D. T. Wang et al., 2018). Debate continues, however, regarding whether fluid inclusions sustain CH₄ fluxes from continental, low-temperature serpentinizing settings (Etiope & Whiticar, 2019; Grozeva et al., 2020).

Abiotic reduction of CO₂ to CH₄ can occur at temperatures at least as low as 20 °C when catalyzed by the transition metal ruthenium (Ru) (Etiope & Ionescu, 2015). Ru is present in considerable abundance in chromitite bodies in ultramafic rock accumulations (Etiope et al., 2018). However, it has not been shown to catalyze CO₂ hydrogenation under aqueous conditions (Etiope & Ionescu, 2015). The relevance of this process, particularly to aquifers whose fluid compositions appear to be dominantly influenced by water/harzburgite reactions, has been questioned (Etiope, 2017; Miller, Matter, et al., 2017).

Low-temperature CH₄ production can also be mediated by microbes called “methanogens”. It has been argued that serpentinizing settings contain only minor amounts of microbial CH₄ because CH₄ in serpentinizing settings is often more ¹³C-enriched than CH₄ in sedimentary settings of microbial methanogenesis (Etiope, 2017; Etiope & Whiticar, 2019). However, cultures of methanogens can produce CH₄ with minimal C isotope fractionation in H₂-rich, CO₂-poor fluids simulating serpentinizing systems (Miller et al., 2018). In these cultures, it has been inferred that the net C isotope effect of methanogenesis was attenuated due to microbial conversion of a large proportion of available CO₂ to CH₄ when CO₂ was the limiting substrate. Such results illustrate that ¹³C-enriched CH₄ in natural serpentinizing settings does not necessarily derive from non-microbial sources. Still, the quantity and isotopic composition of microbial CH₄ in serpentinizing settings remains uncertain.

In this study, we assessed sources and sinks of CH₄ in the Samail Ophiolite of Oman, a site of active, low-temperature serpentinization and carbonation. For this purpose, isotopic compositions of CH₄ and co-occurring short-chain alkanes exsolved from pumped groundwaters were measured, including the multiply-substituted “clumped” isotopologues of CH₄, ¹³CH₃D and ¹²CH₂D₂. To complement the isotopic data, 16S rRNA genes in biomass filter-concentrated from groundwaters were amplified and sequenced. We observed a wide range of C isotopic compositions of CH₄ and short-chain alkanes, intramolecular isotopologue disequilibrium in CH₄, and widespread occurrence of gene sequences affiliated with methanogens, which collectively indicate that substantial quantities of microbial CH₄ are produced and mix with abiotic CH₄ released from fluid inclusions in the Samail Ophiolite. Our finding that microbial methanogenesis proceeds even in hyperalkaline fluids lends insight into the functioning of microbial ecosystems that leverage reactions between water and ultramafic rocks to power metabolic processes on Earth and perhaps on other rocky bodies of the Solar System (Ménez, 2020; Glein & Zolotov, 2020).

2 Geologic Setting

The Samail Ophiolite (Figure 1) consists of pelagic sedimentary rocks (< 0.1 km), volcanic rocks (0.5 km to 2.0 km), sheeted dikes (1 km to 1.5 km), gabbro and igneous peri-

124 dotite (0.5 km to 6.5 km), residual mantle peridotites, (8 km to 12 km), and a metamorphic
 125 sole of greenschist- to granulite-facies metamorphic rocks (< 0.5 km) (Glennie et
 126 al., 1973; Coleman & Hopson, 1981; Lippard et al., 1986; Nicolas, 1989; Nicolas et al.,
 127 2000). The ophiolite crust formed from 96.12 Ma to 95.50 Ma, and convergence began
 128 at about the same time (Rioux et al., 2016), or up to 10 My earlier (Guilmette et al., 2018;
 129 Soret et al., 2020). Ophiolite emplacement continued until 78 Ma to 71 Ma (Rabu et al.,
 130 1993). Part of the ophiolite was subaerially eroded in the Late Cretaceous, then became
 131 covered in parts by Maastrichtian to Eocene limestones due to subsidence and transgres-
 132 sion (Nolan et al., 1990; Skelton et al., 1990).

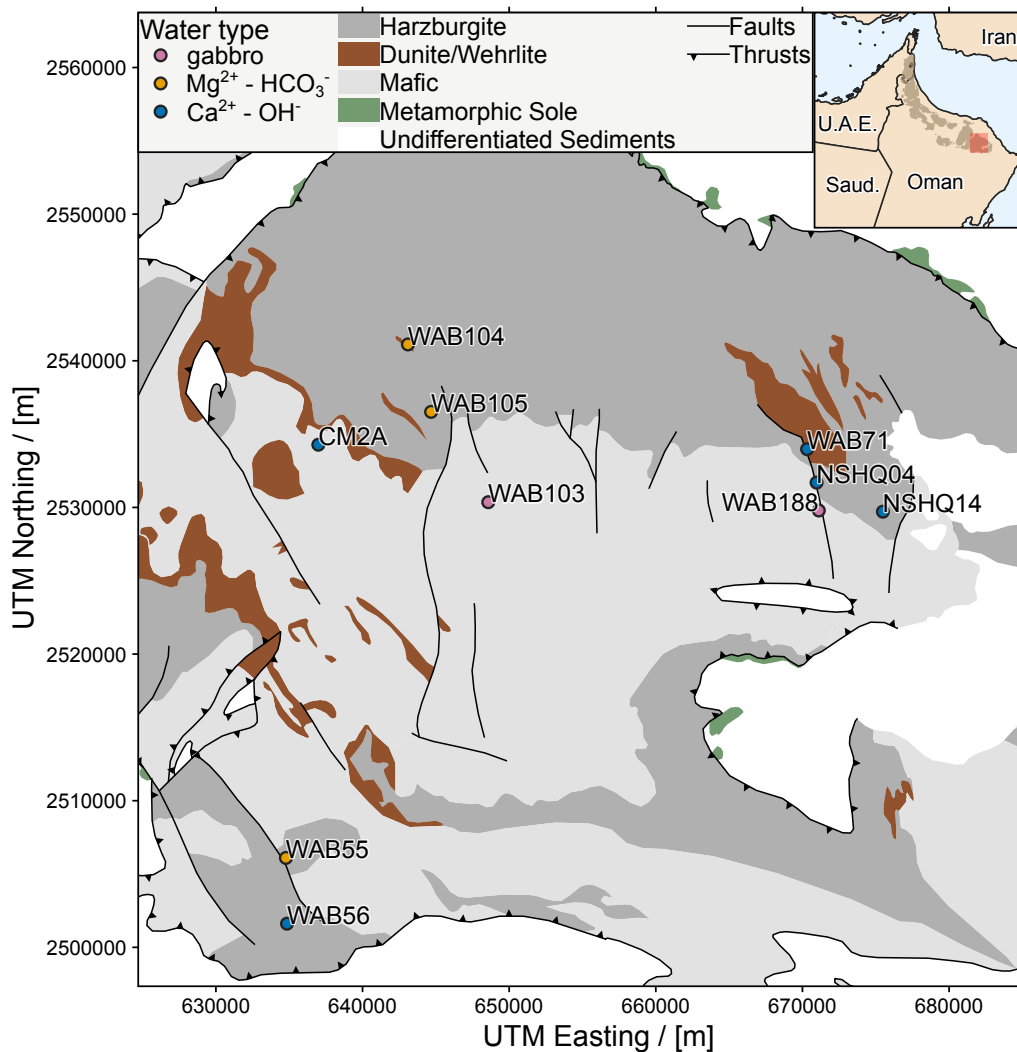


Figure 1. Study area in Samail Ophiolite, Sultanate of Oman. Geologic map data from Nicolas et al. (2000). Inset: overview of Samail Ophiolite (shaded in brown) with study area (larger map) indicated by the red shaded box. A topographic map of the study area is provided in Supporting Information Figure S1.

133 The mantle section of the ophiolite is mainly composed of highly depleted, resid-
 134 ual mantle harzburgites, together with 5 % to 15 % dunite, which both contain a few per-
 135 cent chromian spinel (Godard et al., 2000; Hanghøj et al., 2010; Boudier & Coleman, 1981;
 136 Collier, 2012). The extent of serpentinization is typically 30 % to 60 %, reaching 100 %

137 in some cases (Dewandel et al., 2003; Boudier et al., 2009; Miller et al., 2016; P. Kele-
 138 men et al., 2020). Chromitites are most often found in association with dunitites near the
 139 crust-mantle transition, possibly representing bases of cumulate piles, but are also found
 140 dispersed throughout the mantle section (Rollinson, 2005).

141 Geologic reservoirs of C underlying the ophiolite include Mid Permian to Late Cre-
 142 taceous shallow marine carbonates, which host oil and gas fields in parts of northern Oman
 143 and the United Arab Emirates (Terken, 1999; Alsharhan, 1989; Etiope et al., 2015). Maas-
 144 trictian to Eocene limestones that partially overly the ophiolite have been shown to trans-
 145 fer inorganic C to peridotites where they are in contact (de Obeso & Kelemen, 2018).
 146 C is also stored within the ophiolite, primarily in the form of carbonate minerals (Neal
 147 & Stanger, 1985; P. B. Kelemen & Matter, 2008; P. B. Kelemen et al., 2011; Noël et al.,
 148 2018). Hydration and carbonation of $> 20\,000\text{ km}^3$ of peridotite continue today in the
 149 Samail Ophiolite, largely at $< 60\text{ }^\circ\text{C}$ (Neal & Stanger, 1983, 1985; P. B. Kelemen & Mat-
 150 ter, 2008; P. B. Kelemen et al., 2011; Streit et al., 2012; A. N. Paukert et al., 2012; Chav-
 151 agnac, Ceuleneer, et al., 2013; Chavagnac, Monnin, et al., 2013; Mervine et al., 2014; Falk
 152 et al., 2016; Miller et al., 2016; Vankeuren et al., 2019).

153 3 Methods

154 3.1 Fluid sampling and field measurements

155 Wells were drilled into the Samail Ophiolite by the Ministry of Regional Munic-
 156 ipalities and Water Resources of the Sultanate of Oman prior to 2006 (“WAB” and “NSHQ”
 157 wells in this study) and by the Oman Drilling Project in 2016 through 2018 (“CM”) (Parsons
 158 International & Co., 2005; P. Kelemen et al., 2013). Information on well location, con-
 159 struction, and water level are given in Table 1. In sampling campaigns in 2014 and 2015,
 160 a 12 V submersible Typhoon ® pump (Proactive Env. Products, Bradenton, FL, USA)
 161 with typical flow rates of $5\text{ L}\cdot\text{min}^{-1}$ was used. This pump was used in all years of sam-
 162 pling at well NSHQ04 due to partial obstruction of this well. In all other sampling from
 163 2016 onwards, a larger submersible pump (Grundfos SQ 2-85) with typical flow rates of
 164 $20\text{ L}\cdot\text{min}^{-1}$ was used. The pumping depths are reported in Tables 1 and 2. For fluids sam-
 165 pled in 2018, temperature, conductivity, and pH were measured using a ColeParmer PC100
 166 Meter, while Eh was measured using a Mettler Toledo SG2 SevenGo meter. The ana-
 167 lytical uncertainties for temperature, conductivity, pH, and Eh are $0.5\text{ }^\circ\text{C}$, 1.0% of mea-
 168 sured value, 0.01, and 1 mV, respectively. Each well was pumped for $\geq 20\text{ min}$ prior to
 169 sampling. Sampling commenced once fluid pH and conductivity measurements stabilized.

170 3.2 Chemical and isotopic analyses of fluids

171 To analyze aqueous concentrations (c) of non-carbonaceous chemical species, sam-
 172 ples were collected by passing groundwater through a $0.2\text{ }\mu\text{m}$ filter into polypropylene
 173 conical tubes. Aqueous concentrations of $\sum\text{Na}$, $\sum\text{Ca}$, $\sum\text{Mg}$, $\sum\text{Al}$, $\sum\text{Fe}$, and $\sum\text{Si}$
 174 were measured by inductively coupled plasma (ICP) atomic emission spectroscopy on
 175 a PerkinElmer Optima 5300 (repeatability as median relative standard deviation of 3%).
 176 Aqueous concentrations of Cl^- , Br^- , F^- , and SO_4^{2-} were measured on a Dionex IC25
 177 ion chromatograph with an AS9-HC IonPac column, with the exception of NO_3^- , which
 178 was measured on a Dionex 4500I ion chromatograph with an IonPac AS14 column us-
 179 ing EPA method 300.0 (analytical uncertainty of 2%).

180 The concentration and $\delta^{13}\text{C}$ of dissolved inorganic C ($\sum\text{CO}_2$) were measured by
 181 acidification of water samples and transfer of resultant $\text{CO}_2(\text{g})$ via a Thermo Fisher Gas-
 182 Bench II to a Thermo Delta V Plus isotope ratio mass spectrometer. We optimized the
 183 methods of Assayag et al. (2006) for the wide range of $c_{\sum\text{CO}_2}$ observed in ophiolite ground-
 184 waters. Complete methodological details are available at [http://dx.doi.org/10.17504/](http://dx.doi.org/10.17504/protocols.io.zduf26w)
 185 [protocols.io.zduf26w](http://dx.doi.org/10.17504/protocols.io.zduf26w). Conversion of sample $\delta^{13}\text{C}$ values to the VPDB reference frame

Table 1. Well data and field measurements.

Well	UTM coordinates (WGS-84)		Geologic description	Well depth / [mbgl]	Screen interval / [mbct]	Water level / [mbct]	Pump depth / [mbct]	Conductivity / [$\mu\text{S} \cdot \text{cm}^{-1}$]	Temperature / [$^{\circ}\text{C}$]	pH	E_h / [mV]	f_{O_2} / [bar] ^b
	easting	northing										
WAB103	648 577	2 530 362	Gabbro	101	90 – 98	15	70.	1410	34.9	8.51	167 ^a	$2.99 \cdot 10^{-36}$
WAB188	671 123	2 529 798	Gabbro, near contact with harzburgite	78	34.5 – 51	9.5	50.	1120	35.6	8.16	214 ^a	$2.01 \cdot 10^{-34}$
WAB104	643 099	2 541 124	Harzburgite	120.4	100.8 – 104	40.	85	548	33.7	8.79	133	$1.23 \cdot 10^{-37}$
WAB105	644 678	2 536 524	Harzburgite	120.5	110 – 117	16.5	60.	498	33.7	8.66	162	$2.99 \cdot 10^{-36}$
WAB55	634 777	2 506 101	Harzburgite with abundant carbonate veins, near contact with gabbro	102	8 – 97	7.5 ^a	50. ^a	1183 ^a	36.2 ^a	9.62 ^a	269 ^a	$7.17 \cdot 10^{-25}$
WAB56	634 851	2 501 617	Harzburgite	106	7 – 27	7.62 ^a	30. ^a	930. ^a	35.6 ^a	10.61 ^a	20.2 ^a	$2.81 \cdot 10^{-37}$
NSHQ04	670 971	2 531 699	Harzburgite, near fault with gabbro	304	open > 5.8	4.7	8	3350	33.4	10.51 ^a	-174	$5.14 \cdot 10^{-51}$
WAB71	670 322	2 533 981	Dunite, near fault with harzburgite	136.5	128 – 131	8.3	70.	1970	34.9	11.22	-229	$2.52 \cdot 10^{-51}$
CM2A	636 988	2 534 284	Mostly dunite with occasional gabbro and harzburgite	400.	open > 23.7	13.4	75	2860	33.6	11.32	n.d.	n.d.
NSHQ14	675 495	2 529 716	Harzburgite	304	open > 5.8	9.2	85	2670	36.7	11.39	-253 ^a	$1.19 \cdot 10^{-51}$

Measurements refer to sampling February-March, 2018, unless noted. Well elevations are given in Supporting Information Figure S1. *Abbreviations:* n.d., not determined; mbgl, meters below ground level; mbct, meters below casing top. Casings extend ~ 1 m above ground level.

^aNot determined during 2018 sampling, so most recent prior data is reported (2015 to 2017; Rempfert et al., 2017; Fones et al., 2019).

^bCalculated from temperature, pH, and E_h . Where one or more of these parameters were obtained during different sampling years, f_{O_2} should be considered a representative estimate.

Table 2. Isotopic compositions of CH₄, C₂H₆, and C₃H₈.

Well	Sample year	Pump depth / [mbct]	laboratory	$\delta^{13}\text{C}_{\text{CH}_4}$	$\delta\text{D}_{\text{CH}_4}$	$\Delta^{13}\text{CH}_3\text{D}$	$\Delta^{12}\text{CH}_2\text{D}_2$	$\delta^{13}\text{C}_{\text{C}_2\text{H}_6}$	$\delta^{13}\text{C}_{\text{C}_3\text{H}_8}$
WAB188	2018	50.	CUB	-86.7	n.d.	n.d.	n.d.	n.d.	n.d.
	2017	78	CUB	-60.8	n.d.	n.d.	n.d.	n.d.	n.d.
	2015	20.	LBNL	-71.3	n.d.	n.d.	n.d.	n.d.	n.d.
WAB56	2015	12	LBNL	-83.2	n.d.	n.d.	n.d.	n.d.	n.d.
NSHQ04	2018	8	CUB	4.7	-229	n.d.	n.d.	n.d.	n.d.
			UCLA	4.177	-227.396	0.229 ± 0.288	-24.502 ± 0.944	n.d.	n.d.
	2017	5.8	CUB	6.8	-225	n.d.	n.d.	n.d.	n.d.
			MIT	3.59	-229.67	0.12 ± 0.17	n.d.	n.d.	n.d.
	2015	22	LBNL	0.8	-209	n.d.	n.d.	n.d.	n.d.
			MIT	1.60	-230.00	0.72 ± 0.29	n.d.	n.d.	n.d.
2014	18	LBNL	2.4	-205	n.d.	n.d.	n.d.	n.d.	
WAB71	2018	70.	CUB	3.6	-307	n.d.	n.d.	n.d.	n.d.
	2017	50.	CUB	3.9	-313	n.d.	n.d.	n.d.	n.d.
	2016	50.	LBNL	3.0	n.d.	n.d.	n.d.	n.d.	n.d.
	2015	18	LBNL	2.9	n.d.	n.d.	n.d.	n.d.	n.d.
CM2A	2018	75	CUB	-4.3	-206	n.d.	n.d.	n.d.	n.d.
			MIT	-3.83	-190.32	2.87 ± 0.57	n.d.	n.d.	n.d.
			UCLA	-4.710	-197.73	2.638 ± 0.284	-1.267 ± 0.886	n.d.	n.d.
NSHQ14	2018	85	CUB	-2.3	-314	n.d.	n.d.	n.d.	n.d.
			MIT	-5.02	-311.73	0.77 ± 0.44	n.d.	n.d.	n.d.
			UCLA	-3.352	-293.58	2.074 ± 0.298	-0.204 ± 1.358	n.d.	n.d.
NSHQ14	2017	85	CUB	0.2	-271	n.d.	n.d.	-6.0	+3.3
			MIT	-0.08	-268.82	0.69 ± 0.23	n.d.	n.d.	n.d.
NSHQ14	2016	70.	LBNL	1.8	-273	n.d.	n.d.	n.d.	n.d.
			MIT	-6.89	-308.52	0.69 ± 0.17	n.d.	n.d.	n.d.
NSHQ14	2015	20.	LBNL	3.7	n.d.	n.d.	n.d.	n.d.	n.d.
			2014	260.	LBNL	3.0	-232	n.d.	n.d.

All isotopic values reported in ‰ units. $\delta^{13}\text{C}$ and δD reported in the VPDB and VSMOW reference frames, respectively. Data from 2014 previously reported by Miller et al. (2016). *Abbreviations:* n.d., not determined; mbct, meters below casing top.

186 using measured $\delta^{13}\text{C}$ values of international reference materials (Harding Iceland Spar
187 and LSVEC) were performed using the statistical programming language, R (R Core Team,
188 2019) (Supporting Information Section S1).

189 Water $\delta^{18}\text{O}$ and δD were measured on a Picarro L2120-i cavity ring down spectrom-
190 eter. The instrument analyzed each sample six times, excluding the first three analyses
191 to avoid memory effects. Reported precision is the standard deviation of the last three
192 measurements. Reported accuracy is the mean difference between accepted values and
193 measured values of standards. Mean precision in the run was 0.06 ‰ for $\delta^{18}\text{O}$ and 0.23 ‰
194 for δD ; mean accuracy was 0.04 ‰ for $\delta^{18}\text{O}$ and 0.47 ‰ for δD .

195 Gases dissolved in pumped groundwaters were sampled by injecting water into N₂
196 purged vials for headspace gas analysis using methods described by Miller et al. (2016)
197 in field campaigns occurring from 2014 to 2017. In addition, the bubble strip method
198 (modified from Kampbell et al. (1998) was used from 2016 to 2018. Details on bubble
199 strip gas sampling are available at <http://dx.doi.org/10.17504/protocols.io.2x5gfgq6>.
200 The gas concentrations reported in this study were determined from bubble strip sam-
201 ples. These concentrations were measured on an SRI 8610C gas chromatograph (GC)
202 with N₂ as the carrier gas. H₂, CO, CH₄, and CO₂ were separated with a 2 mm by 1 mm
203 ID micropacked ShinCarbon ST column, whereas alkanes of 2 to 6 C atoms (“C₂–C₆
204 short-chain alkanes”) were separated with a PORAPAK Q 6 ft by 0.085 in ID column.
205 Peak intensities were measured concurrently using a thermal conductivity detector (TCD)
206 and a flame ionization detector (FID) and calibrated with standard gas mixes (Supelco
207 Analytical, Bellefonte, PA, USA; accuracy of $\pm 2\%$ of reported concentration). Measure-

208 ment repeatability expressed as relative standard deviation was 5% over most of the cal-
 209 ibrated range. The limit of quantitation was defined as the signal at which the relative
 210 standard deviation increased to 20%. In 2018, H₂ and CO were analyzed on a Peak Per-
 211 former 1 gas chromatograph equipped with a reducing compound photometer (RCP).
 212 Due to the high sensitivity of the RCP, the signal at limit of quantitation (S_{LQ}) for these
 213 analyses was defined as $S_{LQ} = S_b + 10 \cdot \sigma_b$, where S_{mb} is the mean signal of blanks
 214 prepared in field and σ_b is the population standard deviation of these blanks, in accor-
 215 dance with American Chemical Society guidelines (MacDougall et al., 1980). Gaseous
 216 concentrations were converted to aqueous concentrations using gas solubilities (Sander,
 217 2015) and corrected for temperature and volume changes between sampling and anal-
 218 ysis.

219 Prior to 2017, bulk stable isotope analyses of CH₄ were conducted at the Center
 220 for Isotope Geochemistry at the Lawrence Berkeley National Laboratory (LBNL) by gas
 221 chromatography/combustion/pyrolysis isotope-ratio mass spectrometry (GC/C/Pyr/IRMS)
 222 using methods described by Miller et al. (2016). The measurement repeatability expressed
 223 as 1 sample standard deviation (s) for these analyses is $\pm 0.2\%$ for $\delta^{13}\text{C}$ and $\pm 5\%$ for
 224 δD .

225 From 2017 onwards, bulk stable isotope analyses of CH₄ and co-occurring alkane
 226 gases were conducted at the University of Colorado - Boulder (CUB) by GC/C/Pyr/IRMS
 227 using a Trace 1310 GC equipped with an Agilent J & W GS-CarbonPLOT column (30 m
 228 length, 0.32 mm ID, 3.0 μm film) coupled to a Thermo Scientific MAT253 IRMS. CH₄
 229 isotope standards purchased from Airgas (uncertainties of $\pm 0.3\%$ for $\delta^{13}\text{C}$ and $\pm 5\%$
 230 for δD) were used for calibration. Over the range of peak amplitudes of analyses reported
 231 here, the repeatability expressed as 1 s on analyses of standards is $\pm 0.6\%$ for $\delta^{13}\text{C}$ and
 232 $\pm 7\%$ for δD . The analytical uncertainty (accuracy) expressed as 1 standard error on
 233 a 3-point calibration was $< 0.3\%$ for $\delta^{13}\text{C}$ and $< 9\%$ for δD (Supporting Information
 234 Section S1).

235 The relative abundances of CH₄ isotopologues, including the doubly-substituted
 236 isotopologue, $^{13}\text{CH}_3\text{D}$, were measured at the Massachusetts Institute of Technology (MIT)
 237 by tunable infrared laser direct absorption spectroscopy following the methods described
 238 by Ono et al. (2014). Abundances of CH₄ isotopologues, including both $^{13}\text{CH}_3\text{D}$ and $^{12}\text{CH}_2\text{D}_2$,
 239 were measured at the University of California, Los Angeles (UCLA) by high-mass-resolution
 240 gas-source isotope ratio mass spectrometry following the procedure of E. D. Young et
 241 al. (2016). The abundance of $^{13}\text{CH}_3\text{D}$ relative to a random (stochastic) distribution of
 242 isotopes among the isotopologues in a CH₄ sample is described by its $\Delta^{13}\text{CH}_3\text{D}$ value,
 243 which is defined as: $\Delta^{13}\text{CH}_3\text{D} = \ln Q$, where Q is the reaction quotient of the isotope
 244 exchange reaction:



245 Analogous expressions can be written for doubly-deuterated CH₄, $^{12}\text{CH}_2\text{D}_2$.

246 3.3 16S rRNA gene sequencing and analysis

247 Biomass for DNA extraction was concentrated by pumping 5 L to 20 L of ground-
 248 water through Millipore polycarbonate inline filters (0.45 μm pore diameter, 47 mm fil-
 249 ter diameter). At well NSHQ04, a 0.22 μm pore diameter polyethersulfone Millipore Sterivex
 250 filter was used instead due to the lower-flow pump used at this well (Section 3.1). Fil-
 251 ters were placed in cryovials, transported frozen in liquid N₂, and stored in a -70°C freezer
 252 until extraction. DNA was extracted from one quarter subsamples of each filter using
 253 a Qiagen PowerSoil DNA extraction kit. The V4 hypervariable region of the 16S rRNA
 254 gene was amplified by PCR in duplicate reactions using the 515 (Parada) - 806R (Ap-
 255 prill) primer pair modified to include Illumina adapters and the appropriate error-correcting

256 barcodes. Each 25- μL reaction mixture included 12.5 μL of Promega HotStart Master-
 257 mix, 10.5 μL of PCR-grade water, 1 μL of PCR primers (combined at 10 M), and 1 μL
 258 of purified genomic DNA. PCR consisted of an initial step at 94 °C for 3 min followed
 259 by 35 cycles of 94 °C for 45 s, 50 °C for 1 min, and 72 °C for 1.5 min. PCR concluded with
 260 a final elongation step at 72 °C for 10 min. No-template controls and DNA extraction
 261 controls were subjected to PCR to check for potential contamination in our PCR and
 262 DNA extraction reagents, respectively. Amplification was evaluated via electrophoresis
 263 in a 2 % agar gel. Amplicons from duplicate reactions were pooled, cleaned, and their
 264 concentrations normalized using a Thermo Fisher SequelPrep normalization plate kit.
 265 Amplicons were sequenced on an Illumina MiSeq at the CUB Next-Generation Sequenc-
 266 ing Facility with 2-by-150 bp paired-end chemistry.

267 Sequences were demultiplexed with idemp (<https://github.com/yhwu/idemp>).
 268 The resultant fastq files were quality filtered using Figaro v1.1.1 ([https://github.com/](https://github.com/Zymo-Research/figaro)
 269 [Zymo-Research/figaro](https://github.com/Zymo-Research/figaro)) and the DADA2 v1.16 R package (Callahan et al., 2016). Am-
 270 plicon sequence variants were assigned taxonomy to the genus level using the RDP clas-
 271 sifier (Q. Wang et al., 2007) trained on the Silva SSU 138 reference database (Quast et
 272 al., 2012) using the DADA2 assignTaxonomy function. Species level assignments were
 273 based on exact matching between amplicon sequence variants and sequenced reference
 274 strains using the DADA2 addSpecies function. Sequences assigned to mitochondria, chloro-
 275 plast, and Eukaryota, or not assigned at the domain level (collectively < 1 % of sequences),
 276 were removed. In addition, 16S rRNA gene sequencing data from previous Oman sam-
 277 pling campaigns (2014 through 2017; Miller et al., 2016; Rempfert et al., 2017; Kraus
 278 et al., 2018) were reprocessed in accordance with the methods outlined here to facilitate
 279 comparisons across the data sets (https://github.com/danote/Samail_16S_compilation).
 280 For samples presented in this study, demultiplexed fastq files (without additional pro-
 281 cessing) are accessible on the NCBI Short Read Archive under accession PRJNA655565.

282 4 Results and discussion

283 4.1 Controls on groundwater chemistry

284 To assess the source and reaction histories of Samail Ophiolite groundwaters, we
 285 measured their stable isotopic compositions and solute concentrations. Groundwater δD
 286 and $\delta^{18}\text{O}$ plotted near local and global meteoric water lines (Weyhenmeyer et al., 2002;
 287 Terzer et al., 2013), indicating that the groundwaters derive from rain (Table 3; Support-
 288 ing Information Figure S2; Matter et al., 2006; Miller et al., 2016; Vankeuren et al., 2019).
 289 The sampled groundwaters included oxidized and moderately alkaline $\text{Mg}^{2+} - \text{HCO}_3^-$
 290 waters, typical of reaction with peridotite in communication with the atmosphere, and
 291 reduced and hyperalkaline $\text{Ca}^{2+} - \text{OH}^-$ waters, typical of extensive hydration and ox-
 292 idation of peridotite in closed-system conditions with respect to the atmosphere (Table
 293 3; Barnes et al., 1967; Barnes & O’Neil, 1969; Neal & Stanger, 1985; Bruni et al., 2002;
 294 Cipolli et al., 2004; P. B. Kelemen et al., 2011; A. N. Paukert et al., 2012). $\text{Ca}^{2+} - \text{OH}^-$
 295 waters had higher conductivities (930 $\mu\text{S} \cdot \text{cm}^{-1}$ to 3350 $\mu\text{S} \cdot \text{cm}^{-1}$) than $\text{Mg}^{2+} - \text{HCO}_3^-$
 296 waters (498 $\mu\text{S} \cdot \text{cm}^{-1}$ to 1183 $\mu\text{S} \cdot \text{cm}^{-1}$) (Table 1). The increase in conductivity from
 297 $\text{Mg}^{2+} - \text{HCO}_3^-$ waters to $\text{Ca}^{2+} - \text{OH}^-$ waters is driven by enrichments in Ca^{2+} derived
 298 from dissolution of primary silicate minerals in addition to Na^+ and Cl^- derived from
 299 mineral dissolution, sea spray, and/or leaching of sea salts introduced during subseafloor
 300 alteration and/or ophiolite emplacement (Neal & Stanger, 1985; Stanger, 1986; Murad
 301 & Krishnamurthy, 2004; A. N. Paukert et al., 2012; Rempfert et al., 2017). The increase
 302 in pH from $\text{Mg}^{2+} - \text{HCO}_3^-$ waters (pH 8.66 to 9.62) to $\text{Ca}^{2+} - \text{OH}^-$ waters (10.51 to
 303 11.39) was accompanied by a shift to lower f_{O_2} and Eh ($\sim 10^{-51}$ bar and -174 mV to
 304 -253 mV, respectively, in most $\text{Ca}^{2+} - \text{OH}^-$ waters) (Table 1), indicating reduced con-
 305 ditions in $\text{Ca}^{2+} - \text{OH}^-$ waters.

Table 3. Chemical and isotopic composition of water samples.

Well	δD_{H_2O}	$\delta^{18}O_{H_2O}$	$\sum CO_2$	$\delta^{13}C_{\sum CO_2}$	$\sum Na$	$\sum Ca$	$\sum Mg$	$\sum Fe$	$\sum Si$	NO_3^-	SO_4^{2-}	Cl^-	Br^-
<i>gabbro-hosted groundwaters</i>													
WAB103	-0.5	+0.34	$2.67 \cdot 10^3$	-13.54	$1.18 \cdot 10^3$	$2.58 \cdot 10^2$	$1.87 \cdot 10^3$	7.35	$4.63 \cdot 10^2$	$4.72 \cdot 10^2$	$1.57 \cdot 10^3$	$6.25 \cdot 10^3$	$1.39 \cdot 10^2$
WAB188	-2.1	-0.71	$3.48 \cdot 10^3$	-13.52	$4.06 \cdot 10^3$	$1.41 \cdot 10^3$	$1.82 \cdot 10^3$	$2.90 \cdot 10^1$	$4.77 \cdot 10^2$	$3.21 \cdot 10^2$	$1.41 \cdot 10^3$	$4.22 \cdot 10^3$	$6.78 \cdot 10^1$
<i>Mg²⁺ - HCO₃⁻ groundwaters</i>													
WAB104	-0.5	-0.53	$3.62 \cdot 10^3$	-13.88	$7.53 \cdot 10^2$	$1.96 \cdot 10^2$	$2.30 \cdot 10^3$	3.88	$4.15 \cdot 10^2$	$3.14 \cdot 10^2$	$3.80 \cdot 10^2$	$7.76 \cdot 10^2$	3.55
WAB105	+0.4	+0.50	$3.32 \cdot 10^3$	-10.88	$1.18 \cdot 10^3$	$2.58 \cdot 10^2$	$1.87 \cdot 10^3$	4.83	$2.83 \cdot 10^2$	$3.02 \cdot 10^2$	$2.92 \cdot 10^2$	$8.54 \cdot 10^2$	8.60
WAB55	+2.2	+0.26	$2.40 \cdot 10^3$	-12.63	$4.44 \cdot 10^3$	$5.06 \cdot 10^1$	$3.34 \cdot 10^3$	2.52	$3.58 \cdot 10^1$	$3.02 \cdot 10^2$	$8.03 \cdot 10^2$	$6.54 \cdot 10^3$	$1.12 \cdot 10^2$
<i>Ca²⁺ - OH⁻ groundwaters</i>													
WAB56	n.d.	n.d.	$1.3 \cdot 10^{2a}$	n.d.	$3.56 \cdot 10^{3a}$	$5.43 \cdot 10^{2a}$	1.00^a	n.d.	$2.22 \cdot 10^2$	3.00^a	6.00^b	$1.33 \cdot 10^{1a}$	$1.79 \cdot 10^{-1a}$
NSHQ04	-15 ^a	-3.0 ^a	$1.8 \cdot 10^1$	-29.7	$1.04 \cdot 10^{4a}$	$7.79 \cdot 10^{3a}$	$1.80 \cdot 10^{1a}$	$8.20 \cdot 10^{-1a}$	$3.60 \cdot 10^{1a}$	3.00^a	$6.83 \cdot 10^{2a}$	$1.82 \cdot 10^{4a}$	1.25^a
WAB71	-3.0	-0.40	$< 1.2 \cdot 10^1$	n.d.	$6.25 \cdot 10^3$	$4.14 \cdot 10^3$	$< 2.06 \cdot 10^{-1}$	$8.48 \cdot 10^1$	$2.35 \cdot 10^1$	$1.84 \cdot 10^2$	$6.08 \cdot 10^1$	$1.17 \cdot 10^4$	$1.50 \cdot 10^2$
CM2A	+1.7	+0.67	$< 1.2 \cdot 10^1$	n.d.	$2.07 \cdot 10^4$	$1.75 \cdot 10^3$	9.49	$4.03 \cdot 10^1$	$2.81 \cdot 10^1$	$1.64 \cdot 10^2$	$5.56 \cdot 10^2$	$1.85 \cdot 10^4$	$2.48 \cdot 10^2$
NSHQ14	+0.2	+0.43	$< 1.2 \cdot 10^1$	n.d.	$1.03 \cdot 10^4$	$3.60 \cdot 10^3$	6.23	$8.48 \cdot 10^1$	$1.03 \cdot 10^1$	$3.60 \cdot 10^2$	$1.57 \cdot 10^2$	$1.36 \cdot 10^4$	$1.67 \cdot 10^2$

Concentrations reported in $\mu\text{mol} \cdot \text{L}^{-1}$. \sum indicates the sum of all dissolved species of the element. All δ values reported in ‰ units. $\delta^{18}O$ and δD reported relative to VSMOW. $\delta^{13}C$ reported relative to VPDB. Samples obtained in February–March 2018, unless noted. *Abbreviations*: n.d., not determined.

^aNot determined during 2018 sampling, so most recent prior data is reported (2015 to 2017; Rempfert et al., 2017; Fones et al., 2019).

Concentrations of $\sum \text{CO}_2$ were relatively high in $\text{Mg}^{2+}-\text{HCO}_3^-$ waters and gabbro waters (up to $3490 \mu\text{mol} \cdot \text{L}^{-1}$), but below the limit of quantitation ($< 12 \mu\text{mol} \cdot \text{L}^{-1}$) in most $\text{Ca}^{2+}-\text{OH}^-$ waters (Table 3). This is consistent with water-harzburgite reaction path modeling that terminates at chrysotile-brucite-diopside-calcite equilibrium, corresponding to a $c_{\sum \text{CO}_2}$ of $8 \mu\text{mol} \cdot \text{L}^{-1}$ at 25°C and 1 bar (Leong & Shock, 2020). Literature values for $c_{\sum \text{CO}_2}$ in ophiolitic $\text{Ca}^{2+}-\text{OH}^-$ waters are often higher than those predicted by reaction path modeling, but the lower range of reported values approaches $1 \mu\text{mol} \cdot \text{L}^{-1}$ (Barnes et al., 1967; Barnes & O’Neil, 1969; Barnes et al., 1978; Neal & Stanger, 1985; Bruni et al., 2002; Cipolli et al., 2004; A. N. Paukert et al., 2012; Falk et al., 2016; Brazelton et al., 2017; Canovas III et al., 2017; Crespo-Medina et al., 2017; Rempfert et al., 2017; Fones et al., 2019; Vankeuren et al., 2019). This spread in the data could reflect groundwater mixing, atmospheric contamination during sampling, differences in reaction temperature and progress, and/or kinetic inhibitions to carbonate mineral precipitation. In $\text{Mg}^{2+}-\text{HCO}_3^-$ waters and waters from gabbroic aquifers, $\delta^{13}\text{C}_{\sum \text{CO}_2}$ ranged from -13.54‰ VPDB to -10.88‰ VPDB (Table 3), which is comparable to $\delta^{13}\text{C}_{\sum \text{CO}_2}$ of $\text{Mg}^{2+}-\text{HCO}_3^-$ waters elsewhere in the ophiolite (-15.56‰ VPDB to -13.60‰ VPDB; Matter et al., 2006).

Variable concentrations of H_2 and CH_4 across wells suggest spatial heterogeneities in sources and sinks of these gases in the ophiolite. In some $\text{Ca}^{2+}-\text{OH}^-$ waters, c_{H_2} was high (up to $253 \mu\text{mol} \cdot \text{L}^{-1}$), but c_{H_2} was below limits of quantitation in other $\text{Ca}^{2+}-\text{OH}^-$ waters (Figure 2; Table 4). In $\text{Mg}^{2+}-\text{HCO}_3^-$ waters and waters from gabbroic aquifers, c_{H_2} was generally below limits of quantitation. However, up to $0.992 \mu\text{mol} \cdot \text{L}^{-1}$ H_2 was measured in well WAB188, which is in gabbro near a faulted contact with peridotites that contain $\text{Ca}^{2+}-\text{OH}^-$ waters (Figure 1; Table 1). This suggests production of H_2 within the gabbro host rock or migration of H_2 from peridotites into gabbros surrounding WAB188. In most $\text{Ca}^{2+}-\text{OH}^-$ waters, c_{CH_4} was high (up to $483 \mu\text{mol} \cdot \text{L}^{-1}$; Figure 2, Table 4). However, wells with high c_{CH_4} did not always have high c_{H_2} (Figure 2; Table 4). In $\text{Mg}^{2+}-\text{HCO}_3^-$ waters and gabbro waters, c_{CH_4} was typically lower ($\leq 0.1 \mu\text{mol} \cdot \text{L}^{-1}$), although c_{CH_4} reached $1.83 \mu\text{mol} \cdot \text{L}^{-1}$ in well WAB188, where c_{H_2} was also quantifiable.

4.2 Origin of CH_4 and co-occurring short-chain alkanes in the Samail Ophiolite

In this study, we focus our discussion on fluid and particulate samples from a subset of wells (NSHQ14, NSHQ04, and WAB188) that yielded particularly rich datasets from which we infer key CH_4 cycle processes that likely occur widely in the Samail Ophiolite. We discuss three additional wells (WAB71, WAB56, and CM2A) in Supporting Information Text S1, which illustrate that the processes outlined below are broadly applicable throughout the study area, although nuanced differences in CH_4 dynamics do occur depending on local hydrogeologic factors.

4.2.1 Abiotic, ^{13}C -enriched CH_4 , C_2H_6 , and C_3H_8 mixed with microbial CH_4 produced under C -limited conditions in the $\text{Ca}^{2+}-\text{OH}^-$ waters of well NSHQ14

Well NSHQ14 is situated in a catchment dominated by partially serpentinized harzburgite with meter-scale partially serpentinized dunite bands (Figure 1; Supporting Information Figure S1; Table 1). The well is cased to 5.8 meters below ground level (mbgl) and drilled to 304 mbgl (Table 1). Geophysical logs of NSHQ14 (A. Paukert, 2014; Matter et al., 2018) indicate the presence of moderately fresh water ($1500 \mu\text{S} \cdot \text{cm}^{-1}$) near the water table at 10 mbgl trending to more saline water ($3500 \mu\text{S} \cdot \text{cm}^{-1}$) at 30 mbgl and more gradual, continued increase in conductivity towards the bottom of the well. The pH increases from 10.36 to 11.26, while f_{O_2} decreases from 10^{-30} bar to 10^{-74} bar

Table 4. Aqueous gas concentrations, reported in $\mu\text{mol} \cdot \text{L}^{-1}$.

Well	Sample year	H ₂	CO	CH ₄	C ₂ H ₆	C ₃ H ₈	<i>i</i> -C ₄ H ₁₀	<i>n</i> -C ₄ H ₁₀	<i>i</i> -C ₅ H ₁₂	<i>n</i> -C ₅ H ₁₂	C ₆ H ₁₄ ^a
WAB103	2018	$< 5.98 \cdot 10^{-1}$	$< 1.32 \cdot 10^{-1}$	$1.45 \cdot 10^{-1}$	$< 9.88 \cdot 10^{-4}$	$< 7.60 \cdot 10^{-4}$	$< 4.61 \cdot 10^{-4}$	$6.05 \cdot 10^{-3}$	$< 3.43 \cdot 10^{-4}$	$8.73 \cdot 10^{-4}$	$< 2.81 \cdot 10^{-4}$
WAB188	2018	$< 5.98 \cdot 10^{-1}$	$< 1.32 \cdot 10^{-1}$	$9.17 \cdot 10^{-1}$	$< 9.88 \cdot 10^{-4}$	$< 7.60 \cdot 10^{-4}$	$< 4.61 \cdot 10^{-4}$	$< 5.78 \cdot 10^{-4}$	$< 3.43 \cdot 10^{-4}$	$< 3.81 \cdot 10^{-4}$	$< 2.81 \cdot 10^{-4}$
	2017	$9.92 \cdot 10^{-1}$	$< 2.79 \cdot 10^{-1}$	1.83	$< 1.01 \cdot 10^{-3}$	$< 7.79 \cdot 10^{-4}$	$< 4.72 \cdot 10^{-4}$	$< 6.01 \cdot 10^{-4}$	$< 3.50 \cdot 10^{-4}$	$< 3.91 \cdot 10^{-4}$	$< 2.88 \cdot 10^{-4}$
WAB104	2018	$< 5.98 \cdot 10^{-1}$	$< 1.32 \cdot 10^{-1}$	$< 1.53 \cdot 10^{-2}$	$< 9.88 \cdot 10^{-4}$	$< 7.60 \cdot 10^{-4}$	$4.82 \cdot 10^{-4}$	$< 5.78 \cdot 10^{-4}$	$7.56 \cdot 10^{-4}$	$< 3.81 \cdot 10^{-4}$	$< 2.81 \cdot 10^{-4}$
	2017	$< 4.80 \cdot 10^{-2}$	$< 2.79 \cdot 10^{-1}$	$2.30 \cdot 10^{-2}$	$< 1.01 \cdot 10^{-3}$	$< 7.79 \cdot 10^{-4}$	$< 4.72 \cdot 10^{-4}$	$< 6.01 \cdot 10^{-4}$	$< 3.50 \cdot 10^{-4}$	$< 3.91 \cdot 10^{-4}$	$< 2.88 \cdot 10^{-4}$
WAB105	2018	$< 5.98 \cdot 10^{-1}$	$< 1.32 \cdot 10^{-1}$	$< 1.53 \cdot 10^{-2}$	$< 9.88 \cdot 10^{-4}$	$< 7.60 \cdot 10^{-4}$	$3.70 \cdot 10^{-2}$	$< 5.78 \cdot 10^{-4}$	$< 3.43 \cdot 10^{-4}$	$< 3.81 \cdot 10^{-4}$	$< 2.81 \cdot 10^{-4}$
	2017	$< 4.80 \cdot 10^{-2}$	$< 2.79 \cdot 10^{-1}$	$2.01 \cdot 10^{-2}$	$< 1.01 \cdot 10^{-3}$	$< 7.79 \cdot 10^{-4}$	$< 4.72 \cdot 10^{-4}$	$< 6.01 \cdot 10^{-4}$	$< 3.50 \cdot 10^{-4}$	$< 3.91 \cdot 10^{-4}$	$< 2.88 \cdot 10^{-4}$
WAB55	2018	$< 5.98 \cdot 10^{-1}$	$< 1.32 \cdot 10^{-1}$	$1.15 \cdot 10^{-1}$	$1.55 \cdot 10^{-3}$	$< 7.60 \cdot 10^{-4}$	$2.25 \cdot 10^{-3}$	$7.91 \cdot 10^{-4}$	$1.60 \cdot 10^{-3}$	$< 3.81 \cdot 10^{-4}$	$5.52 \cdot 10^{-3}$
	2017	$< 4.80 \cdot 10^{-2}$	$< 2.79 \cdot 10^{-1}$	$1.06 \cdot 10^{-1}$	$< 1.01 \cdot 10^{-3}$	$< 7.79 \cdot 10^{-4}$	$< 4.72 \cdot 10^{-4}$	$< 6.01 \cdot 10^{-4}$	$< 3.50 \cdot 10^{-4}$	$< 3.91 \cdot 10^{-4}$	$< 2.88 \cdot 10^{-4}$
WAB56	2017	$2.40 \cdot 10^{-1}$	$< 2.79 \cdot 10^{-1}$	$1.60 \cdot 10^{-1}$	$< 1.01 \cdot 10^{-3}$	$< 7.79 \cdot 10^{-4}$	$< 4.72 \cdot 10^{-4}$	$< 6.01 \cdot 10^{-4}$	$< 3.50 \cdot 10^{-4}$	$< 3.91 \cdot 10^{-4}$	$< 2.88 \cdot 10^{-4}$
	2018	$< 5.98 \cdot 10^{-1}$	$< 1.32 \cdot 10^{-1}$	$1.44 \cdot 10^2$	$2.45 \cdot 10^{-2}$	$2.22 \cdot 10^{-3}$	$< 4.61 \cdot 10^{-4}$	$< 5.78 \cdot 10^{-4}$	$< 3.43 \cdot 10^{-4}$	$< 3.81 \cdot 10^{-4}$	$< 2.81 \cdot 10^{-4}$
NSHQ04	2017	$< 4.80 \cdot 10^{-2}$	$< 2.79 \cdot 10^{-1}$	$4.83 \cdot 10^2$	$< 1.01 \cdot 10^{-3}$ b	$1.03 \cdot 10^{-3}$	$< 4.72 \cdot 10^{-4}$	$< 6.01 \cdot 10^{-4}$	$< 3.50 \cdot 10^{-4}$	$< 3.91 \cdot 10^{-4}$	$< 2.88 \cdot 10^{-4}$
	2018	$< 5.98 \cdot 10^{-1}$	$< 1.32 \cdot 10^{-1}$	7.76	$1.00 \cdot 10^{-3}$	$< 7.60 \cdot 10^{-4}$	$< 4.61 \cdot 10^{-4}$	$< 5.78 \cdot 10^{-4}$	$< 3.43 \cdot 10^{-4}$	$< 3.81 \cdot 10^{-4}$	$< 2.81 \cdot 10^{-4}$
WAB71	2017	$5.92 \cdot 10^{-1}$	$< 2.79 \cdot 10^{-1}$	$1.48 \cdot 10^1$	$< 1.01 \cdot 10^{-3}$	$< 7.79 \cdot 10^{-4}$	$< 4.72 \cdot 10^{-4}$	$1.94 \cdot 10^{-2}$	$< 3.50 \cdot 10^{-4}$	$4.79 \cdot 10^{-4}$	$< 2.88 \cdot 10^{-4}$
	2018	3.38	$< 1.32 \cdot 10^{-1}$	$1.52 \cdot 10^2$	$4.11 \cdot 10^{-2}$	$1.75 \cdot 10^{-3}$	$< 4.61 \cdot 10^{-4}$	$6.48 \cdot 10^{-3}$	$< 3.43 \cdot 10^{-4}$	$< 3.81 \cdot 10^{-4}$	$< 2.81 \cdot 10^{-4}$
NSHQ14	2018	$1.31 \cdot 10^2$	$< 1.32 \cdot 10^{-1}$	$7.12 \cdot 10^1$	$7.32 \cdot 10^{-2}$	$7.64 \cdot 10^{-3}$	$2.26 \cdot 10^{-3}$	$2.88 \cdot 10^{-3}$	$1.27 \cdot 10^{-3}$	$2.23 \cdot 10^{-3}$	$1.12 \cdot 10^{-3}$
	2017	$2.53 \cdot 10^2$	$< 2.79 \cdot 10^{-1}$	$1.06 \cdot 10^2$	$7.98 \cdot 10^{-2}$	$9.00 \cdot 10^{-3}$	$1.53 \cdot 10^{-3}$	$4.77 \cdot 10^{-3}$	$< 3.50 \cdot 10^{-4}$	$< 3.91 \cdot 10^{-4}$	$9.70 \cdot 10^{-4}$

^aHexane isomers not chromatographically resolved.^bHigh C₁/(C₂ + C₃) at NSHQ04 resulted in CH₄ tailing into and preventing quantitation of the C₂H₆ peak in 2017. Chromatographic improvements were made between analyses of 2017 and 2018 samples.

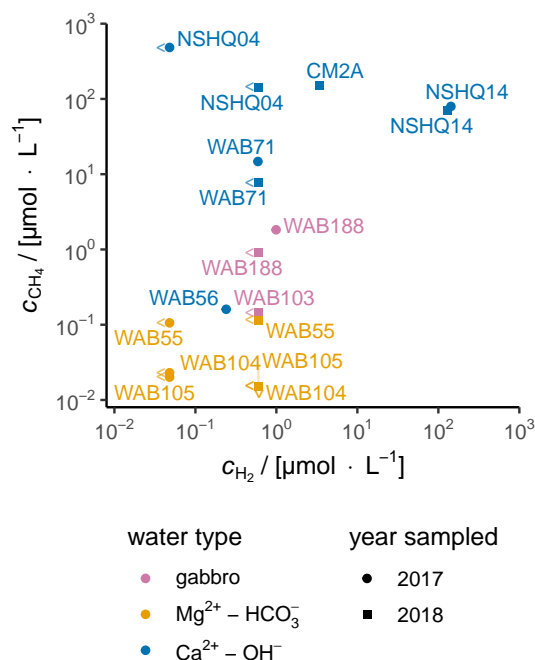
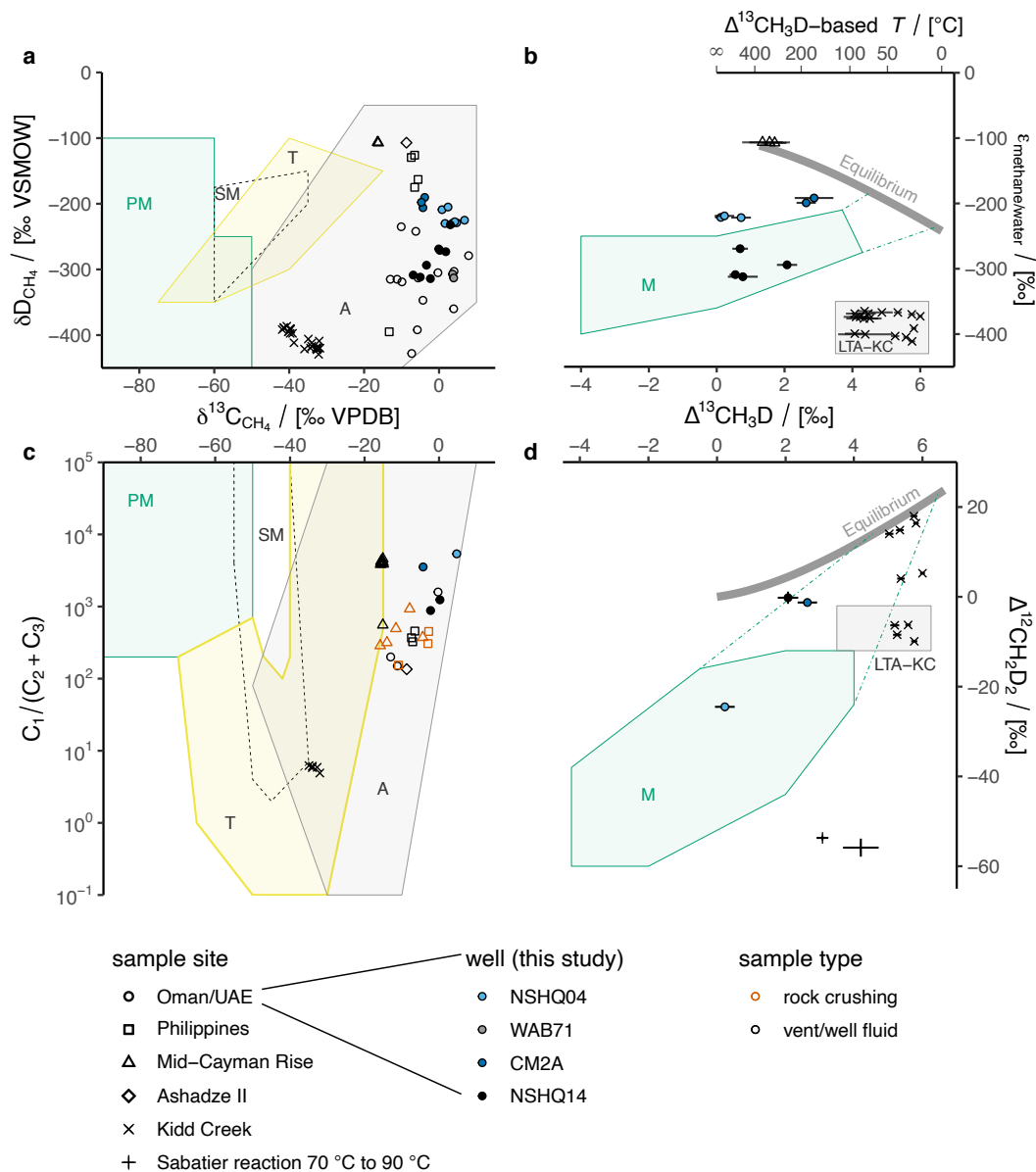


Figure 2. Aqueous concentrations of CH₄ and H₂ in Oman groundwater samples from 2017 and 2018. Left and down carrots denote “below limit of quantitation” for CH₄ and H₂, respectively, with the adjacent point plotted at the limit of quantitation for that gas and year of analysis.

356 and Eh decreases from 142 mV to -582 mV from 10 mbgl to 30 mbgl, and hyperalkaline
 357 and reduced conditions persist to the bottom of the well. These trends suggest that the
 358 upper 20 m of the water column contain a mixture of atmosphere-influenced water and
 359 deep water that has extensively reacted with peridotite in isolation from the atmosphere.
 360 The high extents of reaction experienced by deep fluids sampled from NSHQ14 are ad-
 361 ditionally reflected in their c_{H_2} , which was the highest among the studied wells ($253 \mu\text{mol} \cdot$
 362 L^{-1} and $131 \mu\text{mol} \cdot \text{L}^{-1}$ in 2017 and 2018, respectively; Table 4; Figure 2). NSHQ14 wa-
 363 ters also had high c_{CH_4} ($106 \mu\text{mol} \cdot \text{L}^{-1}$ and $71.2 \mu\text{mol} \cdot \text{L}^{-1}$ in 2017 and 2018, respec-
 364 tively).

365 CH₄ has ranged in $\delta^{13}\text{C}$ from -6.89 ‰ VPDB to $+3.7$ ‰ VPDB in fluid samples
 366 from NSHQ14, with a mean weighted by sample year of -0.8 ‰ VPDB (Figure 3a; Ta-
 367 ble 2). These $\delta^{13}\text{C}$ values are generally higher than those of CH₄ emanating from sediment-
 368 poor seafloor hydrothermal vents, where a dominantly abiogenic origin has been proposed
 369 ((Welhan & Craig, 1983; Merlivat et al., 1987; J. L. Charlou et al., 1996; J. Charlou et
 370 al., 2000, 2002; Proskurowski et al., 2008; Kumagai et al., 2008; McDermott et al., 2015;
 371 D. T. Wang et al., 2018); represented by Mid-Cayman Rise and Ashadze II in Figure 3a),
 372 higher than typical mantle values (Deines, 2002), and similar to marine carbonate (Schidlowski,
 373 2001). CH₄ $\delta^{13}\text{C}$ at NSHQ14 is generally higher than $\delta^{13}\text{C}$ of carbonate veins in NSHQ14
 374 (-7.05 ‰ VPDB to -4.69 ‰ VPDB; Miller et al., 2016), which is opposite to that which
 375 would be expected at equilibrium (Bottinga, 1969), indicating that CH₄ is not in isotopic
 376 equilibrium with co-existing carbonate minerals.

377 CH₄ is accompanied by C₂–C₆ alkanes in fluids from NSHQ14 (Table 4). These
 378 alkanes had $C_1/(C_2 + C_3)$ ratios of 1240 in 2017 and 881 in 2018, which are similar to
 379 fluid samples and rock crushings from other ophiolites and sediment-poor seafloor hy-



380 drothermal vents (Abrajano et al., 1990; J. L. Charlou et al., 2010; McDermott et al.,
 381 2015; Grozeva et al., 2020), but 10^2 times higher than those of Kidd Creek mine, Canada,
 382 for which a low-temperature, abiotic origin of alkanes has been proposed (Sherwood Lollar
 383 et al., 2002, 2008; E. Young et al., 2017) (Figure 3c). Thus, $C_1 / (C_2 + C_3)$ ratios could
 384 reflect differences in alkane formation mechanisms or extents of reaction in Precambrian
 385 shield sites like Kidd Creek versus ophiolites and sediment-poor seafloor hydrothermal
 386 vents.

387 C_2H_6 and C_3H_8 at NSHQ14 are strongly ^{13}C -enriched ($\delta^{13}C$ of $-6.0‰$ VPDB and
 388 $+3.3‰$ VPDB, respectively; Table 2; Figure 4). The observed $\delta^{13}C$ values are $\sim 15‰$
 389 higher than those in the most mature (and therefore most ^{13}C -enriched) thermogenic
 390 C_2H_6 and C_3H_8 samples from confined systems (Milkov & Etiope, 2018; Fiebig et al.,
 391 2019). Increases in $\delta^{13}C_{C_3}$ of $\sim 15‰$ have been attributed to microbial oxidation of short-
 392 chain alkanes, which enriches the residual in ^{13}C (Martini et al., 2003). However, short-
 393 chain alkane oxidizing microbial species (Shennan, 2006; Singh et al., 2017; Laso-Pérez

Figure 3. Molecular and isotopic compositions of natural gases. (a) Plot of δD_{CH_4} vs. $\delta^{13}C_{CH_4}$. Shaded fields of typical gas origin after Milkov and Etiope (2018). *Abbreviations:* PM, primary microbial; SM, secondary microbial; T, thermogenic; A, abiotic. (c) Plot of ratio of methane (C_1) to the sum of ethane (C_2) and propane (C_3) vs. $\delta^{13}C_{CH_4}$. Only analyses for which C_2 was above limit of quantitation are plotted. If C_3 was below limit of quantitation, its contribution to $C_1/(C_2 + C_3)$ was assumed to be negligible, and therefore C_1/C_2 is plotted. Fields and abbreviations same as in (a). In (a) and (c), uncertainties are smaller than plotted symbols. (b) Plot of $\epsilon_{methane/water}$ vs. $\Delta^{13}CH_3D$. X and Y axes are swapped with respect to original publication of this type of plot (D. T. Wang et al., 2015) so that (b) is comparable against (d). The data from (b) are plotted in the D. T. Wang et al. (2015) orientation in Supporting Information Figure S4. Equilibrium line from Horibe and Craig (1995) and E. Young et al. (2017). *Abbreviations:* LTA-KC, low-temperature abiotic (Kidd Creek-type); M, microbial. Green dot-dashed lines in (b) and (d) indicate a range of CH_4 isotopic compositions that have been attributed to either low cell-specific rates of methanogenesis or anaerobic oxidation of methane; that is, they start at isotopic compositions produced by methanogen cultures and end at isotopic equilibrium between 5 °C and 70 °C, which is the range of temperatures over which anaerobic oxidation of methane has been documented (D. T. Wang et al., 2015; Stolper et al., 2015; E. Young et al., 2017; Ash & Egger, 2019; Giunta et al., 2019). (d) Plot of $\Delta^{13}CH_3D$ vs. $\Delta^{12}CH_2D_2$, after E. Young et al. (2017). Fields, abbreviations, and temperature axis same as in (b). In (b) and (d), error bars represent 95 % confidence interval for analyses performed at MIT, and 1 standard error for analyses performed at UCLA. Contextual data from ophiolites: Oman/UAE (Fritz et al., 1992; Etiope et al., 2015; Boulart et al., 2013; Miller et al., 2016; Vacquand et al., 2018), the Philippines (Abrajano et al., 1990; Grozeva et al., 2020); sediment-poor seafloor hydrothermal vents: Mid-Cayman Rise (McDermott et al., 2015; D. T. Wang et al., 2018; Grozeva et al., 2020), Ashadze II (J. L. Charlou et al., 2010); Precambrian Shield: Kidd Creek, Canada (Sherwood Lollar et al., 2008; E. Young et al., 2017); and laboratory Sabatier reaction catalyzed by Ru (E. Young et al., 2017).

394 et al., 2019) were not detected in 16S rRNA gene sequences of DNA obtained from NSHQ14.
 395 Thus, there is not strong evidence to suggest that $\delta^{13}C_{C_2}$ and $\delta^{13}C_{C_3}$ at NSHQ14 re-
 396 sult from post-genetic microbial alteration. Rather, $\delta^{13}C_{C_2}$ and $\delta^{13}C_{C_3}$ should reflect
 397 formation conditions and C source(s).

398 C_2H_6 and C_3H_8 at NSHQ14 are not likely to derive from nearby organic matter.
 399 Hydrocarbon-rich sedimentary formations in northern Oman not only lack a clear struc-
 400 tural connection to the ophiolite aquifer, but also yield oils with $\delta^{13}C$ values (Terken,
 401 1999) at least 20 ‰ lower than those of C_2H_6 and C_3H_8 at NSHQ14. Furthermore, to-
 402 tal organic C in peridotites exposed to alteration at the seafloor, a proxy for organic C
 403 endogenous to the Samail Ophiolite, is also relatively ^{13}C -depleted (approximately $-25 \pm$
 404 5 ‰ VPDB ; Alt et al., 2013; Alt, Garrido, et al., 2012; Alt, Shanks, et al., 2012; Dela-
 405 cour et al., 2008). Closed-system thermal cracking of these organic matter sources is un-
 406 likely to have produced the comparatively ^{13}C -enriched C_2H_6 and C_3H_8 at NSHQ14 and
 407 previously reported elsewhere in the ophiolite (Figure 4; Fritz et al., 1992).

408 Thermal cracking of organic matter and open-system degassing can enrich late-produced
 409 short-chain alkanes in ^{13}C due to kinetic isotope effects associated with the cleavage of
 410 precursor sites in the parent organic matter and the resultant Rayleigh distillation of these
 411 sites (Fiebig et al., 2019). However, this process has only been shown to occur in hydrother-
 412 mal settings where reservoir temperatures are 200 °C to 450 °C (Fiebig et al., 2019), which

are higher than temperatures along groundwater flow paths intersecting the wells in this study. Measured groundwater temperatures in the study area are $\sim 35^\circ\text{C}$ (Table 1), and $\text{H}_2 - \text{H}_2\text{O}$ isotope thermometry and $\text{C} - \text{O}$ clumped isotope thermometry on carbonate veins with significant ^{14}C contents in Samail Ophiolite peridotites both indicate equilibrium $\leq 60^\circ\text{C}$ (P. B. Kelemen & Matter, 2008; P. B. Kelemen et al., 2011; Mervine et al., 2014; Miller et al., 2016). At these low temperatures within the active alteration zone of the Samail Ophiolite, thermal cracking of organic matter is unlikely to proceed at sufficient rates to attain the high extents of reaction progress necessary to explain the observed ^{13}C enrichments in short-chain alkanes at NSHQ14 over relevant timescales.

Alternatively, short-chain alkanes in NSHQ14 fluids may have an abiotic source. Several studies have demonstrated storage of large quantities of CH_4 and associated short-chain alkanes in fluid inclusions in ophiolites (Sachan et al., 2007; Klein et al., 2019; Grozeva et al., 2020). However, the findings of these studies disagree with those of Etiope et al. (2018), who measured relatively low concentrations of CH_4 stored in serpentinized peridotites from Greek ophiolites. Since the rocks analyzed by Etiope et al. (2018) were sampled from outcrops, it is possible that chemical or physical processes associated with surface exposure may have resulted in loss of CH_4 once stored in peridotite-hosted fluid inclusions prior to analysis. Although further study of the quantity and spatial distribution of CH_4 storage in ophiolitic rocks is warranted, the presence of $\text{CH}_4 + \text{H}_2$ inclusions in olivine and $\text{CH}_4 \pm \text{graphite}$ inclusions in orthopyroxene in Samail Ophiolite harzburgites (Miura et al., 2011) requires that fluid inclusions be considered as a potential source for abiotic CH_4 and associated short-chain alkanes at NSHQ14 and elsewhere in the ophiolite.

A fluid inclusion source of CH_4 and short-chain alkanes is compatible with C stable isotopic compositions of these compounds in groundwaters pumped from NSHQ14. CH_4 , C_2H_6 , and C_3H_8 $\delta^{13}\text{C}$ values at NSHQ14 (-6.89‰ VPDB to $+3.7\text{‰}$ VPDB; Table 2) overlap with CH_4 and C_2H_6 $\delta^{13}\text{C}$ values measured by Grozeva et al. (2020) in rock crushing experiments on CH_4 -rich fluid inclusion-bearing peridotites and dunites sampled from the Zambales ophiolite in the Philippines (-12.4‰ VPDB to -0.9‰ VPDB; Figure 4), which, in turn, overlap with $\delta^{13}\text{C}$ values of CH_4 from nearby gas seeps at Los Fuegos Eternos and Nagsasa in the Philippines (-7.4‰ VPDB to -5.6‰ VPDB; Figure 3a; Abrajano et al., 1990; Vacquand et al., 2018). Grozeva et al. (2020) also crushed CH_4 -rich fluid inclusion-bearing rocks from the Mid-Cayman Rise. Of the Mid-Cayman Rise samples that yielded sufficient CH_4 and C_2H_6 for precise C isotopic analysis, which were all mafic intrusive rocks, $\delta^{13}\text{C}$ values ranged from -14.0‰ VPDB to $+0.7\text{‰}$ VPDB. The lower end of Mid-Cayman Rise rock crushing short-chain alkane $\delta^{13}\text{C}$ values are similar to those measured in Mid-Cayman Rise hydrothermal vent fluids (-15.8‰ VPDB to -9.7‰ VPDB; (McDermott et al., 2015)), whereas the higher end are similar to those of NSHQ14 (Figure 4). Furthermore, C_2H_6 and C_3H_8 $\delta^{13}\text{C}$ values of NSHQ14 fluids resemble those of fluids discharging from the sediment-poor hydrothermal vents at Ashadze II, Mid-Atlantic Ridge (Figure 4; J. L. Charlou et al., 2010). The similarities in short-chain alkane $\delta^{13}\text{C}$ values between circulating fluids and rock-hosted fluid inclusions in ophiolites and present-day oceanic lithospheric sites suggest that circulating fluids in both environments derive much of their CH_4 and short-chain alkanes from fluid inclusions.

Sources of CH_4 can also be assessed by measuring H isotopic compositions and clumped isotopologue relative abundances of CH_4 and comparing these isotopic compositions to temperature-dependent equilibria. $\text{CH}_4 - \text{H}_2\text{O}$ H isotopic equilibrium and intra- CH_4 isotopologue equilibrium are related because the dominant mechanism through which intra- CH_4 equilibrium is approached in nature is typically not direct reaction among CH_4 isotopologues (e.g. Equation 1), but rather isotopic exchange reactions involving co-existing compounds like H_2O and H_2 (D. T. Wang et al., 2018). These isotopic equilibria are represented by thick gray lines in Figure 3b and d. Intra- CH_4 equilibrium is governed by the increasing relative stability of bonds between two heavy isotopes (more “clumping”)

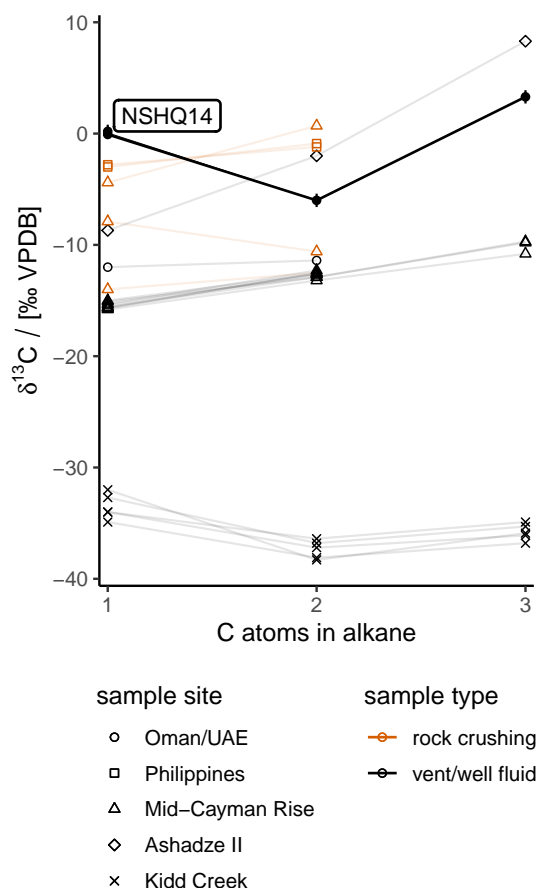


Figure 4. Plot of $\delta^{13}\text{C}$ of CH_4 and co-occurring n -alkanes vs. the number of C atoms per molecule. Error bars represent uncertainties on $\delta^{13}\text{C}$ analyses performed at CUB. Only samples for which $\delta^{13}\text{C}_{\text{C}_2}$ was determined are plotted. Contextual data from ophiolites: Oman/UAE (Fritz et al., 1992), the Philippines (Grozeva et al., 2020); sediment-poor seafloor hydrothermal vents: Mid-Cayman Rise (McDermott et al., 2015; Grozeva et al., 2020), Ashadze II (J. L. Charlou et al., 2010); and Precambrian Shield: Kidd Creek, Canada (Sherwood Lollar et al., 2008).

466 at lower temperatures, which is reflected in higher $\Delta^{13}\text{CH}_3\text{D}$ and $\Delta^{12}\text{CH}_2\text{D}_2$ values. How-
 467 ever, isotopic equilibrium will only be expressed in a sample if kinetics allow it. This is
 468 not always the case because H isotope half-exchange timescales in the CH_4 – H_2O sys-
 469 tem increase from 10 y at 300 °C to 10⁶ y at 200 °C to 10¹² y (extrapolated) at 100 °C
 470 (Koepp, 1978; Reeves et al., 2012). Furthermore, D. T. Wang et al. (2018) showed that
 471 CH_4 - and H_2 - rich gas samples from sediment-poor seafloor hydrothermal vents whose
 472 effluent fluid temperature ranged from 96 °C to 370 °C yielded apparent CH_4 – H_2O H
 473 isotopic and $\Delta^{13}\text{CH}_3\text{D}$ equilibrium temperatures of 270 °C to 360 °C, suggesting a clo-
 474 sure temperature of 270 °C for H isotope exchange in the CH_4 – H_2O and CH_4 – H_2
 475 systems in seafloor hydrothermal settings (e.g. Mid-Cayman Rise in Figure 3b). Thus,
 476 if CH_4 at NSHQ14 were formed exclusively within fluid inclusions and was subsequently
 477 stored at relatively low temperatures (< 200 °C) without subsequent alteration or mix-
 478 ing with CH_4 of other sources, then this CH_4 would be expected to exhibit H isotopic
 479 equilibrium with SMOW-like water and intra- CH_4 equilibrium reflecting temperatures
 480 above 200 °C.

481 Across five years of samples from NSHQ14, δD_{CH_4} has ranged from -232‰ VSMOW
 482 to -311.73‰ VSMOW, with a mean weighted by sample year of -275‰ VSMOW (Fig-
 483 ure 3a; Table 2). This CH_4 is D-enriched with respect to coexisting H_2 ($\delta D_{H_2} = -685\text{‰}$ VSMOW;
 484 Miller et al., 2016) and D-depleted with respect to coexisting water ($\delta D_{H_2O} = +0.2\text{‰}$ VSMOW
 485 in 2018; Table 3). Although H_2 and water reflect H isotopic equilibrium at $\sim 50\text{°C}$ (Miller
 486 et al., 2016), both H_2 and water are in H isotopic disequilibrium with CH_4 (Figure 3b).
 487 Moreover, NSHQ14 fluids exhibit intra- CH_4 disequilibrium, as indicated by $\Delta^{13}CH_3D$
 488 and $\Delta^{12}CH_2D_2$ values (Table 2) plotting below the equilibrium line in Figure 3d. These
 489 non-equilibrium isotopic compositions indicate that post-genetic alteration of CH_4 must
 490 have occurred or that fluid inclusions are not the only source of CH_4 at NSHQ14.

491 One such post-genetic alteration mechanism is diffusion. However, CH_4 at NSHQ14
 492 cannot be the diffusion residual of CH_4 that was originally at intramolecular equilibrium,
 493 as that would have increased $\Delta^{13}CH_3D$ and $\Delta^{12}CH_2D_2$ of the residual (E. Young et al.,
 494 2017), pushing those values above the equilibrium line in Figure 3d. Another potential
 495 alteration mechanism is microbial CH_4 oxidation. Two types of microbial CH_4 oxida-
 496 tion have been studied for their effects on CH_4 clumped isotopologue relative abundances:
 497 anaerobic methane oxidation of the ANME type and aerobic CH_4 oxidation. ANME-type
 498 anaerobic methane oxidation is suggested to be a highly reversible metabolic pathway
 499 (Knittel & Boetius, 2009; Timmers et al., 2017). This reversibility has been proposed
 500 to bring $\Delta^{13}CH_3D$ towards equilibrium at low temperatures (70°C to 30°C) through
 501 continuous breaking and reforming of bonds in the CH_4 molecule (E. Young et al., 2017;
 502 Ash & Egger, 2019; Giunta et al., 2019). Thus, the comparatively low $\Delta^{13}CH_3D$ values
 503 observed in samples from NSHQ14 and other wells in this study (Figure 3b and d) do
 504 not support a major role for anaerobic methane oxidation in the CH_4 cycle within the
 505 study area. Aerobic CH_4 oxidation is less reversible than ANME-type anaerobic methane
 506 oxidation due to differences in the enzymes and electron acceptors used for those respec-
 507 tive processes. For this reason, aerobic CH_4 oxidation does not bring CH_4 into isotopic
 508 equilibrium, but rather imparts a normal, classical kinetic isotope effect during CH_4 con-
 509 sumption. In a study of the effect of aerobic CH_4 oxidation on $\Delta^{13}CH_3D$, D. T. Wang
 510 et al. (2016) found that the fractionation factor for $^{13}CH_3D$ was closely approximated
 511 by the product of the fractionation factors for $^{13}CH_4$ and $^{12}CH_3D$. Although it has not
 512 yet been demonstrated experimentally, it is hypothesized that the fractionation factor
 513 for $^{12}CH_2D_2$ during aerobic CH_4 oxidation is likewise equivalent to the square of the frac-
 514 tionation factor for $^{12}CH_3D$ (E. D. Young, 2020). This “product rule” for isotopic frac-
 515 tionation during aerobic CH_4 oxidation results in decreases in $\Delta^{13}CH_3D$ and $\Delta^{12}CH_2D_2$
 516 with concomitant increases in $\delta^{13}C$ and δD in residual CH_4 (D. T. Wang et al., 2016;
 517 E. D. Young, 2020). Thus, aerobic CH_4 oxidation could in principle draw $\Delta^{13}CH_3D$ and
 518 $\Delta^{12}CH_2D_2$ values originally reflecting 200°C to 360°C equilibrium down below the equi-
 519 librium line in Figure 3d. However, if CH_4 samples from NSHQ14 were originally at 200°C
 520 to 360°C equilibrium with water of SMOW-like isotopic composition, aerobic methane
 521 oxidation would push the residual CH_4 towards higher δD (and $\varepsilon_{methane/water}$) values (above
 522 the equilibrium line in Figure 3b), which is inconsistent with the comparatively low δD_{CH_4}
 523 observed at NSHQ14.

524 For the reasons outlined above, post-genetic alteration of CH_4 in CH_4-H_2O and
 525 intramolecular isotopic equilibrium at 200°C to 360°C does not explain the observed
 526 isotopic compositions of CH_4 sampled from NSHQ14. Therefore, the release of CH_4 stored
 527 in fluid inclusions cannot account for all the CH_4 at NSHQ14. Alternative processes that
 528 do produce CH_4 with $\Delta^{13}CH_3D$ and $\Delta^{12}CH_2D_2$ values lower than equilibrium include
 529 microbial methanogenesis (green shaded area in Figure 3b and d; D. T. Wang et al., 2015;
 530 Stolper et al., 2015; E. Young et al., 2017; Gruen et al., 2018; E. D. Young, 2020) and
 531 low-temperature ($\leq 90\text{°C}$) abiotic reduction of CO_2 or CO through Sabatier or Fischer-
 532 Tropsch-type reactions (represented in Figure 3 d by samples from Kidd Creek (gray shaded
 533 area) (E. Young et al., 2017; Sherwood Lollar et al., 2002, 2008) and Ru-catalyzed Sabatier
 534 reaction experiments (E. Young et al., 2017; Etiope & Ionescu, 2015)).

535 To independently assess the potential influences of microbial processes on CH₄ con-
 536 centration and isotopic composition, DNA was extracted from biomass in pumped ground-
 537 waters and subjected to amplification and sequencing of 16S rRNA genes. 16S rRNA gene
 538 sequences of biomass collected in 2018 were searched for matches to known CH₄-cycling
 539 taxa, as compiled previously by Crespo-Medina et al. (2017). Sequences closely affiliated
 540 with both methanogenic and methanotrophic taxa were found to be widespread in the
 541 aquifer (Figure 5). Based on phylogenetic inference, the dominant methanogenic taxon
 542 was related to the genus *Methanobacterium*, whose members can produce CH₄ from H₂
 543 and CO₂, CO, or formate (Balch et al., 1979). *Methanobacterium* comprised a high pro-
 544 portion (24 %) of 16S rRNA gene sequences at NSHQ14 in 2018. Relative abundances
 545 of *Methanobacterium* 16S rRNA gene reads were similarly high in 2017 (12 %) and 2016
 546 (28 %), but lower (< 1 %) in 2015 and 2014 (Miller et al., 2016; Rempfert et al., 2017;
 547 Kraus et al., 2018). The increase in the relative abundance of 16S rRNA genes affiliated
 548 with *Methanobacterium* in samples collected in 2016 and onwards versus those collected
 549 in 2014 and 2015 coincided with our transition from a smaller, lower-flow pump (max-
 550 imum depth 20 m) to larger, higher-flow pumps (maximum depth 90 m). The obligate
 551 anaerobic nature of this methanogen genus (Boone, 2015) is consistent with its higher
 552 relative gene abundances in fluids sampled from greater depths, which presumably re-
 553 ceive less input of atmospheric O₂ than do shallower fluids.

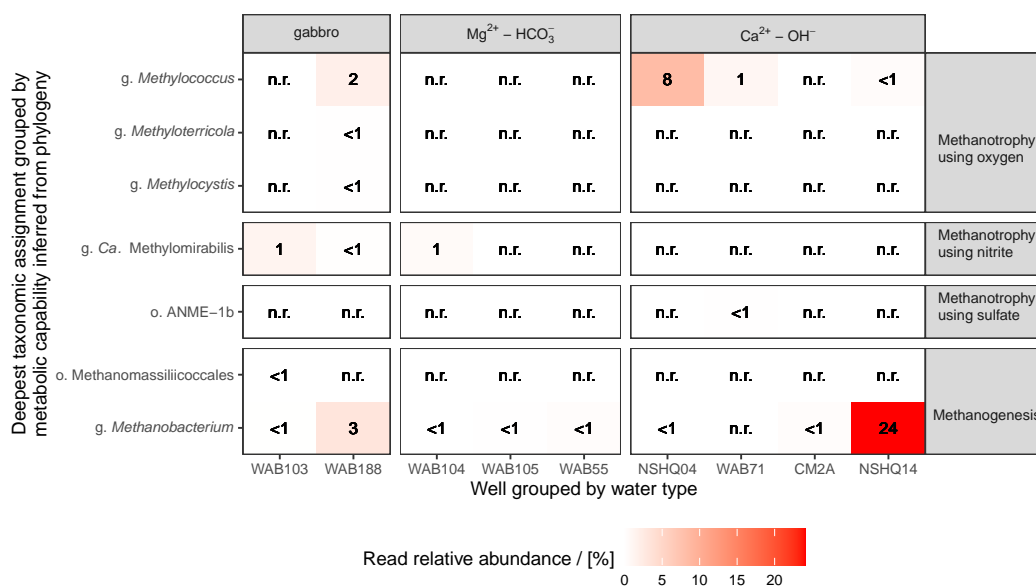


Figure 5. 16S rRNA gene read relative abundances of DNA extracted from Samail Ophiolite groundwaters sampled in 2018 affiliated with CH₄-cycling taxa. Read relative abundances are reported as percentages rounded to the ones place. Cases when a taxon was detected in a sample and was < 1 % read relative abundance after rounding are labeled “< 1”. Cases when no reads of a taxon were detected in a sample are labeled “n.r.”

554 Consortia capable of anaerobic oxidation of CH₄ coupled to SO₄²⁻ reduction, in-
 555 cluding ANME, were not detected by 16S rRNA gene sequencing of samples obtained
 556 from NSHQ14 in 2018 (Figure 5), 2016, or 2014 (Miller et al., 2016; Rempfert et al., 2017),
 557 although sequences affiliated with order ANME-1b were detected in low abundance (<
 558 1 % of reads) in samples obtained from NSHQ14 in 2017 and 2015 (Rempfert et al., 2017;
 559 Kraus et al., 2018). This scarcity of ANME may result from metabolic inhibition by high
 560 CH₂ in groundwaters at NSHQ14 and elsewhere in the Samail Ophiolite. It has been pro-

561 posed that the thermodynamics of “reverse methanogenesis” require low c_{H_2} (0.1 nM to
 562 1 nM at Hydrate Ridge, a marine cold seep environment (Boetius et al., 2000), where CH_4
 563 and SO_4^{2-} concentrations can be a factor of 10 or more higher than those typically mea-
 564 sured in ophiolitic groundwaters such as in Oman). Indeed, the bioenergetics of SO_4^{2-} -
 565 driven oxidation of CH_4 are less favorable than SO_4^{2-} -driven oxidation of H_2 or non- CH_4
 566 organics, or other metabolisms such as methanogenesis or acetogenesis in the Samail Ophi-
 567 olite (Canovas III et al., 2017), as in deep continental settings where radiolytic H_2 ac-
 568 cumulates (Kieft et al., 2005; Moser et al., 2005; Kieft, 2016).

569 While 16S rRNA gene sequences affiliated with anaerobic CH_4 oxidizing microbes
 570 have only occasionally been detected at NSHQ14, 16S rRNA gene sequences affiliated
 571 with the genus *Methylococcus*, which contains aerobic methanotrophs (Hanson & Han-
 572 son, 1996), have been detected in all samples from NSHQ14, ranging from 1 % to < 1 %
 573 of reads in samples obtained from 2014 to 2018 (Figure 5; Miller et al., 2016; Rempfert
 574 et al., 2017; Kraus et al., 2018). Since the aerobic lifestyle of *Methylococcus* is at odds
 575 with that of the obligate anaerobe, *Methanobacterium*, it seems most likely that these
 576 two taxa are spatially separated in the aquifer, and that waters containing each of them
 577 were mixed during open borehole pumping. Still, the > 10 times higher abundances of
 578 *Methanobacterium*-related 16S rRNA genes relative to those of *Methylococcus* at NSHQ14
 579 in samples from 2016 to 2018 suggest that the microbial CH_4 cycle at this well is domi-
 580 nated by CH_4 production, rather than consumption.

581 16S rRNA gene sequencing of subsurface biomass from NSHQ14 is complemented
 582 by other observations that suggest that methanogens are not only prevalent, but active.
 583 The functional potential to perform hydrogenotrophic and acetoclastic methanogenesis
 584 at NSHQ14 has been demonstrated through metagenomic sequencing (Fones et al., 2019),
 585 and genes involved in methanogenesis are actively transcribed (Kraus et al., 2018). Trans-
 586 formation of ^{14}C -labeled HCO_3^- to CH_4 has been shown to occur in water samples from
 587 NSHQ14 at significantly higher rates than in killed controls (Fones et al., 2019), indi-
 588 cating that methanogenesis occurs *in situ*. Taken together with a cell abundance of $1.15 \cdot$
 589 10^5 cells·mL $^{-1}$ in groundwater at NSHQ14 (Fones et al., 2019), these data suggest that
 590 some depths of the aquifer accessed by NSHQ14 host abundant active methanogenic cells
 591 (thousands per mL, assuming $\sim 24\%$ of cells are methanogens based on 16S rRNA gene
 592 data). These active cells could influence CH_4 concentration and isotopic composition.

593 Methanogens could produce CH_4 through direct uptake of $\sum \text{CO}_2$ in H_2 -rich $\text{Ca}^{2+} -$
 594 OH^- water, where kinetic inhibitions to abiotic $\sum \text{CO}_2$ reduction to CH_4 allow for a mod-
 595 est energy yield for hydrogenotrophic methanogens (Leong & Shock, 2020). Methanogens
 596 using $\sum \text{CO}_2$ could benefit from greater chemical disequilibrium if they inhabit zones
 597 where deeply-sourced, H_2 -rich $\text{Ca}^{2+} - \text{OH}^-$ water mixes with shallow, $\text{Mg}^{2+} - \text{HCO}_3^-$
 598 water (Zwicker et al., 2018; Leong & Shock, 2020). This niche could be supported by rapid
 599 microbial O_2 consumption by aerobes, such as those that may belong to the genera *Meio-*
 600 *thermus* and *Hydrogenophaga*, whose 16S rRNA gene sequences have been detected in
 601 multiple years of sampling at NSHQ14 (Supporting Information Figure S3; Miller et al.,
 602 2016; Rempfert et al., 2017; Kraus et al., 2018; Fones et al., 2019), and kinetic limita-
 603 tions on carbonate precipitation (P. B. Kelemen et al., 2011; Gadikota et al., 2014; Na-
 604 tional Academies, 2019; Gadikota et al., 2020; P. B. Kelemen et al., 2020). In addition
 605 to direct uptake of $\sum \text{CO}_2$, carbonate minerals may serve as a C source for methano-
 606 genesis in carbonated peridotites (Miller et al., 2018). Other potential C sources include
 607 formate (HCOO^-) and carbon monoxide (CO). Formate and CO are related to $\sum \text{CO}_2$
 608 through reversible reactions involving H_2 and H_2O , which are known to occur during ser-
 609 pentinization (McCollom & Seewald, 2003; McDermott et al., 2015). CO has always been
 610 below limits of quantitation in Oman wells ($< 132 \text{ nmol} \cdot \text{L}^{-1}$ in 2018; Table 4), and
 611 formate concentrations are $1 \mu\text{mol} \cdot \text{L}^{-1}$ to $2 \mu\text{mol} \cdot \text{L}^{-1}$ in the studied wells (Rempfert
 612 et al., 2017). The relatively low concentrations of these single-C compounds suggest that
 613 they could be limiting substrates for methanogenesis, similarly to $\sum \text{CO}_2$. Further phys-

614 biological studies are needed to determine which C compounds *Methanobacterium* most
 615 actively metabolizes in $\text{Ca}^{2+}-\text{OH}^-$ waters and how substrate selection/limitation under
 616 these conditions affects isotopic compositions of produced CH_4 .

617 The microbiological data from NSHQ14 fluids are compatible with $\delta\text{D}_{\text{CH}_4}$, $\Delta^{13}\text{CH}_3\text{D}$,
 618 and $\Delta^{12}\text{CH}_2\text{D}_2$ values that collectively indicate a substantial addition of microbial CH_4
 619 to an otherwise abiotic pool of CH_4 . Although the data presented here do not enable
 620 us to precisely determine the mole fractions and isotopic compositions of the microbial
 621 and abiotic components of CH_4 at NSHQ14, the high $\delta^{13}\text{C}$ of this CH_4 suggests that the
 622 microbial component is more ^{13}C -enriched than microbial CH_4 formed in sedimentary
 623 environments. The small apparent C isotope fractionation imparted by microbial methano-
 624 genesis at NSHQ14 is perhaps less than that observed by Miller et al. (2018) in growth
 625 of *Methanobacterium* on $\text{CaCO}_3(s)$ at $\text{pH} \sim 9$ ($\alpha_{\text{CO}_2/\text{CH}_4} = 1.028$). This could be a
 626 result of the higher pH in natural $\text{Ca}^{2+}-\text{OH}^-$ fluids (up to $\text{pH} \sim 12$) compared to the
 627 maximum experimental pH of 9.66 at which sufficient CH_4 was produced for isotopic anal-
 628 ysis by Miller et al. (2018) and the potential for increased pH to further limit CO_2 avail-
 629 ability. In natural settings, the suppression of C isotope fractionation during methano-
 630 genesis under severe C limitation is supported by observations of high $\delta^{13}\text{C}$ values (up
 631 to +14 ‰ VPDB) of lipid biomarkers thought to be produced by methanogens at serpentinite-
 632 hosted seeps at Chimaera, Turkey (Zwicker et al., 2018) and at the Lost City Hydrother-
 633 mal Vent Field, Mid-Atlantic Ridge (Bradley et al., 2009). Evaluation of these hypothe-
 634 ses will require further research on the isotope effects of methanogenesis at hyperalka-
 635 line conditions using various C sources.

636 While our data support substantial microbial CH_4 and abiotic, fluid inclusion-derived
 637 CH_4 in NSHQ14 fluids, we find less evidence for abiotic CH_4 production at low temper-
 638 atures ($< 200^\circ\text{C}$). At low temperatures, access of gas-phase H_2 and CO_2 or CO to cat-
 639 alytic metals such as Ru is required for CH_4 to form at appreciable rates (Etiope & Ionescu,
 640 2015; McCollom, 2016). It has been proposed that the spatial concentration of potentially-
 641 catalytic Ru-rich chromites in chromitites is important for catalysis of low-temperature
 642 CO_2 reduction to CH_4 in ophiolites (Etiope & Ionescu, 2015; Etiope et al., 2018). While
 643 peridotites in Oman ubiquitously contain a few percent distributed chromite (Hanghøj
 644 et al., 2010), massive chromitites were not reported in lithologic descriptions of cores or
 645 drill cuttings from NSHQ14 or any of the six additional wells ranging from 300 m to 400 m
 646 depth that have been drilled in the same catchment by the Oman Drilling Project (P. Kele-
 647 men et al., 2020). Nor are chromitites notably abundant in outcrop within this catch-
 648 ment. Furthermore, although some flow paths of meteoric water through the ophiolite
 649 may result in saturation in H_2 and separation of a free gas phase (Canovas III et al., 2017),
 650 the depth to water is < 20 m in all wells in the catchment of NSHQ14, suggesting water-
 651 saturated conditions in the subsurface. Moreover, if free $\text{H}_2(g)$ were generated at high
 652 extents of reaction progress, co-existing $\text{CO}_2(g)$ would be extremely scarce due to pre-
 653 cipitation of carbonate minerals and high pH (Etiope & Ionescu, 2015; Leong & Shock,
 654 2020). It has been proposed that CH_4 in ophiolites can form through reduction of $\text{CO}_2(g)$
 655 from non-atmospheric sources such as magma, the mantle, or sedimentary carbonate for-
 656 mations (Etiope & Ionescu, 2015). A magmatic/mantle CO_2 source is not supported at
 657 NSHQ14 because excess He above air saturation in groundwaters from this well has a
 658 dominantly radiogenic isotopic composition that is distinct from mantle-derived He (Vankeuren
 659 et al., 2019). Further, although sedimentary carbonates are present in the vicinity of NSHQ14
 660 and elsewhere in the ophiolite (Boudier & Coleman, 1981; de Obeso & Kelemen, 2018),
 661 there is no clear mechanism to liberate $\text{CO}_2(g)$ from mineral carbonates and transfer
 662 that $\text{CO}_2(g)$ to catalytic sites of reaction on chromites where $\text{H}_2(g)$ is also present. Thus,
 663 the apparent lack of massive chromites and free gaseous potential reactants suggest that
 664 the subsurface surrounding NSHQ14 is not conducive to low-temperature abiotic CH_4
 665 production.

666 While low-temperature CH_4 production in the catchment of NSHQ14 seems un-
 667 likely, NSHQ14 groundwaters could be mere carriers of CH_4 that was produced elsewhere
 668 in the ophiolite under gaseous conditions and that has subsequently migrated into the
 669 aquifer. Some studies of CH_4 origin in other peridotite bodies have favored such a hy-
 670 pothesis (Etiopie et al., 2016; Marques et al., 2018). However, it is not clear how this hy-
 671 pothesis could be tested in the case of the NSHQ14, nor how it addresses the issue of
 672 CO_2 source.

673 In summary, isotopic and microbiological data lead us to conclude that the high
 674 concentrations of CH_4 ($10^2 \mu\text{mol}\cdot\text{L}^{-1}$) in groundwaters accessed by NSHQ14 primarily
 675 result from microbial methanogenesis and the release of abiotic CH_4 from fluid inclusions.
 676 A portion of this CH_4 may be oxidized by aerobic methanotrophs.

677 **4.2.2 Abundant microbial CH_4 produced under C-limited conditions and** 678 **substantial microbial CH_4 oxidation in the $\text{Ca}^{2+} - \text{OH}^-$ waters** 679 **of well NSHQ04**

680 NSHQ04 is situated in partially serpentinized harzburgite 10 m away from a faulted
 681 contact with crustal gabbros (Figure 1; Supporting Information Figure S1). Surface rock
 682 exposures surrounding NSHQ04 are dominated by serpentinized harzburgites, with lesser
 683 dunites, gabbro lenses, and pyroxenite dikes. NSHQ04 is cased to 5.8 mbgl and drilled
 684 to 304 m depth (Table 1). As of 2017, the well is obstructed at 8 m below the casing top,
 685 precluding deeper sampling (Section 3.1; Table 1).

686 Primary differences in fluid composition between NSHQ04 and NSHQ14 include
 687 lower pH by ~ 1 and higher $c_{\sum \text{Ca}}$ and $c_{\sum \text{Si}}$ at NSHQ04 (Tables 1 and 3; Miller et
 688 al., 2016; Rempfert et al., 2017; Vankeuren et al., 2019; Fones et al., 2019). These dif-
 689 ferences could be related to the scarcity of fresh, near-surface olivine at NSHQ04, which
 690 may result in a greater influence of pyroxene serpentinization at NSHQ04 (Miller et al.,
 691 2016). Low-temperature pyroxene serpentinization generally continues after olivine is
 692 exhausted, and leads to higher $c_{\sum \text{Si}}$ and, depending on pyroxene chemical composition,
 693 can also lead to higher $c_{\sum \text{Ca}}$ and lower pH (Bach et al., 2006; Leong & Shock, 2020).
 694 The relatively low pH and high $c_{\sum \text{Si}}$ could also stem from mixing of $\text{Ca}^{2+} - \text{OH}^-$ wa-
 695 ters with gabbro- or atmosphere-influenced fluids.

696 Compared to NSHQ14, NSHQ04 has generally had lower c_{H_2} (detected in 2014, but
 697 not in 2018, 2017, 2015, or 2012; Table 4; Figure 2; Miller et al., 2016; Rempfert et al.,
 698 2017; Vankeuren et al., 2019)). The relatively low c_{H_2} measured in waters pumped from
 699 NSHQ04 is probably due at least in part to microbial H_2 oxidation. Although there are
 700 multiple enzymes with which a diversity of microbes oxidize H_2 (Peters et al., 2015),
 701 aerobic H_2 oxidation by bacteria of the genus *Hydrogenophaga* has been identified as a
 702 particularly prevalent process in serpentinizing settings, including the Samail Ophiolite
 703 (Suzuki et al., 2014; Rempfert et al., 2017; Marques et al., 2018). Sequences affiliated
 704 with *Hydrogenophaga* accounted for 20% of 16S rRNA gene reads in DNA extracted from
 705 biomass in waters pumped from NSHQ04 in 2018, which is similar to previous years of
 706 sampling at NSHQ04 (6% to 18% in 2014, 2015, and 2017; inter-annual mean of 12%)
 707 and higher than all other studied wells (Supporting Information Figure S3; Rempfert
 708 et al., 2017; Miller et al., 2016; Kraus et al., 2018).

709 While H_2 has only been transiently detected at NSHQ04, c_{CH_4} at this well has con-
 710 sistentlly been the highest among our sample sites ($144 \mu\text{mol}\cdot\text{L}^{-1}$ in 2018 and $483 \mu\text{mol}\cdot$
 711 L^{-1} in 2017. In comparison to NSHQ14, CH_4 at NSHQ04 is more ^{13}C - and D-enriched
 712 (mean weighted by sample year $\delta^{13}\text{C} = +3.3\text{‰}$ VPDB, $s = 1.8\text{‰}$; $\delta\text{D} = -220\text{‰}$ VSMOW,
 713 $s = 11\text{‰}$; $n = 4$; Table 2; Figure 3a). Fluids sampled from NSHQ04 are in $\text{CH}_4 -$
 714 H_2O H isotopic disequilibrium and intra- CH_4 disequilibrium (Figure 3b and d), which
 715 is also true of fluids from NSHQ14. However, CH_4 sampled from NSHQ04 has distinctly

negative $\Delta^{12}\text{CH}_2\text{D}_2$ (-24.502‰) and low $\Delta^{13}\text{CH}_3\text{D}$ (mean weighted by sample year of 0.36‰ , $s = 0.32\text{‰}$, $n = 3$; Table 2). As such, CH_4 from NSHQ04 plots squarely among methanogen culture samples in $\Delta^{13}\text{CH}_3\text{D}/\Delta^{12}\text{CH}_2\text{D}_2$ space (Figure 3d), suggesting that CH_4 is dominantly microbial at NSHQ04. Moreover, alkane gases dissolved in waters pumped from NSHQ04 exhibited a $\text{C}_1/(\text{C}_2 + \text{C}_3)$ ratio of $5.4 \cdot 10^3$ in 2018, which is higher than other wells in this study (Table 4; Figure 3c), further supporting a major component of microbial CH_4 at NSHQ04.

Microbial CH_4 production at NSHQ04 is also indicated by microbiological data. 16S rRNA gene sequences affiliated with *Methanobacterium* have been detected in DNA extracted from biomass filtered from waters pumped from NSHQ04, albeit in low relative abundance ($< 1\%$ of reads in 2018; Figure 5; also detected in $< 1\%$ of reads in 2014, but not detected in 2015 and 2017; Rempfert et al., 2017; Miller et al., 2016; Kraus et al., 2018). The apparent low relative abundance of *Methanobacterium* at NSHQ04 could have resulted from the relatively shallow depth from which samples were collected at NSHQ04 due to well obstruction and the consequential sampling of groundwaters that may have experienced atmospheric O_2 infiltration. High relative read abundances of sequences affiliated with aerobes and transient H_2 across years of sampling NSHQ04 suggest that zones of the aquifer that are not always anoxic were accessed. These conditions may restrict methanogen abundance to greater depths than were sampled, but not constrain the upward diffusion of the product of their metabolism, CH_4 . Nevertheless, fluids obtained from NSHQ04 have yielded robust cultures of *Methanobacterium*. These cultures have been shown to produce CH_4 with suppressed C isotope fractionation when provided H_2 and CaCO_3 (s) at alkaline conditions (Miller et al., 2018). Carbonate minerals could therefore be an important C source for methanogens in subsurface fluids near NSHQ04. Miller et al. (2016) analyzed the isotopic composition of one carbonate mineral sample from NSHQ04 drill cuttings, which yielded a $\delta^{13}\text{C}$ value of -1.48‰ VPDB. This places an upper estimate on the $\delta^{13}\text{C}$ of CH_4 that could be produced from carbonate mineral substrates in the subsurface near NSHQ04. Since this is lower than the measured $\delta^{13}\text{C}$ of CH_4 at NSHQ04 (Table 2), a secondary mechanism, such as methanotrophy, could have further enriched this CH_4 in ^{13}C . High relative abundances of 16S rRNA gene reads of DNA extracted from biomass in waters sampled from NSHQ04 were related to an aerobic methanotroph of the genus *Methylococcus* (8% of reads in 2018; inter-annual mean of 11% ; Figure 5; Miller et al., 2016; Rempfert et al., 2017; Kraus et al., 2018). Greater aerobic methanotrophy at NSHQ04 relative to NSHQ14 may have contributed in part to the lower $\Delta^{13}\text{CH}_3\text{D}$ and $\Delta^{12}\text{CH}_2\text{D}_2$ and higher $\delta^{13}\text{C}$ and δD of CH_4 sampled from NSHQ04.

Methanotrophic activity at NSHQ04 is consistent with the observed ^{13}C -depletion in $\sum \text{CO}_2$ at NSHQ04 (-29.7‰ VPDB $\delta^{13}\text{C}$; Table 2) relative to the other studied wells because environments of active methanotrophy often have ^{13}C -depleted $\sum \text{CO}_2$ (Barker & Fritz, 1981; Michaelis et al., 2002). Indeed, $\delta^{13}\text{C}_{\sum \text{CO}_2}$ at NSHQ04 is compatible with aerobic oxidation of CH_4 of $\sim 0\text{‰}$ VPDB $\delta^{13}\text{C}$ (Barker & Fritz, 1981; Feisthauer et al., 2011). Alternatively, ^{13}C -depletion in $\sum \text{CO}_2$ could be explained by kinetic isotope fractionation during hydroxylation of atmospheric CO_2 upon contact with $\text{Ca}^{2+} - \text{OH}^-$ water, which has been interpreted as the cause of $\delta^{13}\text{C}$ as low as -27.21‰ VPDB in Ca-rich carbonates from hyperalkaline seeps in the Samail Ophiolite (Clark et al., 1992; P. B. Kelemen et al., 2011; Falk et al., 2016). The similarity in $\delta^{13}\text{C}$ of travertines from Samail Ophiolite hyperalkaline seeps and $\sum \text{CO}_2$ in waters pumped from NSHQ04 could reflect a shared mechanism of CO_2 uptake. Considering the relatively shallow sampling depth at NSHQ04 in 2018 (Table 1), it is plausible that the sampled groundwaters continuously interact with atmospheric CO_2 . Although the relative influences of methanotrophy and atmospheric CO_2 hydroxylation cannot be determined based on the available data, both processes could affect $\delta^{13}\text{C}_{\sum \text{CO}_2}$ at NSHQ04.

In summary, low $\Delta^{13}\text{CH}_3\text{D}$ and $\Delta^{12}\text{CH}_2\text{D}_2$, high $\text{C}_1/(\text{C}_2 + \text{C}_3)$, the presence of *Methanobacterium* that were readily cultured, and high 16S rRNA gene relative abundances of *Methylococcus* lead us to conclude that microbial production and consumption of CH_4 are the dominant factors controlling CH_4 concentration and isotopic composition at NSHQ04.

4.2.3 *H₂-limited microbial methanogenesis with classic C isotope effect expressed at well WAB188*

WAB188 is situated 2 km down-gradient from NSHQ04 and is set in gabbro on the opposite side of a fault from NSHQ04 (Figure 1; Supporting Information Figure S1; Table 1). Fluids pumped from WAB188 have had variable pH (8.72 to 5.75) and oxidation-reduction potential (f_{O_2} of 10^{-61} bar to 10^{-34} bar and Eh of -220 mV to $+214$ mV) across four years of sampling (Table 1; Rempfert et al., 2017; Fones et al., 2019). WAB188 has consistently had major ion composition similar to the gabbro-hosted well WAB103, except that WAB188 has had higher $c_{\sum \text{Ca}}$ (Table 3; Rempfert et al., 2017; Fones et al., 2019). H_2 has occasionally been detected in fluids pumped from WAB188 ($c_{\text{H}_2} = 0.992 \mu\text{mol}\cdot\text{L}^{-1}$ in 2017), and CH_4 has consistently been detected at moderate concentrations ($c_{\text{CH}_4} = 1.83 \mu\text{mol}\cdot\text{L}^{-1}$ in 2017 and $0.917 \mu\text{mol}\cdot\text{L}^{-1}$ in 2018) (Table 4; Rempfert et al., 2017; Fones et al., 2019). The high $c_{\sum \text{Ca}}$ and moderate but variable pH, Eh , and c_{H_2} in fluids sampled from WAB188 suggest that fluid chemical composition at WAB188 is dominantly controlled by water-rock reaction with gabbro, but may also be affected by inputs of fresh rainwater and/or H_2 -bearing $\text{Ca}^{2+}-\text{OH}^-$ water flowing from the peridotite aquifer into the gabbro aquifer across a fault at depth. Flows of water from higher-head, lower-permeability peridotite aquifers into gabbro aquifers in the Samail Ophiolite has been proposed on the basis of physical hydrologic data (Dewandel et al., 2005). Instead or in addition, serpentinization of olivine and pyroxene entirely within gabbro might have produced some of the H_2 observed in water samples from WAB188.

Microbial methanogenesis at WAB188 is indicated by high relative abundances of 16S rRNA gene reads affiliated with methanogens in pumped groundwaters. Sequences affiliated with *Methanobacterium* accounted for 3% of 16S rRNA gene reads of DNA extracted from subsurface fluids sampled from WAB188 in 2018, which was second only to NSHQ14 among our sampling sites, and consistent with prior years of sampling at WAB188 (mean 2015 to 2018 of 4%; Figure 5; Rempfert et al., 2017; Kraus et al., 2018). Further, 2% of 16S rRNA gene reads from WAB188 were affiliated with *Methylococcus* in 2018, which was second only to NSHQ04 among our sampling sites, and consistent with prior years of sampling (Figure 5; Rempfert et al., 2017; Kraus et al., 2018). In addition, 16S rRNA gene sequences affiliated with genus *Candidatus* Methylomirabilis, which includes species that mediate anaerobic methane oxidation coupled to nitrite reduction (Ettwig et al., 2010; Luesken et al., 2012; Welte et al., 2016), were detected in samples from WAB188 in 2018 albeit at low relative gene abundance ($< 1\%$). As a whole, the 16S rRNA gene sequencing data from WAB188 fluids are consistent with microbial production of CH_4 and, secondarily, methanotrophy using O_2 and/or NO_2^- .

While subsurface fluids sampled at WAB188, NSHQ14, and NSHQ04 all bear microbiological and isotopic evidence of methanogenic activity, the conditions under which methanogenesis proceeds at WAB188 are fundamentally distinct. In contrast to the $\text{Ca}^{2+}-\text{OH}^-$ fluids from NSHQ14 and NSHQ04, the circumneutral fluids from WAB188 have $\sim 10^2$ to $\sim 10^3$ times higher $c_{\sum \text{CO}_2}$ (inter-annual mean of $2910 \mu\text{mol}\cdot\text{L}^{-1}$, $s = 620 \mu\text{mol}\cdot\text{L}^{-1}$, $n = 3$; Table 3) and $\sim 75\%$ lower $\delta^{13}\text{C}_{\text{CH}_4}$ (inter-annual mean $\delta^{13}\text{C} = -73\%$ VPDB, $s = 13\%$, $n = 3$; Table 2). Since WAB188 fluids contain relatively ^{13}C -depleted CH_4 that is not associated with substantial concentrations of $\text{C}_2 - \text{C}_6$ alkanes (Table 4), a standard interpretation (Bernard et al., 1977; Milkov & Etiope, 2018) would be that the source of CH_4 at WAB188 is dominantly microbial. Such an interpretation is largely pred-

819 icated on data from sedimentary settings, where H_2 is typically more scarce than CO_2 .
 820 H_2 may be the limiting substrate for methanogenesis at WAB188, as indicated by tran-
 821 sient H_2 at moderate concentrations co-occurring with abundant $\sum CO_2$. These condi-
 822 tions contrast starkly with those that prevail in $Ca^{2+}-OH^-$ fluids, where C substrates
 823 for methanogenesis are more scarce than H_2 . Indeed, the apparent α_{CO_2/CH_4} at WAB188
 824 (based on measured $\delta^{13}C_{\sum CO_2}$ of -13.52% VPDB; Table 3) is compatible with that
 825 of CH_4 produced by *Methanobacterium* cultures provided limiting H_2 and excess $HCO_3^- (aq)$,
 826 which was greater than the α_{CO_2/CH_4} observed for parallel cultures under CO_2 -poor con-
 827 ditions (Miller et al., 2018). Therefore, the inverse relationship between $c_{\sum CO_2}$ and $\delta^{13}C_{CH_4}$
 828 across fluids from wells WAB188, NSHQ14, and NSHQ04 is consistent with an effect of
 829 CO_2 availability on α_{CO_2/CH_4} of microbial methanogenesis.

830 5 Conclusions

831 Through integration of isotopic, microbiological, and hydrogeochemical data, we
 832 conclude that substantial microbial CH_4 is produced under varying degrees of C or H_2
 833 limitation in subsurface waters of the Samail Ophiolite and mixes with abiotic CH_4 re-
 834 leased from fluid inclusions. Across subsurface fluids ranging in pH from circumneutral
 835 to 11.39, microbial CH_4 production is evidenced by 16S rRNA gene sequencing and other
 836 microbiological data indicating that methanogens are widespread and active in ground-
 837 waters in the ophiolite. We propose that CH_4 produced by these microbes constitutes
 838 a substantial portion of the total CH_4 pool, which is consistent with our finding of $^{13}CH_3D$
 839 and $^{12}CH_2D_2$ relative abundances significantly less than equilibrium. An abiotic, fluid
 840 inclusion-derived source of CH_4 , C_2H_6 , and C_3H_8 is inferred from the widespread occur-
 841 rence of CH_4 in fluid inclusions in peridotites, including those in Oman, and is supported
 842 by the relatively ^{13}C -enriched C_2H_6 and C_3H_8 measured in gases exsolved from peridotite-
 843 hosted groundwaters in this study. In contrast, abiotic, low-temperature reduction of CO_2
 844 to CH_4 is less likely to contribute substantially to the CH_4 pool in the study area due
 845 to an apparent scarcity of conditions favorable to catalysis: access of gas-phase H_2 and
 846 CO_2/CO to Ru-bearing chromites. The 16S rRNA gene sequencing data also indicate
 847 the presence of microbes capable of CH_4 oxidation, particularly using O_2 as an oxidant,
 848 but this oxidation is apparently not extensive enough to obscure the underlying CH_4 sources.
 849 In addition, we note an inverse relationship between $c_{\sum CO_2}$ and $\delta^{13}C_{CH_4}$ across ground-
 850 waters bearing microbiological evidence of methanogenic activity. This finding supports
 851 the hypothesis that C isotope fractionation between the C substrate used by methanogens
 852 and the CH_4 they produce is suppressed when the C substrate is limiting. Thus, our find-
 853 ing that $\delta^{13}C_{CH_4}$ varies by 90‰ in the Samail Ophiolite suggests that, in some settings,
 854 $\delta^{13}C_{CH_4}$ may be a powerful indicator of transitions from H_2 -limited to C-limited con-
 855 ditions for microbial methanogenesis, rather than a discriminant between microbial ver-
 856 sus abiotic CH_4 .

857 This study supports the premise that H_2 produced from water/rock reaction can
 858 fuel microbial life, even under challenging conditions of high pH and low oxidant avail-
 859 ability. By identifying where and how microbial methanogenesis can reasonably be ex-
 860 pected to occur in H_2 -rich, subsurface environments, this work complements theoreti-
 861 cal models in guiding the search for rock-hosted life, including extraterrestrial life. For
 862 example, our findings substantiate predictions that microbial methanogenesis could oc-
 863 cur in the reduced, alkaline ocean of Saturn’s moon, Enceladus (McKay et al., 2008; Glein
 864 et al., 2015; Waite et al., 2017), and that methanogens may use H_2 and carbonate min-
 865 erals in the Martian subsurface (Kral et al., 2014).

866 Acknowledgments

867 This research was directly supported by the Rock-Powered Life NASA Astrobiol-
 868 ogy Institute (NNA15BB02A). This research also used samples and/or data provided by

869 the Oman Drilling Project. The Oman Drilling Project (OmanDP) has been possible
 870 through co-mingled funds from the International Continental Scientific Drilling Project
 871 (ICDP), the Sloan Foundation – Deep Carbon Observatory (Grant 2014-3-01, Kelemen
 872 PI), the National Science Foundation (NSF-EAR-1516300, Kelemen PI), the NASA As-
 873 trobiology Institute (NNA15BB02A), the German Research Foundation (DFG), the Japanese
 874 Society for the Promotion of Science (JSPS), the European Research Council, the Swiss
 875 National Science Foundation, JAMSTEC, the TAMU-JR Science operator, and contri-
 876 butions from the Sultanate of Oman Ministry of Regional Municipalities and Water Re-
 877 sources, the Oman Public Authority of Mining, Sultan Qaboos University, CRNS-Univ.
 878 Montpellier II, Columbia University, and the University of Southampton. Work at LBNL
 879 was supported by the U.S. Department of Energy, Office of Science, Office of Basic En-
 880 ergy Sciences, Chemical Sciences, Geosciences, and Biosciences Division, under Award
 881 Number DE-AC02-05CH11231.

882 We thank the Ministry of Regional Municipalities and Water Resources in the Sul-
 883 tanate of Oman (particularly Said Al Habsi, Rashid Al Abri, Salim Al Khanbashi, and
 884 Haider Ahmed Mohammed Alajmi) for allowing access to wells and logistical support,
 885 Zaher Al Sulaimani and Mazin Al Sulaimani from the Oman Water Centre and AZD En-
 886 gineering for their technical and logistical support, Jude Coggon for coordinating Oman
 887 Drilling Project activities, Benoît Ildefonse for sharing geologic map data, Eric Ellison
 888 and Kaitlin Rempfert for their assistance in the field and laboratory, Elizabeth Fones
 889 for sharing biomass samples, Emily Kraus for critical discussion of Oman CH₄ cycle pro-
 890 cesses, and Noah Fierer, Jen Reeves, Corinne Walsh, Matthew Gebert, and Angela Oliv-
 891 erio for assisting with DNA sequencing and interpretation.

892 Data (in Excel format) and source code (in R Markdown format) used to produce
 893 the figures, data tables and analyses for this paper (as well as additional data on ana-
 894 lytical uncertainties and trace element concentrations) are available online at [https://](https://github.com/danote/2019_Nothaft_et_al)
 895 github.com/danote/2019_Nothaft_et_al. Additional DNA sequence data processing
 896 codes are available at https://github.com/danote/Samail_16S_compilation. The se-
 897 quences are accessible on the NCBI Short Read Archive under accession PRJNA655565.

898 References

- 899 Abrajano, T., Sturchio, N., Kennedy, B., Lyon, G., Muehlenbachs, K., & Bohlke, J.
 900 (1990). Geochemistry of reduced gas related to serpentinization of the Zam-
 901 bales ophiolite, Philippines. *Appl. Geochem.*, 5(5), 625 - 630. Retrieved from
 902 <http://www.sciencedirect.com/science/article/pii/088329279090060I>
 903 (Water-Rock Interactions Special Memorial Issue Ivan Barnes (1931–1989))
 904 doi: 10.1016/0883-2927(90)90060-I
- 905 Alsharhan, A. S. (1989). PETROLEUM GEOLOGY OF THE UNITED ARAB
 906 EMIRATES. *J. Pet. Geol.*, 12(3), 253-288. Retrieved from [https://](https://onlinelibrary.wiley.com/doi/abs/10.1111/j.1747-5457.1989.tb00197.x)
 907 onlinelibrary.wiley.com/doi/abs/10.1111/j.1747-5457.1989.tb00197.x
 908 doi: 10.1111/j.1747-5457.1989.tb00197.x
- 909 Alt, J. C., Garrido, C. J., Shanks, W., Turchyn, A., Padrón-Navarta, J. A., Sánchez-
 910 Vizcaíno, V. L., ... Marchesi, C. (2012). Recycling of water, carbon, and
 911 sulfur during subduction of serpentinites: A stable isotope study of Cerro del
 912 Almirez, Spain. *Earth Planet. Sci. Lett.*, 327-328, 50 - 60. Retrieved from
 913 <http://www.sciencedirect.com/science/article/pii/S0012821X12000568>
 914 doi: 10.1016/j.epsl.2012.01.029
- 915 Alt, J. C., Schwarzenbach, E. M., Früh-Green, G. L., Shanks, W. C., Bernasconi,
 916 S. M., Garrido, C. J., ... Marchesi, C. (2013). The role of serpentinites in cy-
 917 cling of carbon and sulfur: Seafloor serpentinization and subduction metamor-
 918 phism. *Lithos*, 178, 40 - 54. Retrieved from [http://www.sciencedirect.com/](http://www.sciencedirect.com/science/article/pii/S0024493712004975)
 919 [science/article/pii/S0024493712004975](http://www.sciencedirect.com/science/article/pii/S0024493712004975) (Serpentinites from mid-oceanic
 920 ridges to subduction) doi: 10.1016/j.lithos.2012.12.006

- 921 Alt, J. C., Shanks, W., Crispini, L., Gaggero, L., Schwarzenbach, E. M., Früh-
922 Green, G. L., & Bernasconi, S. M. (2012). Uptake of carbon and sulfur
923 during seafloor serpentinization and the effects of subduction metamorphism
924 in Ligurian peridotites. *Chem. Geol.*, *322-323*, 268 - 277. Retrieved from
925 <http://www.sciencedirect.com/science/article/pii/S0009254112003154>
926 doi: 10.1016/j.chemgeo.2012.07.009
- 927 Ash, J. L., & Egger, M. (2019, Jun). Exchange catalysis during anaer-
928 obic methanotrophy revealed by $^{12}\text{CH}_2\text{D}_2$ and $^{13}\text{CH}_3\text{D}$ in methane.
929 *Geochem. Perspect. Lett.*, *10*, 26–30. Retrieved from [https://www](https://www.geochemicalperspectivesletters.org/article1910)
930 [.geochemicalperspectivesletters.org/article1910](https://www.geochemicalperspectivesletters.org/article1910) doi: 10.7185/
931 geochemlet.1910
- 932 Assayag, N., Rivé, K., Ader, M., Jézéquel, D., & Agrinier, P. (2006). Improved
933 method for isotopic and quantitative analysis of dissolved inorganic carbon in
934 natural water samples. *Rapid Commun. Mass Spectrom.*, *20*(15), 2243–2251.
935 doi: 10.1002/rcm.2585
- 936 Bach, W., Paulick, H., Garrido, C. J., Ildfonse, B., Meurer, W. P., & Humphris,
937 S. E. (2006). Unraveling the sequence of serpentinization reactions: pet-
938 rography, mineral chemistry, and petrophysics of serpentinites from MAR
939 15°N (ODP Leg 209, Site 1274). *Geophys. Res. Lett.*, *33*(13). Retrieved
940 from [https://agupubs.onlinelibrary.wiley.com/doi/abs/10.1029/](https://agupubs.onlinelibrary.wiley.com/doi/abs/10.1029/2006GL025681)
941 [2006GL025681](https://agupubs.onlinelibrary.wiley.com/doi/abs/10.1029/2006GL025681) doi: 10.1029/2006GL025681
- 942 Balch, W. E., Fox, G. E., Magrum, L. J., Woese, C. R., & Wolfe, R. S. (1979, Jun).
943 Methanogens: reevaluation of a unique biological group. *Microbiol. Rev.*,
944 *43*(2), 260. Retrieved from [https://www.ncbi.nlm.nih.gov/pmc/articles/](https://www.ncbi.nlm.nih.gov/pmc/articles/PMC281474)
945 [PMC281474](https://www.ncbi.nlm.nih.gov/pmc/articles/PMC281474)
- 946 Barker, J. F., & Fritz, P. (1981, Sep). Carbon isotope fractionation during microbial
947 methane oxidation. *Nature*, *293*(5830), 289–291. doi: 10.1038/293289a0
- 948 Barnes, I., LaMarche, j. V., & Himmelberg, G. (1967). Geochemical evidence of
949 present-day serpentinization. *Science*, *156*(3776), 830–832. doi: 10.1126/
950 science.156.3776.830
- 951 Barnes, I., O'Neil, J., & Trescases, J. (1978). Present day serpentinization in New
952 Caledonia, Oman and Yugoslavia. *Geochim. Cosmochim. Acta*, *42*(1), 144 -
953 145. Retrieved from [http://www.sciencedirect.com/science/article/pii/](http://www.sciencedirect.com/science/article/pii/0016703778902259)
954 [0016703778902259](http://www.sciencedirect.com/science/article/pii/0016703778902259) doi: 10.1016/0016-7037(78)90225-9
- 955 Barnes, I., & O'Neil, J. R. (1969). The relationship between fluids in some
956 fresh alpine-type ultramafics and possible modern serpentinization, west-
957 ern United States. *Geol. Soc. Am. Bull.*, *80*(10), 1947–1960. doi: 10.1130/
958 0016-7606(1969)80[1947:TRBFIS]2.0.CO;2
- 959 Bernard, B., Brooks, J. M., Sackett, W. M., et al. (1977). A geochemical model for
960 characterization of hydrocarbon gas sources in marine sediments. In *Offshore*
961 *technology conference* (p. 435-438). doi: 10.4043/2934-MS
- 962 Boetius, A., Ravensschlag, K., Schubert, C. J., Rickert, D., Widdel, F., Gieseke, A.,
963 ... Pfannkuche, O. (2000). A marine microbial consortium apparently medi-
964 ating anaerobic oxidation of methane. *Nature*, *407*(6804), 623–626. Retrieved
965 from <https://doi.org/10.1038/35036572> doi: 10.1038/35036572
- 966 Boone, D. R. (2015). Methanobacterium. In *Bergey's manual of system-*
967 *atics of archaea and bacteria* (p. 1-8). American Cancer Society. Re-
968 trieved from [https://onlinelibrary.wiley.com/doi/abs/10.1002/](https://onlinelibrary.wiley.com/doi/abs/10.1002/9781118960608.gbm00495)
969 [9781118960608.gbm00495](https://onlinelibrary.wiley.com/doi/abs/10.1002/9781118960608.gbm00495) doi: 10.1002/9781118960608.gbm00495
- 970 Bottinga, Y. (1969). Calculated fractionation factors for carbon and hydrogen
971 isotope exchange in the system calcite-carbon dioxide-graphite-methane-
972 hydrogen-water vapor. *Geochim. Cosmochim. Acta*, *33*(1), 49 - 64. Re-
973 trieved from [http://www.sciencedirect.com/science/article/pii/](http://www.sciencedirect.com/science/article/pii/0016703769900921)
974 [0016703769900921](http://www.sciencedirect.com/science/article/pii/0016703769900921) doi: 10.1016/0016-7037(69)90092-1
- 975 Boudier, F., Baronnet, A., & Mainprice, D. (2009, Aug). Serpentine Mineral

- 976 Replacements of Natural Olivine and their Seismic Implications: Oceanic
 977 Lizardite versus Subduction-Related Antigorite. *J. Petrol.*, 51(1-2), 495–512.
 978 doi: 10.1093/petrology/egp049
- 979 Boudier, F., & Coleman, R. G. (1981). Cross section through the peri-
 980 dotite in the Samail Ophiolite, southeastern Oman Mountains. *J. Geo-
 981 phys. Res.: Solid Earth*, 86(B4), 2573–2592. Retrieved from [https://
 982 agupubs.onlinelibrary.wiley.com/doi/abs/10.1029/JB086iB04p02573](https://agupubs.onlinelibrary.wiley.com/doi/abs/10.1029/JB086iB04p02573)
 983 doi: 10.1029/JB086iB04p02573
- 984 Boulart, C., Chavagnac, V., Monnin, C., Delacour, A., Ceuleneer, G., & Hoareau,
 985 G. (2013). Differences in gas venting from ultramafic-hosted warm springs:
 986 the example of Oman and Voltri ophiolites. *Ophioliti*, 38(2), 142–156. doi:
 987 10.4454/ofioliti.v38i2.423
- 988 Bradley, A. S., Hayes, J. M., & Summons, R. E. (2009). Extraordinary ^{13}C en-
 989 richment of diether lipids at the Lost City Hydrothermal Field indicates a
 990 carbon-limited ecosystem. *Geochim. Cosmochim. Acta*, 73(1), 102–118. doi:
 991 10.1016/j.gca.2008.10.005
- 992 Brazelton, W. J., Thornton, C. N., Hyer, A., Twing, K. I., Longino, A. A., Lang,
 993 S. Q., ... Schrenk, M. O. (2017). Metagenomic identification of active
 994 methanogens and methanotrophs in serpentinite springs of the Voltri Mas-
 995 sif, Italy. *PeerJ*, 5, e2945. doi: 10.7717/peerj.2945
- 996 Bruni, J., Canepa, M., Chiodini, G., Cioni, R., Cipolli, F., Longinelli, A., ... Zuc-
 997 colini, M. V. (2002). Irreversible water–rock mass transfer accompanying
 998 the generation of the neutral, Mg–HCO₃ and high-pH, Ca–OH spring wa-
 999 ters of the Genova province, Italy. *Appl. Geochem.*, 17(4), 455–474. doi:
 1000 10.1016/S0883-2927(01)00113-5
- 1001 Callahan, B. J., McMurdie, P. J., Rosen, M. J., Han, A. W., Johnson, A. J. A., &
 1002 Holmes, S. P. (2016, May). DADA2: High-resolution sample inference from
 1003 Illumina amplicon data. *Nat. Methods*, 13(7), 581. doi: 10.1038/nmeth.3869
- 1004 Canovas III, P. A., Hoehler, T., & Shock, E. L. (2017). Geochemical bioenergetics
 1005 during low-temperature serpentinization: An example from the Samail ophio-
 1006 lite, Sultanate of Oman. *J. Geophys. Res.: Biogeosci.*, 122(7), 1821–1847. doi:
 1007 10.1002/2017JG003825
- 1008 Charlou, J., Donval, J., Douville, E., Jean-Baptiste, P., Radford-Knoery, J.,
 1009 Fouquet, Y., ... Stievenard, M. (2000). Compared geochemical sig-
 1010 natures and the evolution of Menez Gwen (37°50'N) and Lucky Strike
 1011 (37°17'N) hydrothermal fluids, south of the Azores Triple Junction on
 1012 the Mid-Atlantic Ridge. *Chem. Geol.*, 171(1), 49 - 75. Retrieved from
 1013 <http://www.sciencedirect.com/science/article/pii/S0009254100002448>
 1014 doi: 10.1016/S0009-2541(00)00244-8
- 1015 Charlou, J., Donval, J., Fouquet, Y., Jean-Baptiste, P., & Holm, N. (2002). Geo-
 1016 chemistry of high H₂ and CH₄ vent fluids issuing from ultramafic rocks at the
 1017 Rainbow hydrothermal field (36° 14' N, MAR). *Chem. Geol.*, 191(4), 345–359.
 1018 doi: 10.1016/S0009-2541(02)00134-1
- 1019 Charlou, J. L., Donval, J. P., Konn, C., Ondréas, H., Fouquet, Y., Jean-Baptiste, P.,
 1020 & Fourné, E. (2010). High production and fluxes of H₂ and CH₄ and evidence
 1021 of abiotic hydrocarbon synthesis by serpentinization in ultramafic-hosted hy-
 1022 drothermal systems on the Mid-Atlantic Ridge. In *Diversity of hydrothermal
 1023 systems on slow spreading ocean ridges* (p. 265-296). American Geophysical
 1024 Union (AGU). Retrieved from [https://agupubs.onlinelibrary.wiley.com/
 1025 doi/abs/10.1029/2008GM000752](https://agupubs.onlinelibrary.wiley.com/doi/abs/10.1029/2008GM000752) doi: 10.1029/2008GM000752
- 1026 Charlou, J. L., Fouquet, Y., Donval, J. P., Auzende, J. M., Jean-Baptiste, P., Stie-
 1027 venard, M., & Michel, S. (1996). Mineral and gas chemistry of hydrothermal
 1028 fluids on an ultrafast spreading ridge: East Pacific Rise, 17° to 19°S (Naudur
 1029 cruise, 1993) phase separation processes controlled by volcanic and tectonic
 1030 activity. *J. Geophys. Res.: Solid Earth*, 101(B7), 15899-15919. Retrieved from

- 1031 <https://agupubs.onlinelibrary.wiley.com/doi/abs/10.1029/96JB00880>
1032 doi: 10.1029/96JB00880
- 1033 Chavagnac, V., Ceuleneer, G., Monnin, C., Lansac, B., Hoareau, G., & Boulart,
1034 C. (2013). Mineralogical assemblages forming at hyperalkaline warm
1035 springs hosted on ultramafic rocks: A case study of Oman and Ligurian ophi-
1036 olites. *Geochem., Geophys., Geosyst.*, 14(7), 2474-2495. Retrieved from
1037 <https://agupubs.onlinelibrary.wiley.com/doi/abs/10.1002/ggge.20146>
1038 doi: 10.1002/ggge.20146
- 1039 Chavagnac, V., Monnin, C., Ceuleneer, G., Boulart, C., & Hoareau, G. (2013).
1040 Characterization of hyperalkaline fluids produced by low-temperature ser-
1041 pentinization of mantle peridotites in the Oman and Ligurian ophiolites.
1042 *Geochem., Geophys., Geosyst.*, 14(7), 2496–2522. doi: 10.1002/ggge.20147
- 1043 Cipolli, F., Gambardella, B., Marini, L., Ottonello, G., & Zuccolini, M. V. (2004).
1044 Geochemistry of high-pH waters from serpentinites of the Gruppo di Voltri
1045 (Genova, Italy) and reaction path modeling of CO₂ sequestration in ser-
1046 pentinite aquifers. *Appl. Geochem.*, 19(5), 787 - 802. Retrieved from
1047 <http://www.sciencedirect.com/science/article/pii/S0883292703002105>
1048 doi: 10.1016/j.apgeochem.2003.10.007
- 1049 Clark, I. D., Fontes, J.-C., & Fritz, P. (1992). Stable isotope disequilibria in traver-
1050 tine from high pH waters: Laboratory investigations and field observations
1051 from Oman. *Geochim. Cosmochim. Acta*, 56(5), 2041 - 2050. Retrieved from
1052 <http://www.sciencedirect.com/science/article/pii/001670379290328G>
1053 doi: 10.1016/0016-7037(92)90328-G
- 1054 Coleman, R. G., & Hopson, C. A. (1981). Introduction to the Oman Ophiolite
1055 Special Issue. *J. Geophys. Res.: Solid Earth*, 86(B4), 2495-2496. Retrieved
1056 from [https://agupubs.onlinelibrary.wiley.com/doi/abs/10.1029/
1057 JB086iB04p02495](https://agupubs.onlinelibrary.wiley.com/doi/abs/10.1029/JB086iB04p02495) doi: 10.1029/JB086iB04p02495
- 1058 Collier, M. L. (2012). *Spatial-Statistical Properties of Geochemical Variability as*
1059 *Constraints on Magma Transport and Evolution Processes at Ocean Ridges*
1060 (Doctoral dissertation, Columbia University). doi: 10.7916/D82V2P43
- 1061 Crespo-Medina, M., Twing, K. I., Sánchez-Murillo, R., Brazelton, W. J., McCol-
1062 lom, T. M., & Schrenk, M. O. (2017, May). Methane Dynamics in a Tropical
1063 Serpentinizing Environment: The Santa Elena Ophiolite, Costa Rica. *Front.*
1064 *Microb.*, 8. Retrieved from <http://dx.doi.org/10.3389/fmicb.2017.00916>
1065 doi: 10.3389/fmicb.2017.00916
- 1066 de Obeso, J. C., & Kelemen, P. B. (2018). Fluid rock interactions on residual man-
1067 tle peridotites overlain by shallow oceanic limestones: Insights from Wadi
1068 Fins, Sultanate of Oman. *Chem. Geol.*, 498, 139 - 149. Retrieved from
1069 <http://www.sciencedirect.com/science/article/pii/S0009254118304625>
1070 doi: 10.1016/j.chemgeo.2018.09.022
- 1071 Deines, P. (2002). The carbon isotope geochemistry of mantle xenoliths. *Earth-Sci.*
1072 *Rev.*, 58(3), 247 - 278. Retrieved from [http://www.sciencedirect.com/
1073 science/article/pii/S0012825202000648](http://www.sciencedirect.com/science/article/pii/S0012825202000648) doi: 10.1016/S0012-8252(02)
1074 00064-8
- 1075 Delacour, A., Früh-Green, G. L., Bernasconi, S. M., Schaeffer, P., & Kelley, D. S.
1076 (2008). Carbon geochemistry of serpentinites in the Lost City Hydrother-
1077 mal System (30°N, MAR). *Geochim. Cosmochim. Acta*, 72(15), 3681 - 3702.
1078 Retrieved from [http://www.sciencedirect.com/science/article/pii/
1079 S0016703708002585](http://www.sciencedirect.com/science/article/pii/S0016703708002585) doi: 10.1016/j.gca.2008.04.039
- 1080 Dewandel, B., Boudier, F., Kern, H., Warsi, W., & Mainprice, D. (2003). Seis-
1081 mic wave velocity and anisotropy of serpentinized peridotite in the Oman
1082 ophiolite. *Tectonophysics*, 370(1), 77 - 94. Retrieved from [http://
1083 www.sciencedirect.com/science/article/pii/S0040195103001781](http://www.sciencedirect.com/science/article/pii/S0040195103001781) (Phys-
1084 ical Properties of Rocks and other Geomaterials, a Special Volume to honour
1085 Professor H. Kern) doi: 10.1016/S0040-1951(03)00178-1

- 1086 Dewandel, B., Lachassagne, P., Boudier, F., Al-Hattali, S., Ladouche, B., Pinault, J.-
 1087 L., & Al-Suleimani, Z. (2005, 5). A conceptual hydrogeological model of ophi-
 1088 olite hard-rock aquifers in Oman based on a multiscale and a multidisciplinary
 1089 approach. *Hydrogeol. J.*, *13*(5-6), 708–726. doi: 10.1007/s10040-005-0449-2
- 1090 Etiope, G. (2017). Methane origin in the Samail ophiolite: Comment on “Modern
 1091 water/rock reactions in Oman hyperalkaline peridotite aquifers and impli-
 1092 cations for microbial habitability” [*Geochim. Cosmochim. Acta* 179 (2016)
 1093 217–241]. *Geochim. Cosmochim. Acta*, *197*, 467 - 470. Retrieved from
 1094 <http://www.sciencedirect.com/science/article/pii/S0016703716304379>
 1095 doi: 10.1016/j.gca.2016.08.001
- 1096 Etiope, G., Ifandi, E., Nazzari, M., Procesi, M., Tsikouras, B., Ventura, G., ... Szat-
 1097 mari, P. (2018, Jun). Widespread abiotic methane in chromitites. *Sci. Rep.*,
 1098 *8*(1). Retrieved from <http://dx.doi.org/10.1038/s41598-018-27082-0>
 1099 doi: 10.1038/s41598-018-27082-0
- 1100 Etiope, G., & Ionescu, A. (2015). Low-temperature catalytic CO₂ hydrogenation
 1101 with geological quantities of ruthenium: a possible abiotic CH₄ source
 1102 in chromitite-rich serpentinitized rocks. *Geofluids*, *15*(3), 438–452. doi:
 1103 10.1111/gfl.12106
- 1104 Etiope, G., Judas, J., & Whiticar, M. (2015). Occurrence of abiotic methane in
 1105 the eastern United Arab Emirates ophiolite aquifer. *Arabian J. Geosci.*, *8*(12),
 1106 11345–11348. doi: 10.1007/s12517-015-1975-4
- 1107 Etiope, G., Vadillo, I., Whiticar, M., Marques, J., Carreira, P., Tiago, I., ... Ur-
 1108 resti, B. (2016). Abiotic methane seepage in the Ronda peridotite mas-
 1109 sif, southern Spain. *Appl. Geochem.*, *66*, 101–113. doi: doi.org/10.1016/
 1110 j.apgeochem.2015.12.001
- 1111 Etiope, G., & Whiticar, M. (2019). Abiotic methane in continental ultramafic
 1112 rock systems: Towards a genetic model. *Appl. Geochem.*, *102*, 139 - 152.
 1113 Retrieved from [http://www.sciencedirect.com/science/article/pii/](http://www.sciencedirect.com/science/article/pii/S0883292719300204)
 1114 [S0883292719300204](http://www.sciencedirect.com/science/article/pii/S0883292719300204) doi: 10.1016/j.apgeochem.2019.01.012
- 1115 Ettwig, K. F., Butler, M. K., Le Paslier, D., Pelletier, E., Mangenot, S., Kuypers,
 1116 M. M. M., ... Strous, M. (2010, Mar). Nitrite-driven anaerobic methane
 1117 oxidation by oxygenic bacteria. *Nature*, *464*(7288), 543. doi: 10.1038/
 1118 nature08883
- 1119 Evans, B. W. (1977). Metamorphism of alpine peridotite and serpenti-
 1120 nite. *Annu. Rev. Earth Planet. Sci.*, *5*(1), 397-447. Retrieved from
 1121 <https://doi.org/10.1146/annurev.ea.05.050177.002145> doi: 10.1146/
 1122 annurev.ea.05.050177.002145
- 1123 Falk, E., Guo, W., Paukert, A., Matter, J., Mervine, E., & Kelemen, P. (2016).
 1124 Controls on the stable isotope compositions of travertine from hyperalkaline
 1125 springs in Oman: Insights from clumped isotope measurements. *Geochim. Cos-*
 1126 *mochim. Acta*, *192*, 1 - 28. Retrieved from [http://www.sciencedirect.com/](http://www.sciencedirect.com/science/article/pii/S0016703716303568)
 1127 [science/article/pii/S0016703716303568](http://www.sciencedirect.com/science/article/pii/S0016703716303568) doi: 10.1016/j.gca.2016.06.026
- 1128 Feisthauer, S., Vogt, C., Modrzynski, J., Szlenkier, M., Krüger, M., Siegert, M., &
 1129 Richnow, H.-H. (2011). Different types of methane monooxygenases produce
 1130 similar carbon and hydrogen isotope fractionation patterns during methane
 1131 oxidation. *Geochim. Cosmochim. Acta*, *75*(5), 1173 - 1184. Retrieved from
 1132 <http://www.sciencedirect.com/science/article/pii/S0016703710006691>
 1133 doi: 10.1016/j.gca.2010.12.006
- 1134 Fiebig, J., Stefánsson, A., Ricci, A., Tassi, F., Viveiros, F., Silva, C., ... Mountain,
 1135 B. W. (2019). Abiogenesis not required to explain the origin of volcanic-
 1136 hydrothermal hydrocarbons. *Geochem. Perspect. Lett.*, *11*, 23–27. Retrieved
 1137 from <http://www.geochemicalperspectivesletters.org/article1920> doi:
 1138 10.7185/geochemlet.1920
- 1139 Fones, E. M., Colman, D. R., Kraus, E. A., Nothhaft, D. B., Poudel, S., Rempfert,
 1140 K. R., ... Boyd, E. S. (2019). Physiological adaptations to serpentinization in

- 1141 the Samail Ophiolite, Oman. *ISME J.*, 1. doi: 10.1038/s41396-019-0391-2
- 1142 Fritz, P., Clark, I., Fontes, J.-C., Whiticar, M., & Faber, E. (1992). Deuterium and
1143 ^{13}C evidence for low temperature production of hydrogen and methane in a
1144 highly alkaline groundwater environment in Oman. In *International symposium*
1145 *on water-rock interaction* (Vol. 1, pp. 793–796). AA Balkema Rotterdam.
- 1146 Frost, B. R. (1985, Feb). On the Stability of Sulfides, Oxides, and Native Metals in
1147 Serpentine. *J. Petrol.*, 26(1), 31–63. doi: 10.1093/petrology/26.1.31
- 1148 Gadikota, G., Matter, J., Kelemen, P., Brady, P. V., & Park, A.-H. A. (2020). Elu-
1149 cidating the differences in the carbon mineralization behaviors of calcium and
1150 magnesium bearing alumino-silicates and magnesium silicates for CO_2 storage.
1151 *Fuel*, 277, 117900. Retrieved from [http://www.sciencedirect.com/science/](http://www.sciencedirect.com/science/article/pii/S0016236120308966)
1152 [article/pii/S0016236120308966](http://www.sciencedirect.com/science/article/pii/S0016236120308966) doi: 10.1016/j.fuel.2020.117900
- 1153 Gadikota, G., Matter, J., Kelemen, P., & Park, A.-h. A. (2014). Chemical and mor-
1154 phological changes during olivine carbonation for CO_2 storage in the presence
1155 of NaCl and NaHCO_3 . *Phys. Chem. Chem. Phys.*, 16(10), 4679–4693. doi:
1156 10.1039/C3CP54903H
- 1157 Giunta, T., Young, E. D., Warr, O., Kohl, I., Ash, J. L., Martini, A., ... Lol-
1158 lar, B. S. (2019). Methane sources and sinks in continental sedimentary
1159 systems: New insights from paired clumped isotopologues $^{13}\text{CH}_3\text{D}$ and
1160 $^{12}\text{CH}_2\text{D}^2$. *Geochim. Cosmochim. Acta*, 245, 327 - 351. Retrieved from
1161 <http://www.sciencedirect.com/science/article/pii/S0016703718306161>
1162 doi: 10.1016/j.gca.2018.10.030
- 1163 Glein, C. R., Baross, J. A., & Waite Jr, J. H. (2015). The pH of Enceladus' ocean.
1164 *Geochim. Cosmochim. Acta*, 162, 202–219. doi: 10.1016/j.gca.2015.04.017
- 1165 Glein, C. R., & Zolotov, M. Y. (2020, 02). Hydrogen, Hydrocarbons, and Habitabil-
1166 ity Across the Solar System. *Elements*, 16(1), 47-52. Retrieved from [https://](https://doi.org/10.2138/gselements.16.1.47)
1167 doi.org/10.2138/gselements.16.1.47 doi: 10.2138/gselements.16.1.47
- 1168 Glennie, K., Boeuf, M., Clarke, M. H., Moody-Stuart, M., Pilaar, W., & Reinhardt,
1169 B. (1973). Late Cretaceous nappes in Oman Mountains and their geologic
1170 evolution. *AAPG Bull.*, 57(1), 5–27. doi: 10.1306/819A4240-16C5-11D7
1171 -8645000102C1865D
- 1172 Godard, M., Jousselin, D., & Bodinier, J.-L. (2000). Relationships between geo-
1173 chemistry and structure beneath a palaeo-spreading centre: a study of the
1174 mantle section in the Oman ophiolite. *Earth Planet. Sci. Lett.*, 180(1), 133 -
1175 148. Retrieved from [http://www.sciencedirect.com/science/article/pii/](http://www.sciencedirect.com/science/article/pii/S0012821X00001497)
1176 [S0012821X00001497](http://www.sciencedirect.com/science/article/pii/S0012821X00001497) doi: 10.1016/S0012-821X(00)00149-7
- 1177 Grozeva, N. G., Klein, F., Seewald, J. S., & Sylva, S. P. (2020, FEB 21).
1178 Chemical and isotopic analyses of hydrocarbon-bearing fluid inclusions in
1179 olivine-rich rocks [Article]. *Philos. Trans. R. Soc., A*, 378(2165, SI). doi:
1180 10.1098/rsta.2018.0431
- 1181 Gruen, D. S., Wang, D. T., Könneke, M., Topçuoğlu, B. D., Stewart, L. C., Gold-
1182 hammer, T., ... Ono, S. (2018). Experimental investigation on the con-
1183 trols of clumped isotopologue and hydrogen isotope ratios in microbial
1184 methane. *Geochim. Cosmochim. Acta*, 237, 339 - 356. Retrieved from
1185 <http://www.sciencedirect.com/science/article/pii/S0016703718303442>
1186 doi: 10.1016/j.gca.2018.06.029
- 1187 Guilmette, C., Smit, M. A., van Hinsbergen, D. J. J., Gürer, D., Corfu, F., Charette,
1188 B., ... Savard, D. (2018). Forced subduction initiation recorded in the
1189 sole and crust of the Semail Ophiolite of Oman. *Nat. Geosci.*, 11(9), 688–
1190 695. Retrieved from <https://doi.org/10.1038/s41561-018-0209-2> doi:
1191 10.1038/s41561-018-0209-2
- 1192 Hanghøj, K., Kelemen, P. B., Hassler, D., & Godard, M. (2010, Jan). Com-
1193 position and Genesis of Depleted Mantle Peridotites from the Wadi Tayin
1194 Massif, Oman Ophiolite; Major and Trace Element Geochemistry, and
1195 Os Isotope and PGE Systematics. *J. Petrol.*, 51(1-2), 201–227. doi:

- 10.1093/petrology/egp077
- 1196 Hanson, R. S., & Hanson, T. E. (1996). Methanotrophic bacteria. *Microbiol. Mol.*
1197 *Biol. Rev.*, *60*(2), 439–471. Retrieved from [https://mbr.asm.org/content/](https://mbr.asm.org/content/60/2/439)
1198 [https://mbr.asm.org/content/](https://mbr.asm.org/content/60/2/439)
1199 [60/2/439](https://mbr.asm.org/content/60/2/439)
- 1200 Henry, E. A., Devereux, R., Maki, J. S., Gilmour, C. C., Woese, C. R., Man-
1201 delco, L., ... Mitchell, R. (1994). Characterization of a new thermophilic
1202 sulfate-reducing bacterium. *Arch. Microbiol.*, *161*(1), 62–69. Retrieved from
1203 <https://doi.org/10.1007/BF00248894> doi: 10.1007/BF00248894
- 1204 Horibe, Y., & Craig, H. (1995). DH fractionation in the system methane-hydrogen-
1205 water. *Geochim. Cosmochim. Acta*, *59*(24), 5209–5217. doi: 10.1016/0016
1206 -7037(95)00391-6
- 1207 Kampbell, D., Wilson, J., & McInnes, D. (1998). Determining dissolved hydrogen,
1208 methane, and vinyl chloride concentrations in aqueous solution on a nanomolar
1209 scale with the bubble strip method. In *Proceedings of the 1998 conference on*
1210 *hazardous waste research* (p. 176-190).
- 1211 Kelemen, P., Al Rajhi, A., Godard, M., Ildefonse, B., Köpke, J., MacLeod, C., ...
1212 Teagle, D. (2013). Scientific drilling and related research in the samail ophio-
1213 lite, sultanate of Oman. *Scientific Drilling 2013 (2013)*, Nr. 15, 2013(15), 64–
1214 71. Retrieved from [https://www.repo.uni-hannover.de/handle/123456789/](https://www.repo.uni-hannover.de/handle/123456789/1086)
1215 [1086](https://www.repo.uni-hannover.de/handle/123456789/1086)
- 1216 Kelemen, P., Matter, J., Teagle, D., Coggon, J., & the Oman Drilling Project Sci-
1217 ence Team. (2020). Proceedings of the oman drilling project. In *Proceed-*
1218 *ings of the oman drilling project* (p. All pages.). College Station, TX. doi:
1219 [10.14379/OmanDP.proc.2020](https://doi.org/10.14379/OmanDP.proc.2020)
- 1220 Kelemen, P. B., & Matter, J. (2008). In situ carbonation of peridotite for CO₂ stor-
1221 age. *Proc. Natl. Acad. Sci. U. S. A.*, *105*(45), 17295–17300. doi: 10.1073/pnas
1222 .0805794105
- 1223 Kelemen, P. B., Matter, J., Streit, E. E., Rudge, J. F., Curry, W. B., & Blusz-
1224 tajn, J. (2011). Rates and mechanisms of mineral carbonation in peri-
1225 dotite: natural processes and recipes for enhanced, in situ CO₂ capture
1226 and storage. *Annu. Rev. Earth Planet. Sci.*, *39*, 545–576. doi: 10.1146/
1227 annurev-earth-092010-152509
- 1228 Kelemen, P. B., McQueen, N., Wilcox, J., Renforth, P., Dipple, G., & Vankeuren,
1229 A. P. (2020). Engineered carbon mineralization in ultramafic rocks for CO₂
1230 removal from air: Review and new insights. *Chem. Geol.*, *550*, 119628.
1231 Retrieved from [http://www.sciencedirect.com/science/article/pii/](http://www.sciencedirect.com/science/article/pii/S0009254120301674)
1232 [S0009254120301674](http://www.sciencedirect.com/science/article/pii/S0009254120301674) doi: 10.1016/j.chemgeo.2020.119628
- 1233 Kelley, D. S. (1996). Methane-rich fluids in the oceanic crust. *J. Geophys. Res.:*
1234 *Solid Earth*, *101*(B2), 2943–2962. doi: 10.1029/95JB02252
- 1235 Kelley, D. S., & Früh-Green, G. L. (1999). Abiogenic methane in deep-seated mid-
1236 ocean ridge environments: Insights from stable isotope analyses. *J. Geophys.*
1237 *Res.: Solid Earth*, *104*(B5), 10439–10460. doi: 10.1029/1999JB900058
- 1238 Kieft, T. L. (2016). Microbiology of the Deep Continental Biosphere. In *Their*
1239 *world: A diversity of microbial environments* (pp. 225–249). Cham: Springer
1240 International Publishing. Retrieved from [https://doi.org/10.1007/978-3-](https://doi.org/10.1007/978-3-319-28071-4_6)
1241 [3-319-28071-4_6](https://doi.org/10.1007/978-3-319-28071-4_6) doi: 10.1007/978-3-319-28071-4_6
- 1242 Kieft, T. L., McCuddy, S. M., Onstott, T. C., Davidson, M., Lin, L.-H., Mislowack,
1243 B., ... van Heerden, A. (2005). Geochemically Generated, Energy-Rich
1244 Substrates and Indigenous Microorganisms in Deep, Ancient Groundwater.
1245 *Geomicrobiol. J.*, *22*(6), 325–335. Retrieved from [https://doi.org/10.1080/](https://doi.org/10.1080/01490450500184876)
1246 [01490450500184876](https://doi.org/10.1080/01490450500184876) doi: 10.1080/01490450500184876
- 1247 Klein, F., & Bach, W. (2009, 02). Fe–Ni–Co–O–S Phase Relations in Peridotite–
1248 Seawater Interactions. *J. Petrol.*, *50*(1), 37–59. Retrieved from [https://doi](https://doi.org/10.1093/petrology/egn071)
1249 [.org/10.1093/petrology/egn071](https://doi.org/10.1093/petrology/egn071) doi: 10.1093/petrology/egn071
- 1250 Klein, F., Bach, W., Jöns, N., McCollom, T., Moskowitz, B., & Berquó, T. (2009).

- 1251 Iron partitioning and hydrogen generation during serpentinization of abyssal
1252 peridotites from 15 °N on the Mid-Atlantic Ridge. *Geochim. Cosmochim.*
1253 *Acta*, 73(22), 6868 - 6893. Retrieved from [http://www.sciencedirect.com/
1254 science/article/pii/S0016703709005353](http://www.sciencedirect.com/science/article/pii/S0016703709005353) doi: 10.1016/j.gca.2009.08.021
- 1255 Klein, F., Grozeva, N. G., & Seewald, J. S. (2019). Abiotic methane synthesis and
1256 serpentinization in olivine-hosted fluid inclusions. *Proc. Natl. Acad. Sci. U. S.*
1257 *A.*, 116(36), 17666–17672. Retrieved from [https://www.pnas.org/content/
1258 116/36/17666](https://www.pnas.org/content/116/36/17666) doi: 10.1073/pnas.1907871116
- 1259 Knittel, K., & Boetius, A. (2009). Anaerobic Oxidation of Methane: Progress with
1260 an Unknown Process. *Annu. Rev. Microbiol.*, 63(1), 311-334. Retrieved from
1261 <https://doi.org/10.1146/annurev.micro.61.080706.093130> (PMID:
1262 19575572) doi: 10.1146/annurev.micro.61.080706.093130
- 1263 Koepf, M. (1978). D/H isotope exchange reaction between petroleum and water: a
1264 contributory determinant for D/H- isotope ratios in crude oils. In R. E. Zart-
1265 man (Ed.), *Short papers of the fourth international conference, geochronology,
1266 cosmochronology, isotope geology, 1978* (p. 221-222). doi: 10.3133/ofr78701
- 1267 Kral, T. A., Birch, W., Lavender, L. E., & Virden, B. T. (2014). Potential use
1268 of highly insoluble carbonates as carbon sources by methanogens in the
1269 subsurface of Mars. *Planet. Space Sci.*, 101, 181 - 185. Retrieved from
1270 <http://www.sciencedirect.com/science/article/pii/S0032063314002049>
1271 doi: 10.1016/j.pss.2014.07.008
- 1272 Kraus, E. A., Stamps, B. W., Rempfert, K. R., Nothhaft, D. B., Boyd, E. S., Mat-
1273 ter, J. M., ... Spear, J. R. (2018, December). Biological methane cycling in
1274 serpentinization-impacted fluids of the Samail ophiolite of Oman. *AGU Fall
1275 Meeting Abstracts*.
- 1276 Kumagai, H., Nakamura, K., Toki, T., Morishita, T., Okino, K., Ishibashi, J.-i.,
1277 ... Takai, K. (2008, nov). Geological background of the Kairei and Ed-
1278 mond hydrothermal fields along the Central Indian Ridge : Implications
1279 for the distinct chemistry between their vent fluids. *Geofluids*, 8(4), 239-
1280 251. Retrieved from <https://ci.nii.ac.jp/naid/120006389526/en/> doi:
1281 10.1111/j.1468-8123.2008.00223.x
- 1282 Laso-Pérez, R., Hahn, C., van Vliet, D. M., Tegetmeyer, H. E., Schubotz, F., Smit,
1283 N. T., ... Wegener, G. (2019). Anaerobic Degradation of Non-Methane
1284 Alkanes by “Candidatus Methanoliparia” in Hydrocarbon Seeps of the Gulf of
1285 Mexico. *mBio*, 10(4). Retrieved from [https://mbio.asm.org/content/10/4/
1286 e01814-19](https://mbio.asm.org/content/10/4/e01814-19) doi: 10.1128/mBio.01814-19
- 1287 Leong, J. A. M., & Shock, E. L. (2020). Thermodynamic constraints on the geo-
1288 chemistry of low-temperature, continental, serpentinization-generated fluids.
1289 *Am. J. Sci.*, 320(3), 185–235. doi: 10.2475/03.2020.01
- 1290 Lippard, S., Shelton, A., & Gass, I. (1986). *The Ophiolite of Northern Oman*
1291 (Vol. 11). Geological Society of London. Retrieved from [https://
1292 mem.lyellcollection.org/content/11/1/39](https://mem.lyellcollection.org/content/11/1/39) doi: 10.1144/GSL.MEM
1293 .1986.011.01.03
- 1294 Luesken, F. A., Wu, M. L., Op den Camp, H. J. M., Keltjens, J. T., Stunnen-
1295 berg, H., Francoijs, K.-J., ... Jetten, M. S. M. (2012). Effect of oxygen
1296 on the anaerobic methanotroph ‘Candidatus Methylopirabilis oxyfera’: ki-
1297 netic and transcriptional analysis. *Environ. Microbiol.*, 14(4), 1024-1034.
1298 Retrieved from [https://onlinelibrary.wiley.com/doi/abs/10.1111/
1299 j.1462-2920.2011.02682.x](https://onlinelibrary.wiley.com/doi/abs/10.1111/j.1462-2920.2011.02682.x) doi: 10.1111/j.1462-2920.2011.02682.x
- 1300 MacDougall, D., Crummett, W. B., et al. (1980). Guidelines for data acquisition
1301 and data quality evaluation in environmental chemistry. *Anal. Chem.*, 52(14),
1302 2242–2249.
- 1303 Marques, J., Etiope, G., Neves, M., Carreira, P., Rocha, C., Vance, S., ...
1304 Suzuki, S. (2018). Linking serpentinization, hyperalkaline mineral wa-
1305 ters and abiotic methane production in continental peridotites: an inte-

- 1306 grated hydrogeological-bio-geochemical model from the Cabeço de Vide
1307 CH₄-rich aquifer (Portugal). *Appl. Geochem.*, *96*, 287 - 301. Retrieved from
1308 <http://www.sciencedirect.com/science/article/pii/S0883292718301987>
1309 doi: 10.1016/j.apgeochem.2018.07.011
- 1310 Martini, A. M., Walter, L. M., Ku, T. C. W., Budai, J. M., McIntosh, J. C., &
1311 Schoell, M. (2003, 08). Microbial production and modification of gases
1312 in sedimentary basins: A geochemical case study from a Devonian shale
1313 gas play, Michigan basin. *AAPG Bull.*, *87*(8), 1355-1375. Retrieved from
1314 <https://doi.org/10.1306/031903200184> doi: 10.1306/031903200184
- 1315 Matter, J. M., Pezard, P. A., Moe, K., Henry, G., Paris, J., Brun, L., ... Coggon,
1316 J. A. (2018, December). Advanced downhole hydrogeophysical logging during
1317 Oman Drilling Project Phase 2 - Correlation of hydraulic and fluid properties.
1318 *AGU Fall Meeting Abstracts*.
- 1319 Matter, J. M., Waber, H., Loew, S., & Matter, A. (2006). Recharge ar-
1320 eas and geochemical evolution of groundwater in an alluvial aquifer sys-
1321 tem in the Sultanate of Oman. *Hydrogeol. J.*, *14*(1-2), 203–224. doi:
1322 10.1007/s10040-004-0425-2
- 1323 McCollom, T. M. (2016). Abiotic methane formation during experimental serpen-
1324 tization of olivine. *Proc. Natl. Acad. Sci. U. S. A.*, *113*(49), 13965–13970.
1325 doi: 10.1073/pnas.1611843113
- 1326 McCollom, T. M., & Bach, W. (2009). Thermodynamic constraints on hydrogen
1327 generation during serpentinization of ultramafic rocks. *Geochim. Cosmochim.*
1328 *Acta*, *73*(3), 856–875. doi: 10.1016/j.gca.2008.10.032
- 1329 McCollom, T. M., & Seewald, J. S. (2003). Experimental constraints on the hy-
1330 drothermal reactivity of organic acids and acid anions: I. Formic acid and
1331 formate. *Geochim. Cosmochim. Acta*, *67*(19), 3625 - 3644. Retrieved from
1332 <http://www.sciencedirect.com/science/article/pii/S0016703703001364>
1333 doi: 10.1016/S0016-7037(03)00136-4
- 1334 McDermott, J. M., Seewald, J. S., German, C. R., & Sylva, S. P. (2015). Pathways
1335 for abiotic organic synthesis at submarine hydrothermal fields. *Proc. Natl.*
1336 *Acad. Sci. U. S. A.*, *112*(25), 7668–7672. doi: 10.1073/pnas.1506295112
- 1337 McKay, C. P., Porco, C. C., Altheide, T., Davis, W. L., & Kral, T. A. (2008).
1338 The Possible Origin and Persistence of Life on Enceladus and Detection of
1339 Biomarkers in the Plume. *Astrobiology*, *8*(5), 909-919. Retrieved from
1340 <https://doi.org/10.1089/ast.2008.0265> (PMID: 18950287) doi:
1341 10.1089/ast.2008.0265
- 1342 Ménez, B. (2020, 02). Abiotic Hydrogen and Methane: Fuels for Life. *Elements*,
1343 *16*(1), 39-46. Retrieved from [https://doi.org/10.2138/gselements.16.1](https://doi.org/10.2138/gselements.16.1.39)
1344 .39 doi: 10.2138/gselements.16.1.39
- 1345 Merlivat, L., Pineau, F., & Javoy, M. (1987). Hydrothermal vent waters at
1346 13 °N on the East Pacific Rise: isotopic composition and gas concentra-
1347 tion. *Earth Planet. Sci. Lett.*, *84*(1), 100 - 108. Retrieved from [http://](http://www.sciencedirect.com/science/article/pii/0012821X87901804)
1348 www.sciencedirect.com/science/article/pii/0012821X87901804 doi:
1349 10.1016/0012-821X(87)90180-4
- 1350 Mervine, E. M., Humphris, S. E., Sims, K. W., Kelemen, P. B., & Jenkins,
1351 W. J. (2014). Carbonation rates of peridotite in the Samail Ophio-
1352 lite, Sultanate of Oman, constrained through ¹⁴C dating and stable iso-
1353 topes. *Geochim. Cosmochim. Acta*, *126*, 371 - 397. Retrieved from
1354 <http://www.sciencedirect.com/science/article/pii/S0016703713006467>
1355 doi: 10.1016/j.gca.2013.11.007
- 1356 Michaelis, W., Seifert, R., Nauhaus, K., Treude, T., Thiel, V., Blumenberg, M., ...
1357 Gulin, M. B. (2002). Microbial Reefs in the Black Sea Fueled by Anaer-
1358 obic Oxidation of Methane. *Science*, *297*(5583), 1013–1015. Retrieved
1359 from <https://science.sciencemag.org/content/297/5583/1013> doi:
1360 10.1126/science.1072502

- 1361 Milkov, A. V., & Etiope, G. (2018). Revised genetic diagrams for natural gases
1362 based on a global dataset of $\approx 20,000$ samples. *Org. Geochem.*, *125*, 109–120.
1363 doi: 10.1016/j.orggeochem.2018.09.002
- 1364 Miller, H. M., Chaudhry, N., Conrad, M. E., Bill, M., Kopf, S. H., & Templeton,
1365 A. S. (2018). Large carbon isotope variability during methanogenesis under
1366 alkaline conditions. *Geochim. Cosmochim. Acta*, *237*, 18 - 31. Retrieved from
1367 <http://www.sciencedirect.com/science/article/pii/S0016703718303223>
1368 doi: 10.1016/j.gca.2018.06.007
- 1369 Miller, H. M., Matter, J. M., Kelemen, P., Ellison, E. T., Conrad, M., Fierer, N.,
1370 ... Templeton, A. S. (2017). Reply to “Methane origin in the Samail ophi-
1371 olite: Comment on ‘Modern water/rock reactions in Oman hyperalkaline
1372 peridotite aquifers and implications for microbial habitability’” [*Geochim. Cos-
1373 mochim. Acta* 179 (2016) 217–241]. *Geochim. Cosmochim. Acta*, *197*, 471 -
1374 473. Retrieved from <http://www.sciencedirect.com/science/article/pii/S0016703716306482>
1375 doi: 10.1016/j.gca.2016.11.011
- 1376 Miller, H. M., Matter, J. M., Kelemen, P., Ellison, E. T., Conrad, M. E., Fierer,
1377 N., ... Templeton, A. S. (2016). Modern water/rock reactions in Oman
1378 hyperalkaline peridotite aquifers and implications for microbial habit-
1379 ability. *Geochim. Cosmochim. Acta*, *179*, 217 - 241. Retrieved from
1380 <http://www.sciencedirect.com/science/article/pii/S0016703716300205>
1381 doi: 10.1016/j.gca.2016.01.033
- 1382 Miller, H. M., Mayhew, L. E., Ellison, E. T., Kelemen, P., Kubo, M., & Templeton,
1383 A. S. (2017). Low temperature hydrogen production during experimental hy-
1384 dration of partially-serpentinized dunite. *Geochim. Cosmochim. Acta*, *209*, 161
1385 - 183. Retrieved from [http://www.sciencedirect.com/science/article/
1386 pii/S0016703717302454](http://www.sciencedirect.com/science/article/pii/S0016703717302454) doi: 10.1016/j.gca.2017.04.022
- 1387 Miura, M., Arai, S., & Mizukami, T. (2011). Raman spectroscopy of hydrous in-
1388 clusions in olivine and orthopyroxene in ophiolitic harzburgite: Implications
1389 for elementary processes in serpentinization. *J. Mineral. Petrol. Sci., adu*
1390 *pub*, 1103030170-1103030170. doi: 10.2465/jmps.101021d
- 1391 Moser, D. P., Gihring, T. M., Brockman, F. J., Fredrickson, J. K., Balkwill,
1392 D. L., Dollhopf, M. E., ... Onstott, T. C. (2005). Desulfotomaculum and
1393 Methanobacterium spp. Dominate a 4- to 5-Kilometer-Deep Fault. *Appl. En-
1394 viron. Microbiol.*, *71*(12), 8773–8783. Retrieved from [https://aem.asm.org/
1395 content/71/12/8773](https://aem.asm.org/content/71/12/8773) doi: 10.1128/AEM.71.12.8773-8783.2005
- 1396 Murad, A. A., & Krishnamurthy, R. (2004). Factors controlling ground-
1397 water quality in Eastern United Arab Emirates: a chemical and iso-
1398 topic approach. *J. Hydro.*, *286*(1), 227 - 235. Retrieved from [http://
1399 www.sciencedirect.com/science/article/pii/S0022169403003949](http://www.sciencedirect.com/science/article/pii/S0022169403003949) doi:
1400 10.1016/j.jhydrol.2003.09.020
- 1401 National Academies. (2019). *Negative Emissions Technologies and Reliable Seques-
1402 tration: A Research Agenda*. Washington, DC: National Academies Press. doi:
1403 10.17226/25259
- 1404 Neal, C., & Stanger, G. (1983). Hydrogen generation from mantle source rocks
1405 in Oman. *Earth Planet. Sci. Lett.*, *66*, 315 - 320. Retrieved from [http://
1406 www.sciencedirect.com/science/article/pii/0012821X83901449](http://www.sciencedirect.com/science/article/pii/0012821X83901449) doi: 10
1407 .1016/0012-821X(83)90144-9
- 1408 Neal, C., & Stanger, G. (1985). Past and present serpentinisation of ultramafic
1409 rocks; an example from the Semail Ophiolite Nappe of Northern Oman. In *The
1410 chemistry of weathering* (pp. 249–275). Springer. doi: 10.1007/978-94-009-5333
1411 -8.15
- 1412 Nicolas, A. (1989). *Structures of Ophiolites and Dynamics of Oceanic Lithosphere* |
1413 *SpringerLink*. Springer, Dordrecht. doi: 10.1007/978-94-009-2374-4
- 1414 Nicolas, A., Boudier, F., Ildefonse, B., & Ball, E. (2000). Accretion of Oman and
1415 United Arab Emirates ophiolite—discussion of a new structural map. *Marine*

- 1416 *Geophysical Researches*, 21(3-4), 147–180. doi: 10.1023/A:1026769727917
- 1417 Noël, J., Godard, M., Oliot, E., Martinez, I., Williams, M., Boudier, F., ...
- 1418 Gouze, P. (2018). Evidence of polygenetic carbon trapping in the Oman
- 1419 Ophiolite: Petro-structural, geochemical, and carbon and oxygen iso-
- 1420 tope study of the Wadi Dima harzburgite-hosted carbonates (Wadi Tayin
- 1421 massif, Sultanate of Oman). *Lithos*, 323, 218 - 237. Retrieved from
- 1422 <http://www.sciencedirect.com/science/article/pii/S0024493718302998>
- 1423 (ABYSS) doi: 10.1016/j.lithos.2018.08.020
- 1424 Nolan, S. C., Skelton, P. W., Clissold, B. P., & Smewing, J. D. (1990). Maas-
- 1425 trichtian to early Tertiary stratigraphy and palaeogeography of the Central
- 1426 and Northern Oman Mountains. *Geological Society, London, Special Publica-*
- 1427 *tions*, 49(1), 495–519. Retrieved from [https://sp.lyellcollection.org/](https://sp.lyellcollection.org/content/49/1/495)
- 1428 [content/49/1/495](https://sp.lyellcollection.org/content/49/1/495) doi: 10.1144/GSL.SP.1992.049.01.31
- 1429 Ono, S., Wang, D. T., Gruen, D. S., Sherwood Lollar, B., Zahniser, M. S., Mc-
- 1430 Manus, B. J., & Nelson, D. D. (2014). Measurement of a Doubly Sub-
- 1431 stituted Methane Isotopologue, $^{13}\text{CH}_3\text{D}$, by Tunable Infrared Laser Direct
- 1432 Absorption Spectroscopy. *Anal. Chem.*, 86(13), 6487-6494. Retrieved
- 1433 from <https://doi.org/10.1021/ac5010579> (PMID: 24895840) doi:
- 1434 10.1021/ac5010579
- 1435 Parsons International & Co., L. (2005, December). *Report on Findings of Explo-*
- 1436 *ration Program of Deep Groundwater in Northern Sharqiyah* (Tech. Rep.). PO
- 1437 Box 162, Postal Code 117, Wadi Al Kabir, Sultanate of Oman: Ministry of
- 1438 Regional Municipalities, Environment and Water Resources.
- 1439 Paukert, A. (2014). *Mineral Carbonation in Mantle Peridotite of the Samail*
- 1440 *Ophiolite, Oman: Implications for permanent geological carbon dioxide*
- 1441 *capture and storage* (Doctoral dissertation, Columbia University). doi:
- 1442 10.7916/D85M63WZ
- 1443 Paukert, A. N., Matter, J. M., Kelemen, P. B., Shock, E. L., & Havig, J. R. (2012).
- 1444 Reaction path modeling of enhanced in situ CO_2 mineralization for carbon
- 1445 sequestration in the peridotite of the Samail Ophiolite, Sultanate of Oman.
- 1446 *Chem. Geol.*, 330, 86–100. doi: 10.1016/j.chemgeo.2012.08.013
- 1447 Peters, J. W., Schut, G. J., Boyd, E. S., Mulder, D. W., Shepard, E. M., Broder-
- 1448 ick, J. B., ... Adams, M. W. (2015). [FeFe]- and [NiFe]-hydrogenase diver-
- 1449 sity, mechanism, and maturation. *Biochim. Biophys. Acta, Mol. Cell Res.*,
- 1450 1853(6), 1350 - 1369. Retrieved from [http://www.sciencedirect.com/](http://www.sciencedirect.com/science/article/pii/S0167488914004194)
- 1451 [science/article/pii/S0167488914004194](http://www.sciencedirect.com/science/article/pii/S0167488914004194) (SI: Fe/S proteins) doi:
- 1452 10.1016/j.bbamcr.2014.11.021
- 1453 Proskurowski, G., Lilley, M. D., Seewald, J. S., Früh-Green, G. L., Olson, E. J.,
- 1454 Lupton, J. E., ... Kelley, D. S. (2008). Abiogenic hydrocarbon produc-
- 1455 tion at Lost City hydrothermal field. *Science*, 319(5863), 604–607. doi:
- 1456 10.1126/science.1151194
- 1457 Quast, C., Pruesse, E., Gerken, J., Peplies, J., Yarza, P., Yilmaz, P., ... Glöckner,
- 1458 F. O. (2012, Nov). The SILVA ribosomal RNA gene database project: im-
- 1459 proved data processing and web-based tools. *Nucleic Acids Res.*, 41(D1),
- 1460 D590–D596. doi: 10.1093/nar/gks1219
- 1461 R Core Team. (2019). *R: A Language and Environment for Statistical Computing*.
- 1462 Vienna, Austria. Retrieved from <https://www.R-project.org/>
- 1463 Rabu, D., Nehlig, P., & Roger, J. (1993). Stratigraphy and structure of the Oman
- 1464 Mountains. *Documents- B. R. G. M.*
- 1465 Reeves, E. P., Seewald, J. S., & Sylva, S. P. (2012). Hydrogen isotope ex-
- 1466 change between n-alkanes and water under hydrothermal conditions.
- 1467 *Geochim. Cosmochim. Acta*, 77, 582 - 599. Retrieved from [http://](http://www.sciencedirect.com/science/article/pii/S0016703711005953)
- 1468 www.sciencedirect.com/science/article/pii/S0016703711005953 doi:
- 1469 10.1016/j.gca.2011.10.008
- 1470 Rempfert, K. R., Miller, H. M., Bompard, N., Nothaft, D., Matter, J. M., Kelemen,

- 1471 P., ... Templeton, A. S. (2017, February). Geological and geochemical controls
1472 on subsurface microbial life in the Samail Ophiolite, Oman. *Front. Microb.*,
1473 8(56), 1-21. doi: 10.3389/fmicb.2017.00056
- 1474 Rioux, M., Garber, J., Bauer, A., Bowring, S., Searle, M., Kelemen, P., & Hacker, B.
1475 (2016). Synchronous formation of the metamorphic sole and igneous crust of
1476 the Semail ophiolite: New constraints on the tectonic evolution during ophiolite
1477 formation from high-precision U–Pb zircon geochronology. *Earth Planet.
1478 Sci. Lett.*, 451, 185 - 195. Retrieved from [http://www.sciencedirect.com/
1479 science/article/pii/S0012821X16303387](http://www.sciencedirect.com/science/article/pii/S0012821X16303387) doi: 10.1016/j.epsl.2016.06.051
- 1480 Rollinson, H. (2005). Chromite in the mantle section of the Oman ophiolite: A
1481 new genetic model. *Island Arc*, 14(4), 542-550. Retrieved from [https://
1482 onlinelibrary.wiley.com/doi/abs/10.1111/j.1440-1738.2005.00482.x](https://onlinelibrary.wiley.com/doi/abs/10.1111/j.1440-1738.2005.00482.x)
1483 doi: 10.1111/j.1440-1738.2005.00482.x
- 1484 Sachan, H. K., Mukherjee, B. K., & Bodnar, R. J. (2007). Preservation of
1485 methane generated during serpentinization of upper mantle rocks: Ev-
1486 idence from fluid inclusions in the Nidar ophiolite, Indus Suture Zone,
1487 Ladakh (India). *Earth Planet. Sci. Lett.*, 257(1), 47 - 59. Retrieved from
1488 <http://www.sciencedirect.com/science/article/pii/S0012821X07000969>
1489 doi: 10.1016/j.epsl.2007.02.023
- 1490 Sander, R. (2015). Compilation of Henry's law constants (version 4.0) for water as
1491 solvent. *Atmos. Chem. Phys.*, 15(8). doi: 10.5194/ACP-15-4399-2015
- 1492 Schidlowski, M. (2001). Carbon isotopes as biogeochemical recorders of life over 3.8
1493 Ga of Earth history: evolution of a concept. *Precambrian Res.*, 106(1), 117 -
1494 134. Retrieved from [http://www.sciencedirect.com/science/article/pii/
1495 S0301926800001285](http://www.sciencedirect.com/science/article/pii/S0301926800001285) doi: 10.1016/S0301-9268(00)00128-5
- 1496 Sekiguchi, Y., Muramatsu, M., Imachi, H., Narihiro, T., Ohashi, A., Harada,
1497 H., ... Kamagata, Y. (2008). *Thermodesulfovibrio aggregans* sp. nov.
1498 and *Thermodesulfovibrio thiophilus* sp. nov., anaerobic, thermophilic,
1499 sulfate-reducing bacteria isolated from thermophilic methanogenic sludge,
1500 and emended description of the genus *Thermodesulfovibrio* [Journal Ar-
1501 ticle]. *Int. J. Syst. Evol. Microbiol.*, 58(11), 2541-2548. Retrieved from
1502 [https://www.microbiologyresearch.org/content/journal/ijsem/
1503 10.1099/ijms.0.2008/000893-0](https://www.microbiologyresearch.org/content/journal/ijsem/10.1099/ijms.0.2008/000893-0) doi: 10.1099/ijms.0.2008/000893-0
- 1504 Shennan, J. L. (2006). Utilisation of C2–C4 gaseous hydrocarbons and isoprene by
1505 microorganisms. *J. Appl. Chem. Biotechnol.*, 81(3), 237-256. Retrieved from
1506 <https://onlinelibrary.wiley.com/doi/abs/10.1002/jctb.1388> doi: 10
1507 .1002/jctb.1388
- 1508 Sherwood Lollar, B., Lacrampe-Couloume, G., Voglesonger, K., Onstott, T., Pratt,
1509 L., & Slater, G. (2008). Isotopic signatures of CH₄ and higher hydrocar-
1510 bon gases from Precambrian Shield sites: A model for abiogenic polymer-
1511 ization of hydrocarbons. *Geochim. Cosmochim. Acta*, 72(19), 4778 - 4795.
1512 Retrieved from [http://www.sciencedirect.com/science/article/pii/
1513 S0016703708004250](http://www.sciencedirect.com/science/article/pii/S0016703708004250) doi: 10.1016/j.gca.2008.07.004
- 1514 Sherwood Lollar, B., Westgate, T. D., Ward, J. A., Slater, G. F., & Lacrampe-
1515 Couloume, G. (2002, Apr). Abiogenic formation of alkanes in the Earth's
1516 crust as a minor source for global hydrocarbon reservoirs. *Nature*, 416(6880),
1517 522–524. doi: 10.1038/416522a
- 1518 Shock, E. L. (1992). Chemical Environments of Submarine Hydrothermal Sys-
1519 tems. In *Marine Hydrothermal Systems and the Origin of Life* (pp. 67–107).
1520 Springer, Dordrecht. doi: 10.1007/978-94-011-2741-7_5
- 1521 Singh, R., Guzman, M. S., & Bose, A. (2017). Anaerobic Oxidation of Ethane,
1522 Propane, and Butane by Marine Microbes: A Mini Review. *Front. Microb.*,
1523 8, 2056. Retrieved from [https://www.frontiersin.org/article/10.3389/
1524 fmicb.2017.02056](https://www.frontiersin.org/article/10.3389/fmicb.2017.02056) doi: 10.3389/fmicb.2017.02056
- 1525 Skelton, P. W., Nolan, S. C., & Scott, R. W. (1990). The Maastrichtian transgres-

- 1526 sion onto the northwestern flank of the Proto-Oman Mountains: sequences of
 1527 rudist-bearing beach to open shelf facies. *Geological Society, London, Special*
 1528 *Publications*, 49(1), 521–547. Retrieved from [https://sp.lyellcollection](https://sp.lyellcollection.org/content/49/1/521)
 1529 [.org/content/49/1/521](https://sp.lyellcollection.org/content/49/1/521) doi: 10.1144/GSL.SP.1992.049.01.32
- 1530 Soret, M., Bonnet, G., Larson, K., Agard, P., Cottle, J., Dubacq, B., & Button, M.
 1531 (2020, January). Slow subduction initiation forces fast ophiolite formation
 1532 Soret. In *International conference on ophiolites and the oceanic lithosphere: Results of the oman drilling project and related research* (p. 232).
 1533
- 1534 Stanger, G. (1986). *The hydrogeology of the Oman Mountains* (Unpublished doctoral
 1535 dissertation). Open University.
- 1536 Stolper, D., Martini, A., Clog, M., Douglas, P., Shusta, S., Valentine, D., . . . Eiler,
 1537 J. (2015). Distinguishing and understanding thermogenic and biogenic sources
 1538 of methane using multiply substituted isotopologues. *Geochim. Cosmochim.*
 1539 *Acta*, 161, 219 - 247. Retrieved from [http://www.sciencedirect.com/](http://www.sciencedirect.com/science/article/pii/S0016703715002082)
 1540 [science/article/pii/S0016703715002082](http://www.sciencedirect.com/science/article/pii/S0016703715002082) doi: 10.1016/j.gca.2015.04.015
- 1541 Streit, E., Kelemen, P., & Eiler, J. (2012, Nov 01). Coexisting serpentine and quartz
 1542 from carbonate-bearing serpentinitized peridotite in the Samail Ophiolite,
 1543 Oman. *Contrib. Mineral. Petrol.*, 164(5), 821–837. Retrieved from [https://](https://doi.org/10.1007/s00410-012-0775-z)
 1544 doi.org/10.1007/s00410-012-0775-z doi: 10.1007/s00410-012-0775-z
- 1545 Suzuki, S., Kuenen, J. G., Schipper, K., van der Velde, S., Ishii, S., Wu, A., . . .
 1546 Neelson, K. H. (2014, May). Physiological and genomic features of highly alkali-
 1547 philic hydrogen-utilizing Betaproteobacteria from a continental serpentinitizing
 1548 site. *Nat. Commun.*, 5, 3900. doi: 10.1038/ncomms4900
- 1549 Terken, J. M. J. (1999, Apr). The Natih Petroleum System of North Oman. *GeoAra-*
 1550 *bia*, 4(2), 157–180. Retrieved from [https://pubs.geoscienceworld.org/](https://pubs.geoscienceworld.org/geoarabia/article/4/2/157/566618)
 1551 [geoarabia/article/4/2/157/566618](https://pubs.geoscienceworld.org/geoarabia/article/4/2/157/566618)
- 1552 Terzer, S., Wassenaar, L. I., Araguás-Araguás, L. J., & Aggarwal, P. K. (2013).
 1553 Global isoscapes for $\delta^{18}\text{O}$ and $\delta^2\text{H}$ in precipitation: improved prediction using
 1554 regionalized climatic regression models. *Hydrol. Earth Syst. Sci.*, 17(11), 4713–
 1555 4728. Retrieved from [https://www.hydrol-earth-syst-sci.net/17/4713/](https://www.hydrol-earth-syst-sci.net/17/4713/2013/)
 1556 [2013/](https://www.hydrol-earth-syst-sci.net/17/4713/2013/) doi: 10.5194/hess-17-4713-2013
- 1557 Timmers, P. H., Welte, C. U., Koehorst, J. J., Plugge, C. M., Jetten, M. S., &
 1558 Stams, A. J. (2017). Reverse methanogenesis and respiration in methan-
 1559 otrophic archaea. *Archaea*, 2017. doi: 10.1155/2017/1654237
- 1560 USGS. (2010). *Digital Elevation - Global Multi-resolution Terrain Elevation Data*
 1561 *2010 (GMTED2010)*. doi: /10.5066/F7J38R2N
- 1562 Vacquand, C., Deville, E., Beaumont, V., Guyot, F., Sissmann, O., Pillot, D., . . .
 1563 Prinzhofer, A. (2018). Reduced gas seepages in ophiolitic complexes: evidences
 1564 for multiple origins of the $\text{H}_2\text{-CH}_4\text{-N}_2$ gas mixtures. *Geochim. Cosmochim.*
 1565 *Acta*, 223, 437–461. doi: 10.1016/j.gca.2017.12.018
- 1566 Vankeuren, A. N. P., Matter, J. M., Stute, M., & Kelemen, P. B. (2019). Multitracer
 1567 determination of apparent groundwater ages in peridotite aquifers within the
 1568 Samail ophiolite, Sultanate of Oman. *Earth Planet. Sci. Lett.*, 516, 37–48. doi:
 1569 [10.1016/j.epsl.2019.03.007](https://doi.org/10.1016/j.epsl.2019.03.007)
- 1570 Waite, J. H., Glein, C. R., Perryman, R. S., Teolis, B. D., Magee, B. A., Miller, G.,
 1571 . . . Bolton, S. J. (2017). Cassini finds molecular hydrogen in the Enceladus
 1572 plume: Evidence for hydrothermal processes. *Science*, 356(6334), 155–159.
 1573 Retrieved from <https://science.sciencemag.org/content/356/6334/155>
 1574 doi: 10.1126/science.aai8703
- 1575 Wang, D. T., Gruen, D. S., Lollar, B. S., Hinrichs, K.-U., Stewart, L. C., Holden,
 1576 J. F., . . . others (2015). Nonequilibrium clumped isotope signals in microbial
 1577 methane. *Science*, 348(6233), 428–431. doi: 10.1126/science.aaa4326
- 1578 Wang, D. T., Reeves, E. P., McDermott, J. M., Seewald, J. S., & Ono, S. (2018).
 1579 Clumped isotopologue constraints on the origin of methane at seafloor
 1580 hot springs. *Geochim. Cosmochim. Acta*, 223, 141–158. doi: 10.1016/

- 1581 j.gca.2017.11.030
1582 Wang, D. T., Welander, P. V., & Ono, S. (2016). Fractionation of the methane iso-
1583 topologues $^{13}\text{CH}_4$, $^{12}\text{CH}_3\text{D}$, and $^{13}\text{CH}_3\text{D}$ during aerobic oxidation of methane
1584 by *Methylococcus capsulatus* (Bath). *Geochim. Cosmochim. Acta*, *192*, 186–
1585 202. doi: 10.1016/j.gca.2016.07.031
- 1586 Wang, Q., Garrity, G. M., Tiedje, J. M., & Cole, J. R. (2007). Naïve Bayesian
1587 Classifier for Rapid Assignment of rRNA Sequences into the New Bacterial
1588 Taxonomy. *Appl. Environ. Microbiol.*, *73*(16), 5261–5267. Retrieved from
1589 <https://aem.asm.org/content/73/16/5261> doi: 10.1128/AEM.00062-07
- 1590 Welhan, J. A., & Craig, H. (1983). Methane, Hydrogen and Helium in Hydrothermal
1591 Fluids at 21 °N on the East Pacific Rise. In *Hydrothermal processes at seafloor*
1592 *spreading centers* (pp. 391–409). Boston, MA: Springer US. Retrieved from
1593 https://doi.org/10.1007/978-1-4899-0402-7_17 doi: 10.1007/978-1-4899
1594 -0402-7_17
- 1595 Welte, C. U., Rasigraf, O., Vaksmaa, A., Versantvoort, W., Arshad, A., Op den
1596 Camp, H. J., ... Reimann, J. (2016). Nitrate- and nitrite-dependent anaerobic
1597 oxidation of methane. *Environ. Microbiol. Rep.*, *8*(6), 941–955. Retrieved from
1598 <https://onlinelibrary.wiley.com/doi/abs/10.1111/1758-2229.12487>
1599 doi: 10.1111/1758-2229.12487
- 1600 Weyhenmeyer, C. E., Burns, S. J., Waber, H. N., Macumber, P. G., & Matter, A.
1601 (2002). Isotope study of moisture sources, recharge areas, and groundwater
1602 flow paths within the eastern Batinah coastal plain, Sultanate of Oman. *Water*
1603 *Resources Research*, *38*(10). doi: 10.1029/2000WR000149
- 1604 Whiticar, M. J. (1999). Carbon and hydrogen isotope systematics of bacterial forma-
1605 tion and oxidation of methane. *Chem. Geol.*, *161*(1), 291 - 314. Retrieved from
1606 <http://www.sciencedirect.com/science/article/pii/S0009254199000923>
1607 doi: 10.1016/S0009-2541(99)00092-3
- 1608 Young, E., Kohl, I., Lollar, B. S., Etiope, G., Rumble Iii, D., Li, S., ... others
1609 (2017). The relative abundances of resolved $^{12}\text{CH}_2\text{D}_2$ and $^{13}\text{CH}_3\text{D}$ and mech-
1610 anisms controlling isotopic bond ordering in abiotic and biotic methane gases.
1611 *Geochim. Cosmochim. Acta*, *203*, 235–264. doi: 10.1016/j.gca.2016.12.041
- 1612 Young, E. D. (2020). A Two-Dimensional Perspective on CH_4 Isotope Clumping :
1613 Distinguishing Process from Source. In *Deep carbon : Past to present* (p. 388-
1614 414). Cambridge University Press. Retrieved from [https://www.cambridge](https://www.cambridge.org/us/academic/subjects/earth-and-environmental-science/geochemistry-and-environmental-chemistry/deep-carbon-past-present?format=HB&isbn=9781108477499#resources)
1615 [.org/us/academic/subjects/earth-and-environmental-science/](https://www.cambridge.org/us/academic/subjects/earth-and-environmental-science/geochemistry-and-environmental-chemistry/deep-carbon-past-present?format=HB&isbn=9781108477499#resources)
1616 [geochemistry-and-environmental-chemistry/deep-carbon-past-present](https://www.cambridge.org/us/academic/subjects/earth-and-environmental-science/geochemistry-and-environmental-chemistry/deep-carbon-past-present?format=HB&isbn=9781108477499#resources)
1617 [?format=HB&isbn=9781108477499#resources](https://www.cambridge.org/us/academic/subjects/earth-and-environmental-science/geochemistry-and-environmental-chemistry/deep-carbon-past-present?format=HB&isbn=9781108477499#resources) doi: 10.1017/9781108677950
- 1618 Young, E. D., Rumble, D., Freedman, P., & Mills, M. (2016). A large-radius high-
1619 mass-resolution multiple-collector isotope ratio mass spectrometer for analysis
1620 of rare isotopologues of O_2 , N_2 , CH_4 and other gases. *Int. J. Mass Spectrom.*,
1621 *401*, 1 - 10. Retrieved from [http://www.sciencedirect.com/science/](http://www.sciencedirect.com/science/article/pii/S138738061600035X)
1622 [article/pii/S138738061600035X](http://www.sciencedirect.com/science/article/pii/S138738061600035X) doi: 10.1016/j.ijms.2016.01.006
- 1623 Zwicker, J., Birgel, D., Bach, W., Richoz, S., Smrzka, D., Grasemann, B., ... oth-
1624 ers (2018). Evidence for archaeal methanogenesis within veins at the onshore
1625 serpentinite-hosted Chimaera seeps, Turkey. *Chem. Geol.*, *483*, 567–580. doi:
1626 10.1016/j.chemgeo.2018.03.027

Figure 1.

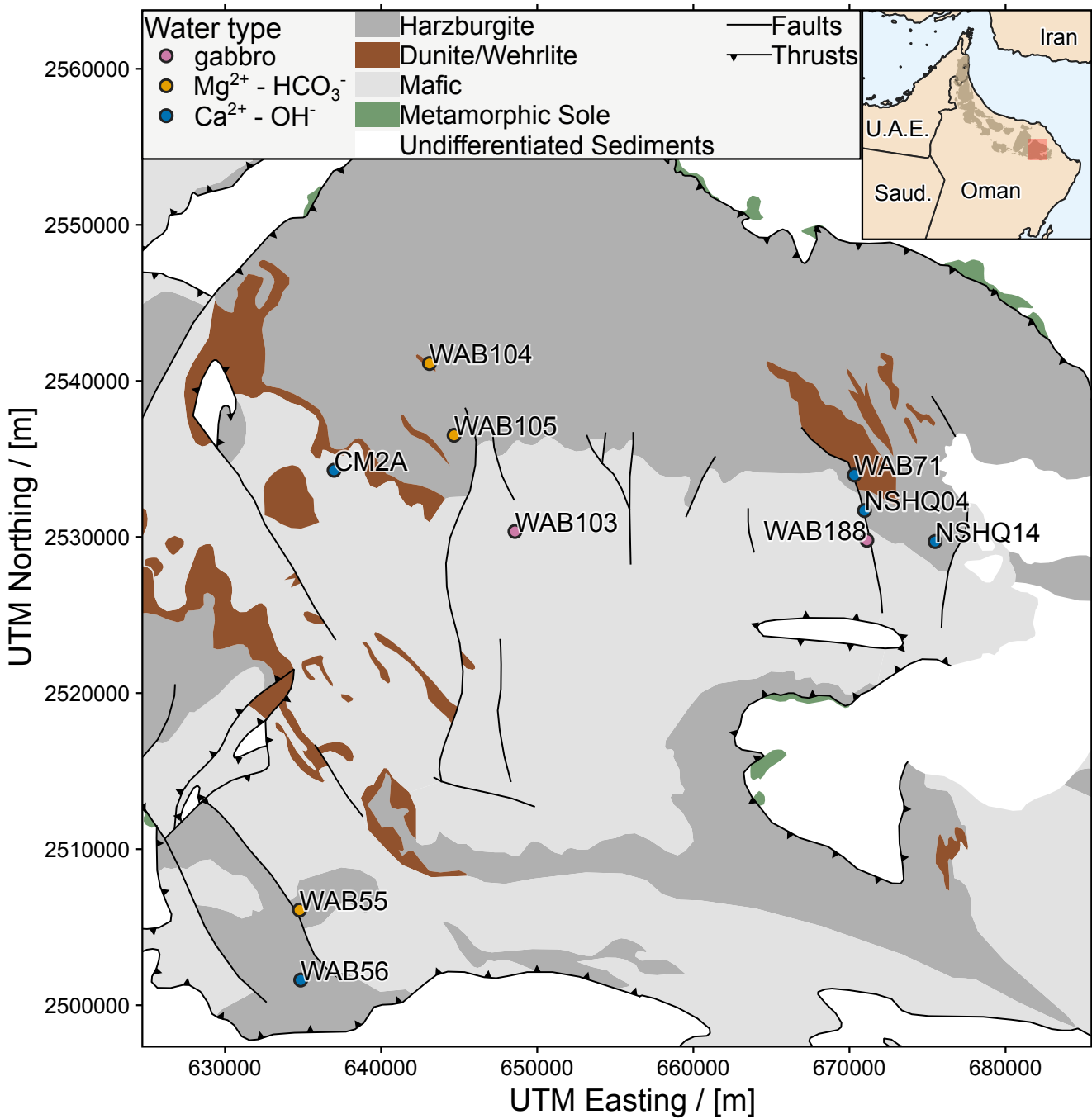
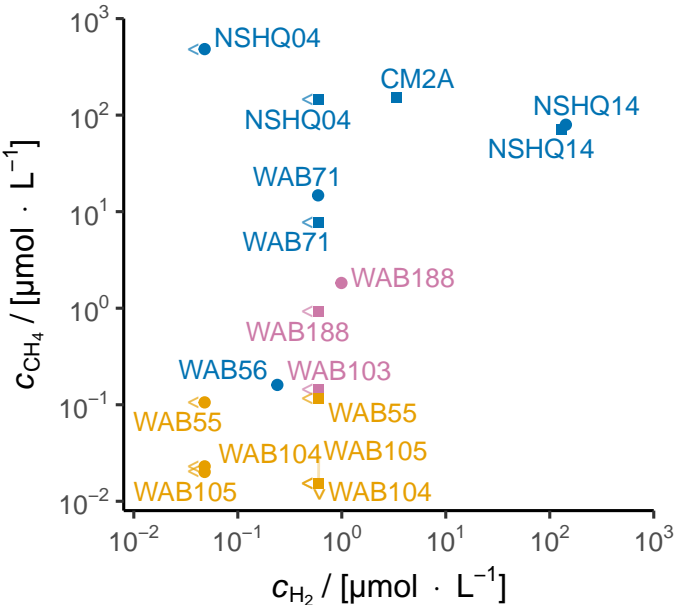


Figure 2.



water type

● gabbro

● $\text{Mg}^{2+} - \text{HCO}_3^-$

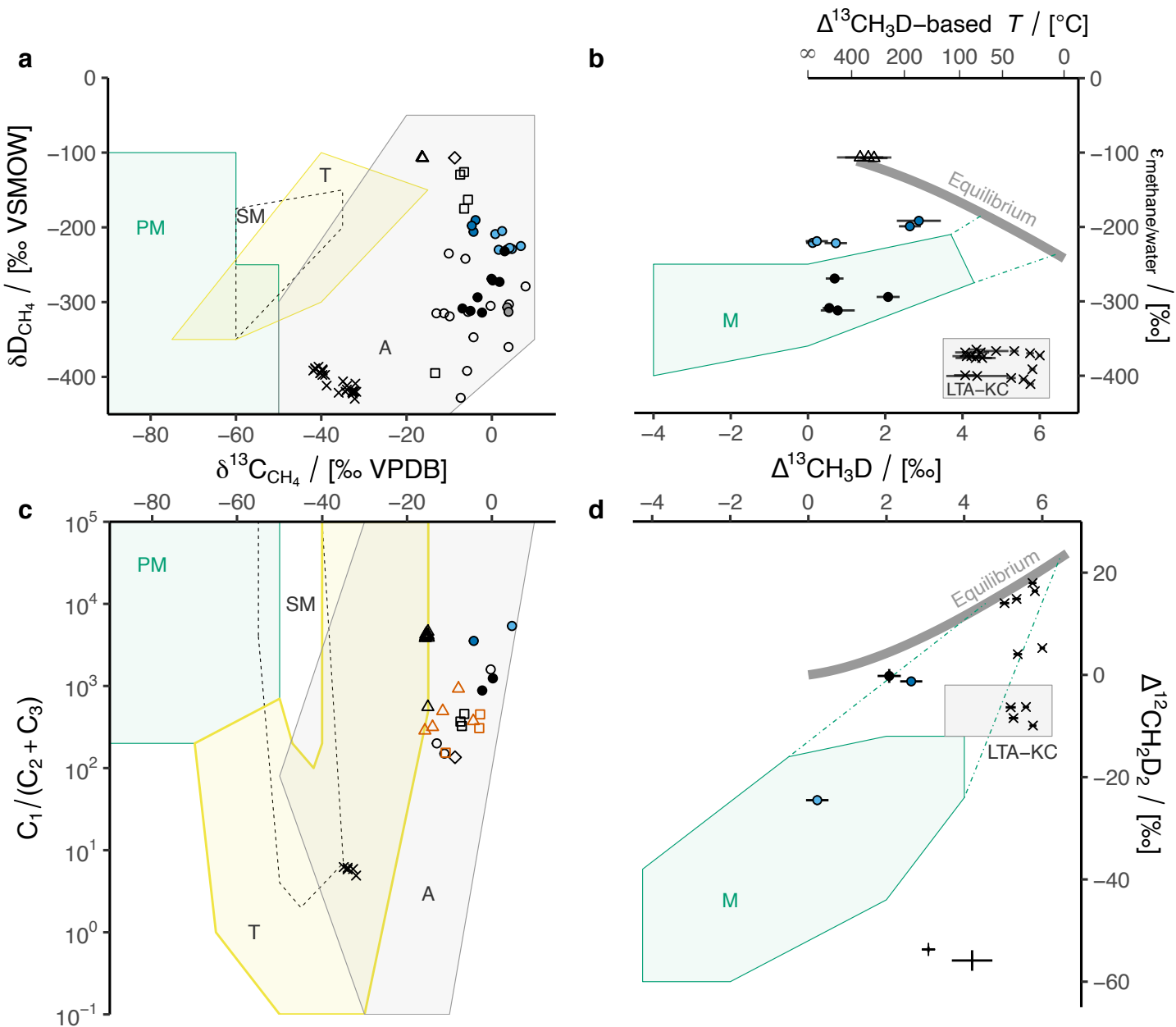
● $\text{Ca}^{2+} - \text{OH}^-$

year sampled

● 2017

■ 2018

Figure 3.



sample site

- Oman/UAE
- Philippines
- △ Mid-Cayman Rise
- ◇ Ashadze II
- × Kidd Creek

well (this study)

- NSHQ04
- WAB71
- CM2A
- NSHQ14

sample type

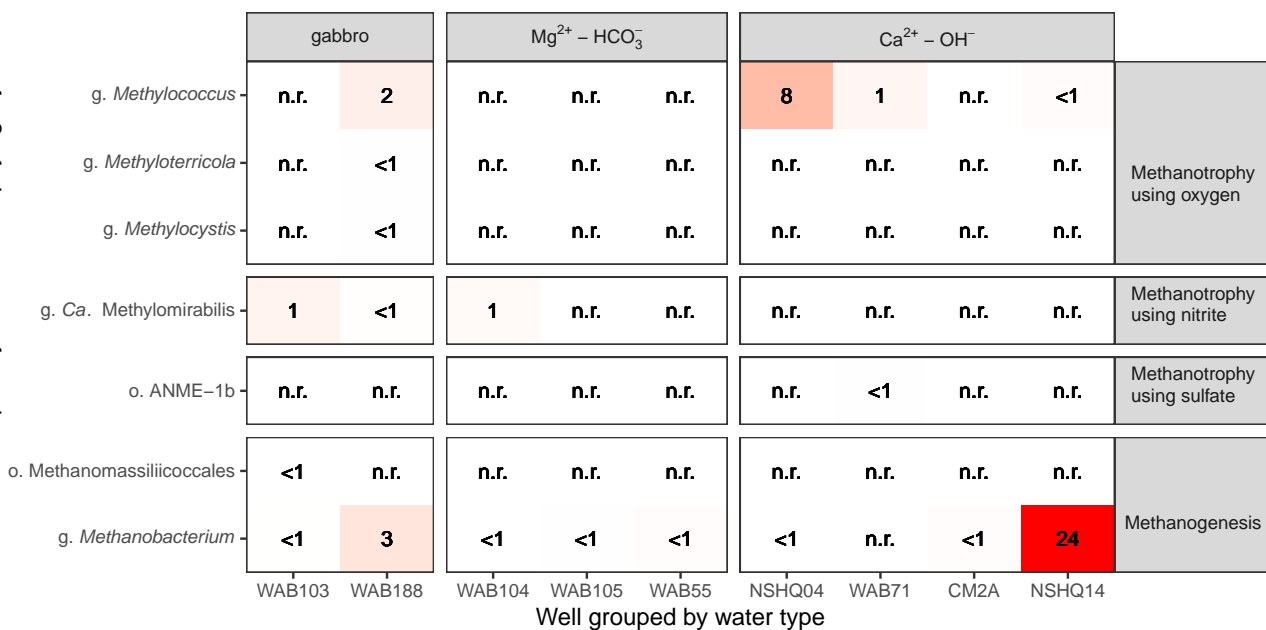
- rock crushing
- vent/well fluid

+ Sabatier reaction 70 °C to 90 °C

Figure 4.

Figure 5.

Deepest taxonomic assignment grouped by metabolic capability inferred from phylogeny



Well grouped by water type

Read relative abundance / [%]

